International Scientific-Technical and Production Journal

The Paton WELDING JOURNAL

June 2009 # 6

English translation of the monthly «Avtomaticheskaya Svarka» (Automatic Welding) journal published in Russian since 1948

Founders: *E.O. Paton Electric Welding Institute of the NAS of Ukraine, International Association «Welding»*

Publisher: *International Association «Welding»*

Address:

E.O. Paton Electric Welding Institute, International Association «Welding», 11, Bozhenko str., 03680, Kyiv, Ukraine

Tel.: (38044) 287 67 57

Fax: (38044) 528 04 86

E-mail: journal@paton.kiev.ua

http://www.nas.gov.ua/pwj

State Registration Certificate KV 4790 of 09.01.2001

Subscriptions:

$324, 12 issues per year, postage and packaging included. Back issues available.

CONTENTS

ESTIMATION OF GROWTH OF FATIGUE CRACKS IN LOAD-BEARING WELDED STRUCTURES AT RANDOM SPECTRUM OF CYCLIC LOADING

V.I. MAKHNENKO and I.Yu. ROMANOVA
E.O. Paton Electric Welding Institute, NASU, Kiev, Ukraine

Considered is the procedure for estimation of growth of fatigue cracks in reinforcement of one-sided butt weld on a longitudinal beam of freight flat car at the preset range of random cyclic loading. It is shown that sequence of application of the loading spectrum elements has a substantial effect on the fatigue life of a structure. The use of the Monte-Carlo method in calculations allows generating probabilistic characteristics of failure related to random application of cyclic loading.

Keywords: *welded structures, freight flat car, fatigue crack, cyclic loading, Monte-Carlo method, probability of failure, amplification factor, estimation of fatigue life*

Many modern critical durable structures (constructions) experience the effect of alternating time-dependent loads, which are of a random character, the elements of spectra of these loads, i.e. their ranges and frequency, being well studied. However, the sequence of application of ranges of such time-dependent loads causes certain difficulties in estimation of the development of fatigue cracks because of its substantial non-linearity with regard to geometric sizes of a crack. Normally, the most conservative method is used in this case. With this method, elements of the loading spectrum are ranked in sequence, starting from the highest range of loads, and ending with the lowest one [1]. The extent of conservatism of such an approach at corresponding loading spectra may be much beyond the reasonable limits, i.e. lead to a high disagreement between the calculated and experimental results. In this connection, when choosing the sequence of ranking of the loading spectrum elements, noteworthy is the use of methods of the theory of random events [2], etc. This study is dedicated particularly to this issue.

The study considers a surface (semielliptical) crack (Figure 1), when its characteristic geometrical sizes c and a grow according to equation (1) per cycle $\Delta N = 1$ [1]:

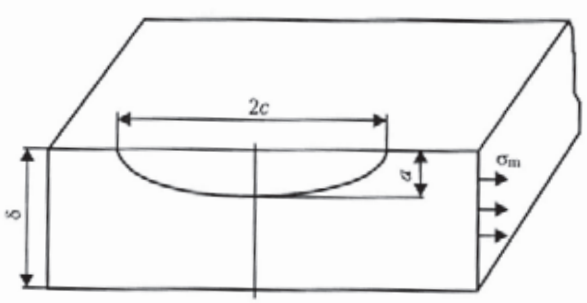

Figure 1. Schematic of surface (semielliptical) crack in structure element with thickness δ loaded by membrane stresses σ_m

$$\frac{dl}{dN} = C_0 \Delta K_I^m(l), \text{ if } \Delta K_I^l > \Delta K_{th}(R) \ (l = a, c);$$
$$\frac{dl}{dN} = 0, \text{ if } \Delta K_I^l < \Delta K_{th}(R), \quad (1)$$

where ΔK_I^l is the range of variations in stress intensity factor $K_I(l)$, respectively, at apex of the crack with sizes c and a (see Figure 1):

$$\Delta K_I^l = K_I^{max}(l) - K_I^{min}(l); \quad (2)$$

$$R = K_I^{min}/K_I^{max}; \quad (3)$$

C_0 and m are the experimental characteristics of a material within the crack zone [1]; and $\Delta K_{th}(R)$ is the threshold value of $K_I(l)$ obtained experimentally [1].

The values of $K_I^{max}(l)$ and $K_I^{min}(l)$ are found from the known values given in [1] and from the other dependencies, allowing for sizes of cracks, l, and preset elements of loading spectrum, P_j (Figure 2), as well as non-relaxed residual stresses σ_{res} within the crack zone.

Numerical integration of equations (1) through (3) at the preset initial sizes of a crack, $l_0 = a_0, c_0$, allows finding $l(N)$ depending upon N up to critical sizes of the crack, l_{cr}, at which the period of its spontaneous growth takes place, which is determined by the following condition:

$$Y = -K_r + f(L_r) < 0, \quad (4)$$

where $K_r = \dfrac{K_I^{max}(l_l)}{K_{IC}}$; $L_r = \dfrac{\sigma_{ref}}{\sigma_y} \le L_r^{max} = \dfrac{\sigma_y + \sigma_t}{2\sigma_y}$; K_{IC} is the fracture toughness of the material in the crack zone; σ_y is the yield stress; σ_t is the tensile strength of the material in the crack zone; $\sigma_{ref} = \sigma_{ref}(l)$ are the stresses in the crack zone under load $P_j^{max}(N)$, which are responsible for the plastic instability mechanism [1].

It is assumed in (4) that $f(L_r) = 0$ at $L_r > L_r^{max}$, which corresponds to fracture by the plastic instability mechanism.

Dependence $f(L_r)$ at $L_r \le L_r^{max}$ is usually approximated by the following equation [1]:

$$f(L_r) = (1 - 0.14L_r^2)\,[0.3 + 0.7\exp(-0.65L_r^6)]. \quad (5)$$

Equations (1) through (5) describe growth of a fatigue crack ($a_0 \times 2c_0$) at the deterministic sequence of application of elements of the cycling loading spectrum (see Figure 2). To allow for the random character of application of such a load, this study suggests using the Monte-Carlo method [3], according to which spectrum element j is selected at each tracing step by using random number counter $0 \le \Phi \le 1$ and table of correspondence between j and Φ. Resulting critical values $l_{cr} = a_{cr}$, c_{cr} and N_{cr} are random values. By repeating the tracing process Z times, we obtain a sample of the N_{cr} values, for which we find a mean value of fatigue life, $N_{cr}(Z)$. The sample being sufficiently representable ($N_{cr}(Z) \approx$ const with increase in Z), we calculate failure probability curves $P_f(N_{cr})$.

Consider a specific example of using the above approach. Figure 3 shows a schematic of one-sided butt weld of reinforcement of the longitudinal beam of a freight flat car made from steel 09G2S.

It is postulated that the root of the butt weld may have some lacks of penetration in the form of surface cracks $a_0 \times 2c_0$ in size. Longitudinal stresses related to vertical load (bend of frame), σ_{st}, act across the butt weld with respect to axis of the car frame. According to [4], depending upon the flat car speed, it is possible to determine the amplitude of dynamic (cyclic) stresses using calculated amplification factor K_{d_j} (j = 1–10):

$$\sigma_a = 0.5K_d\sigma_{st}. \quad (6)$$

The Table gives the values of K_{d_j} [4] obtained depending upon the speed of the flat car, w_j, as well as the share of p_j in the total number of loading cycles during movement of the car at the above speed, this allowing the number of loading cycles, ΔN_j, to be determined for basic fatigue life N_0 at a range of membrane stresses within the butt weld zone equal to $\Delta\sigma_j = 2K_{d_j}\sigma_{st}$.

Calculated values of K_{d_j} depending upon w_j and number of loading cycles ΔN_j normalised in [4] in total fatigue life of $N_\delta = 1\cdot10^7$ cycles

j	w_j, m/s	K_{d_j}	p_j	$\Delta N_j \cdot 10^{-5}$, cycle
1	6.25	0.0625	0.03	3
2	13.75	0.1375	0.07	7
3	16.25	0.1800	0.09	9
4	18.75	0.2400	0.12	12
5	21.25	0.3000	0.16	16
6	23.75	0.3600	0.19	19
7	26.25	0.4200	0.16	16
8	28.75	0.4800	0.10	10
9	31.25	0.5400	0.06	6
10	33.75	0.6000	0.02	2

Note. $\Delta N_j = p_j N_\delta$.

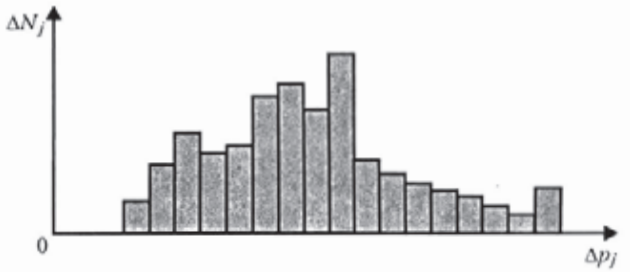

Figure 2. Schematic of cyclic loading spectrum ΔN_j at preset load range Δp_j

Dependencies (1) through (6), according to [1], were used in the calculations at

$$m = 3;\ C_0 = 5\cdot10^{-13}\left[\frac{\text{mm}}{(\text{MPa}\sqrt{\text{m}})^m}\right];$$

$$K_I^{\max} = \sigma_{\max}\frac{\sqrt{\pi l}}{Q}F_l;\ Q = [1 + 1.464(a/c)^{1.65}]^{0.5}; \quad (7)$$

$$F_l = [M_1 + M_2(a/\delta)^2 + M_3(a/\delta)^4]q_l;$$

$$q_a = 1;\ q_c = 1.1 + 0.35(a/\delta)^2;\ M_1 = 1.13 - 0.09(a/\delta);$$

$$M_2 = -0.54 + \frac{0.89}{0.2 + (a/c)}; \quad (8)$$

$$M_3 = 0.5 + \frac{1}{0.65 + (a/c)} + 14(1 - a/c)^{24} \text{ at } a/c < 1.0.$$

The value of $K_I^{\min}$ is calculated from (7), with $\sigma_{\min}$ being substituted for $\sigma_{\max}$.

The value of ΔK_{th} in (1) for carbon and low-alloy steels within the welded joint zone, according to [4], is determined from the following relationships:

$$\Delta K_{th} = 190 - 144R, \text{ not less than } 62\ \text{MPa}\cdot\text{mm}^{1/2}; \quad (9)$$

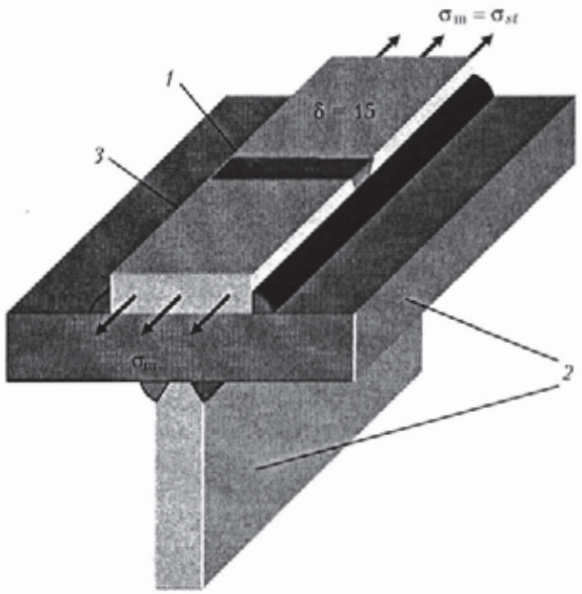

Figure 3. Schematic of longitudinal connection of flat car frame with reinforcement in the form of a cover strip with one-sided butt weld: *1* — one-sided butt weld; *2* — longitudinal connection of frame; *3* — reinforcing cover plate

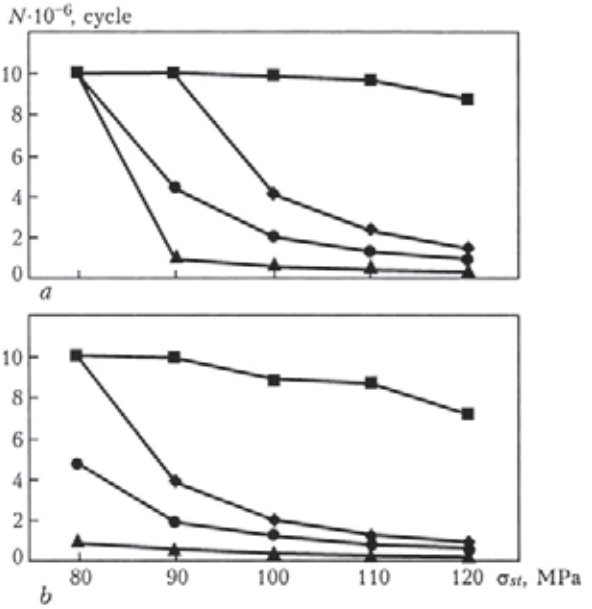

Figure 4. Results of calculation of fatigue life for postulated crack with size $a_0 \times 2c_0 = 1 \times 6$ mm (*a*) and deeper initial crack with size $a_0 \times 2c_0 = 2 \times 6$ mm (*b*) at different values of load σ_{st} obtained by deterministic calculations and calculations by the Monte-Carlo method ($P_f = 0.05$): ◆ — proportional application of load; ■▲— sequential applications of cyclic load at $j = 1$ and 10, respectively; ●— by Monte-Carlo method

$$\sigma_{ref} = \sigma_{\max}\frac{\delta}{\sigma - a};\ \sigma_y = 330\ \text{MPa};\quad L_r^{\max} = 1.33;$$
$$\delta = 15\ \text{mm};\ K_{1C} = 2210\ \text{MPa}\cdot\text{mm}^{1/2}. \qquad (10)$$

Figure 4, *a* shows the results of deterministic calculations of growth of the postulated crack (a_0 = = 1 mm, c_0 = 3 mm) to critical sizes determined by conditions (4) and (5) at sequential application of

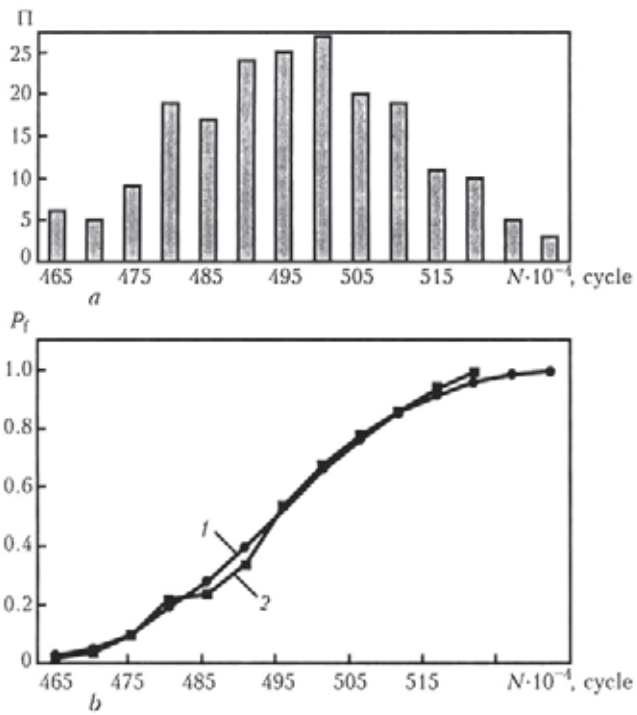

Figure 5. Frequency $\Pi(N)$ (*a*) and failure probability $P_f(N)$ (*b*) depending upon life N, determined for crack-like defect ($a_0 = 2$ mm, $c_0 = 3$ mm) at $\sigma_{st} = 80$ MPa: *a* — 200 random variants; *b* — 200 (*1*) and 50 (*2*) random variants

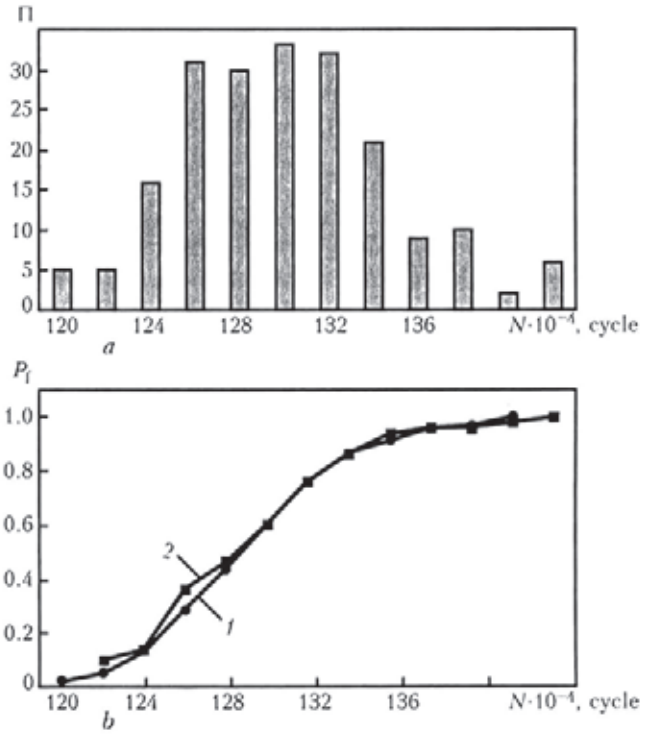

Figure 6. Same as in Figure 5, but at $\sigma_{st} = 100$ MPa

cyclic load (Table) from $j = 1$ to 10, and from 10 to 1, and at proportional presence of all j-th spectrum elements in tracing step $\Delta N_s = 1000$ cycles, i.e. $\Delta N_s^j = 1000(\Delta N_j / N_\delta)$, as well as the results of calculations by the Monte-Carlo method at failure probability $P_f = 0.05$. Similar data obtained for a deeper initial crack ($a_0 \times 2c_0 = 2 \times 6$ mm) are shown in Figure 4, *b*. It can be seen from them that the most conservative results on the fatigue life correspond to the deterministic calculation for sequence from the highest load. The calculation by the Monte-Carlo method at $P_f = 0.05$ is less conservative. The calculations in sequence from the lowest load to the highest one involve the risk of

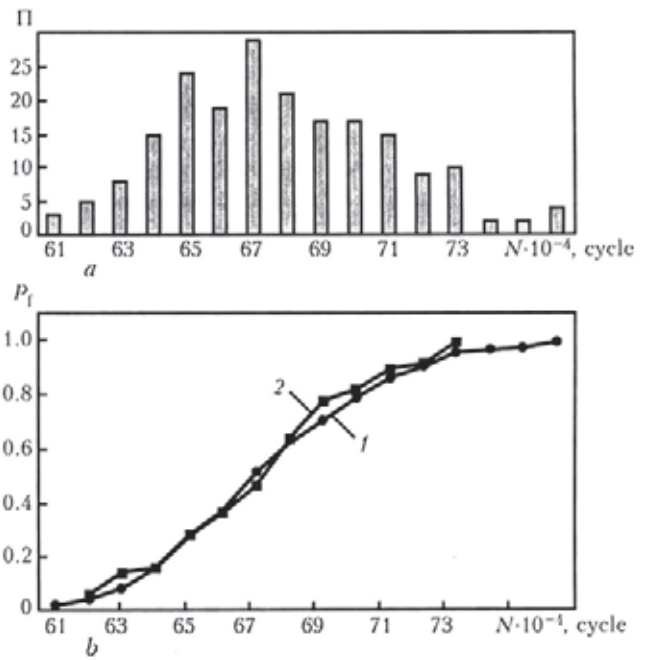

Figure 7. Same as in Figure 5, but at $\sigma_{st} = 120$ MPa

overestimation of the fatigue life. This, but to a lesser degree, takes place at the proportional presence of all elements of the load spectrum at each tracing step. The Monte-Carlo method takes the most complete account for the random character of application of the load spectrum elements, thus making it possible to obtain the probability characteristics of failure related to random application of cyclic load (Figures 5–7). Owing to these data, we can sufficiently clearly reveal the region of effectively varied values of the fatigue life. With the failure probability varied from 0.05 to 0.95, this region for the initial crack (a_0 = 2 mm, $2c_0$ = 6 mm) at σ_{st} = 80 MPa is $N = (4.7–5.2)\cdot10^6$ cycles, at σ_{st} = 110 MPa it is $N = (1.22–1.38)\cdot10^6$ cycles, and at σ_{st} = 120 MPa it is $N = (0.620–0.725)\cdot10^6$ cycles.

Therefore, at a preset spectrum of random cyclic loading the deterministic approach to estimation of growth of a fatigue crack to the critical state yields the results which substantially differ from sequence of application of the loading spectrum elements. The use of the Monte-Carlo method allows the problem of the random character of loading to be solved with a sufficient validity within the framework of the available deterministic schemes of calculation of growth of fatigue cracks and criteria of their reaching the critical sizes.

1. (1996) Recommendations for fatigue design of welded joints and components. *IIW Doc. XIII-1539–96/XV-845–96.*
2. *ISO SD 16708*: Petroleum and natural gas industrial. Pipeline transportation system. Reliability-Based Limit State Methods. Introd. Oct. 2000.
3. Sobol, I.M. (1973) *Monte-Carlo numerical methods.* Moscow: Nauka.
4. (1996) *Norms for calculation and design of railway cars of the Ministry of Communications for the 1520 mm track (non-self propelled).* Moscow: GosNIIV-VNIIZhI.

SELECTION OF THERMAL CONDITIONS OF WELDING HARDENING STEELS OF DIFFERENT STRUCTURE CLASSES

V.Yu. SKULSKY

E.O. Paton Electric Welding Institute, NASU, Kiev, Ukraine

The Implant method was used for the comparative evaluation of influence of preheating temperature on the rate of HAZ metal cooling and resistance of welded joints of martensite and bainite steels against cold crack formation. During experiments the martensite chromium steel of 10Kh9MFB type and bainite steels 10GN2MFA and 20KhN4FA were used. It was defined that the high level of resistance against cold crack formation in welding of martensite and bainite steels is attained at the cooling rate $w_{6/5} \le 8–10$ and $w_{6/5} \le 12–14$ °C/s respectively.

Keywords: *arc welding, welded joints, phase transformation, hardening, bainite, martensite, cold crack, preheating, cooling rate, tempering*

Preliminary (concurrent) preheating in welding of hardening steels is a required technological procedure to prevent the cold crack formation. As applied to perfectly studied steels a number of recommendations (with those included into standard documents) and empirical dependencies for the selection of temperature of preheating were worked out [1–3]. In spite of flexibility of such approaches the temperature of preheating should be still specified experimentally [1]. Sometimes the preheating temperature is used higher to provide the higher guarantee of resistance against cold crack formation. However such approach can lead to undesirable consequences, i.e. to embrittlement due to a low-temperature ageing, deterioration of service properties [1, 2, 4]. In this connection the temperature of preheating should be maintained at the minimum level, sufficient for elimination of crack formation.

It is reasonable to realize the selection of thermal conditions of welding with account for the thermokinetic peculiarities of austenite transformation [5, 6]. Coming from the nature of its decay, the complex-alloyed steels with special service properties (for example, those used in power mechanical engineering) can be conditionally divided into the following groups: with a mixed transformation (martensite + bainite) + (ferrite + pearlite) (Figure 1, *a*), and with a pure martensite transformation (Figure 1, *b*). The first group includes low- and medium-alloyed steels. The passing through the equilibrium high-temperature decay (upper region limited by a dash line) is characteristic of joints of low-alloyed steels with a low content of carbon of 12Kh1MF and 15Kh1M1F type, though under conditions of welding such joints acquire not purely pearlite, but sorbite-troostite structure [7]. With increase in a cooling rate the formation of intermediate transformation products is probable. With increase in a total degree of alloying the stability of austenite is increased. The region of an equilibrium transformation is shifted towards the lower values of cooling rate (dashed region in Figure 1, *a*). It results in predominant formation of bainite-martensite hardening structure in welding. The hardening level depends on the cooling rate and is determined by the thermal conditions of welding. The example of steels

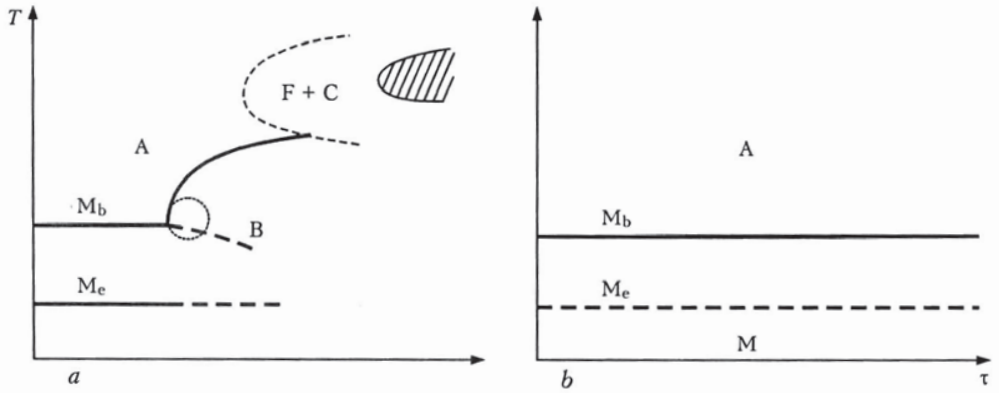

Figure 1. Peculiarities of thermokinetic transformations of austenite in welding of complex-alloyed heat-resistant steels: *a* — martensite-bainite; *b* — martensite; A — austenite; B — bainite; M — martensite (indexes «b» and «e» — beginning and end of martensite transformation); F — ferrite; C — carbide

with bainite-martensite transformation of austenite is the steels of 2.25–3Cr–1Mo, 10GN2MFA, 20KhN4FA type. The second group includes steels containing chromium of more than 7 wt.%. The homogeneity of martensite structure of such steels is provided at the content of chromium-equivalent Cr_{eq} of up to 10 wt.%, at the higher content of ferritizers in martensite a fraction of unhardenable phase, i.e. δ-ferrite, is increased [8, 9]. Steels of the mentioned group include new heat-resistant steels with 9 wt.% Cr (X10CrMoVNb91, 10Kh9MFB and other types).

With increase in alloying level and appropriately increase in stability of austenite under conditions of overcooling the degree of hardening of metal in the zone of welded joints increases, thus resulting in deterioration of weldability. So, the bainite steels are hardened to a less degree in welding and characterized by the better weldability than, for example, the martensite steels alloyed with chromium [10]. Therefore, the thermal conditions of these steels should have definite distinctions. To widen the concept of weldability of martensite steels with increased content of chromium and steels of bainite class, the study of specifics of effect of welding thermal conditions on the resistance of their welded joints against cold crack formation is of a particular interest.

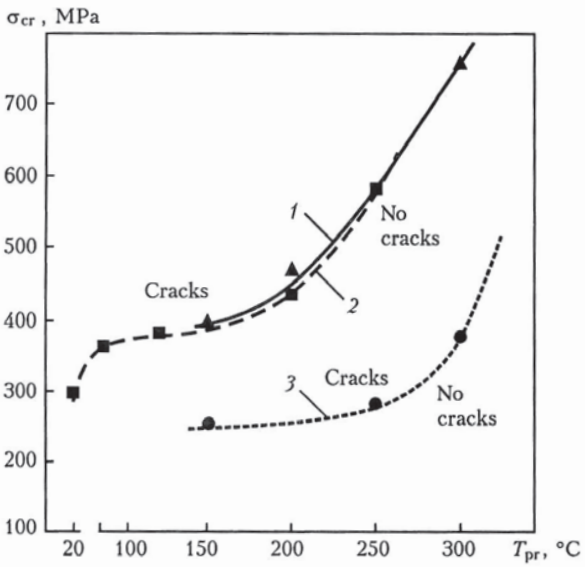

Figure 2. Effect of preheating temperature T_{pr} on critical stresses σ_{cr} provoking cold crack formation: *1* — steel 20KhN4FA; *2* — 10GN2MFA; *3* — 10Kh9MFB

The aim of this work is a comparative estimation of thermal conditions for welding steels with martensite-bainite and martensite transformation of austenite, sufficient to provide high resistance to a delayed fracture of welded joints.

To study the tendency of welded joints to cold cracking, the Implant method was used (the design of test equipment for the mentioned method is described in work [11]). The welding-on of specimens-inserts of test steels to the plate was performed using a manual arc welding with covered electrodes. The cooling rate $w_{6/5}$ of metal in HAZ was determined by thermal cycles, recorded using thermocouples. They were passed through the holes drilled in the plate and welded directly to the specimens at the 1.5–2.0 mm distance from the fusion line. For comparison the specimens of steels 10GN2MFA, 20KhN4FA and 10Kh9MFB were used.

Figure 2 shows the results of investigations of crack resistance of two steels with martensite-bainite transformation (20KhN4FA and 10GN2MFA). The electrodes TML-3U were used for welding, the concentration of diffusive hydrogen H_{diff} in deposited metal (alcohol method) was 2.48 $cm^3/100$ g. In spite of some difference in the alloying level (at averaged content 11 and 7 wt.% of chromium- and nickel-equivalents $Cr_{eq} + Ni_{eq}$ [12] for the first and second steels respectively and carbon equivalent [6] P_{cm} of 0.36 and 0.25 wt.%) the steels are characterized by the affinity as to the nature of thermokinetic transformation of austenite and close critical points of phase transitions. Under the conditions of their arc welding the mixed structure is formed, consisting of martensite and bainite, here the fraction of each one is defined by the joint cooling rate.

As is seen from the Figure 2, the test steels with martensite-bainite transformation have almost the same crack resistance, which is estimated in this case by critical stresses σ_{cr} provoking the crack formation. There are two ranges of increase in resistance against cracks on the curves depending on preheating temperature, i.e. at increase in temperature from room up to 100–150 above 200 °C. The preheating up to 300 °C

provides rate of joint cooling at the level of 6–8 °C/s and significant growth of σ_{cr}. However, thermal conditions with the increased temperature of preheating (taking into account also possible additional increase of temperature due to autoheating by welding arc) are not desirable [4]. In welding of steels with bainite transformation it is recommended to maintain the temperature in welded joint at the level providing the most complete transformation of austenite [4]. It is reasonably to perform preheating up to the temperature close to the lower point of phase $\gamma \rightarrow \alpha$ transition, for example, for steels of mentioned type at the level of temperature M_e equal approximately to 180–200 °C. As is seen from Figure 2, the noticeable increase in crack resistance can be achieved at the preheating temperature from 100 up to 200 °C. This range is quite favourable for welding of such type of steels, as at the temperature above 80 °C the steels with martensite-bainite transformation have high resistance against a delayed fracture [13], and moreover, the conditions are created for completion of austenite transformation. Taking into account the fact that at the preheating temperature of 150–200 °C the even more increase of critical stresses is observed (see Figure 2), it is more probable that the higher effect in providing of higher crack resistance will be achieved at the preheating up to this temperature. Under the conditions of conducted tests the cooling rate in welding with preheating up to 150–200 °C was $w_{6/5} \approx$ ≈ 12–14 °C/s.

According to results of experiments the noticeable increase in crack resistance of welded joints of steels with martensite-bainite transformation was observed at the cooling rate corresponding to the transition from martensite to martensite-bainite transformation (this region in Figure 1, *a* is marked by circle). In the considered steels the transition begins at $w_{6/5} <$ < 20–16 °C/s (Figure 3). It is most probable that for the guaranteed beginning of bainite transformation the cooling rate of austenite should be not more than 15 °C/s. Consequently, with account for critical conditions revealed during test using «Implant» method and peculiarities of thermokinetic transformation of austenite it can be assumed that the high crack resistance of welded joints of steels with martensite-bainite transformation (of 10GN2MFA steel type) occurs at cooling rate of welded joints of not more than 12–14 °C/s, that is achieved at preheating up to 150–200 °C. Depending on the thickness of welded joints and parameters of welding conditions the values of preheating temperature T_{pr}, which provide optimal cooling rate of the joint, should be corrected.

It should be also noted that the delayed cooling of steels leads to the shifting of bainite transformation into the high-temperature region and formation of upper bainite, which is a more rigid structural component and characterized by a lower ductility than the metal with more homogeneous and dispersed structure of lower bainite. Therefore, the maintaining of increased cooling rate providing the beginning of transition to

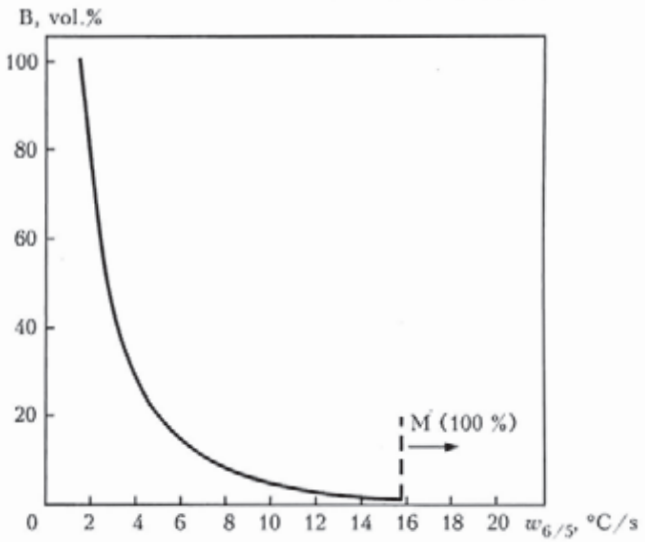

Figure 3. Effect of rate of joints cooling on volumetric fraction of bainite formed during transformation of austenite in steel 10GN2MFA

bainite transformation will, probably, contribute to the formation of fine-dispersed structure of martensite and lower bainite and producing of welded joints with better service properties after tempering [1].

As a result of high level of volumetrical strengthening at phase cold-working the welded joints of martensite steels with increased content of chromium are more sensitive to external loading. The delayed fracture of these joints occurs at the lowest critical stresses (see Figure 2, welding is performed using the ESAB electrodes OK76.98), the concentration of H_{diff} in the deposited metal is 0.78 $cm^3/100$ g.

It should be noted that deposited chromium martensite metal is characterized by much lower concentration of H_{diff} than the low- and medium-alloyed one. The usual level of concentration of H_{diff} attained in use of chromium martensite electrodes with the a basic type of coating is 0.6–0.8 $cm^3/100$ g. In this case it can be connected with the high density of traps (boundaries, dislocations) retaining H_{diff} in martensite deposited metal. Some decrease of H_{diff} concentration is also promoted by decrease of its diffusive mobility due to intensification of its adsorption by iron lattice in chromium alloying [14].

The results of estimation of effect of chromium alloying on H_{diff} concentration in the deposited metal are presented in Figure 4. To obtain pencil samples, the test electrodes were used, manufactured on the base of unalloyed wire Sv-08A with the coating of a basic type and auxiliary adding of different chromium content into the coating. It resulted in obtaining the specimens of deposited metal which differed not only by the chromium content, but also by resultant structure. Figure 4 shows that at the transition from unalloyed ferrite metal to martensite one at a mass fraction of 9 % Cr the H_{diff} concentration decreased from 3.5 down to 0.86 $cm^3/100$ g.

In spite of low concentration of H_{diff} in martensite metal the presence of hydrogen factor exerts a signifi-

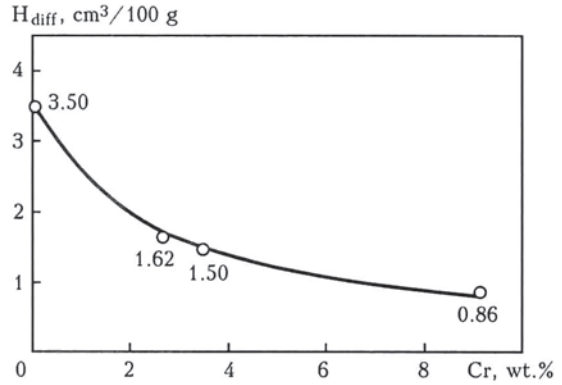

Figure 4. Effect of chromium alloying of deposited metal on concentration of diffusive hydrogen H_{diff}

cant influence on crack resistance of welded joints of 9 % Cr martensite steel, that was confirmed by test results (Figure 5). In given experiments, to change the content of diffusive hydrogen the electrodes of basic type after different period of open storage and different conditions of calcination, and also specially manufactured with addition of mica-muscovite (with approximately 3.97 $cm^3/100$ of H_{diff} concentration after calcination) were used. It is seen from the Figure that with increase in H_{diff} concentration the level of critical stresses is noticeably decreased.

High resistance of welded joints with a martensite structure against cold crack formation is achieved under the conditions of a delayed cooling providing low-temperature volumetric weakening of hardened solid solution (the first stage of martensite tempering) [15] and evolution of hydrogen from it. As the results of experiments showed these conditions during tests using Implant method are created at the preheating up to 250–300 °C, providing the welded joint cooling rate $w_{6/5} \leq 8$–10 °C/s.

The efficiency of mentioned limitation in cooling rate of welded joints of martensite steel 10Kh9MFB was additionally checked in welding of 14 mm thick butt joints with a groove similar to the Tekken sample. To strengthen the rigidity of joints the butts were welded to 30 mm thick plate. Thermal conditions were controlled by preheating of as-assembled joints up to different temperature. Cooling rate was estimated by

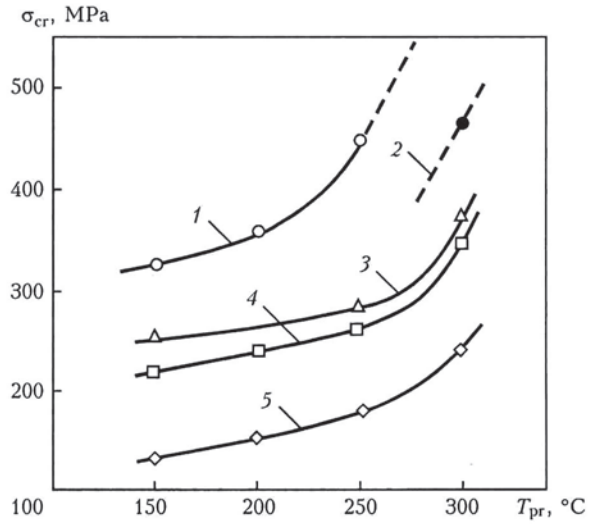

Figure 5. Effect of diffusive hydrogen concentration in deposited metal on critical stresses during tests of welded joints of martensite steel 10Kh9MFB using Implant method: *1* — 0.35; *2* — 0.35 (under conditions of 100 % air humidity); *3* — 0.78; *4* — 0.96; *5* — 3.97 $cm^3/100$ g

thermal cycles, recorded by thermocouples. They were welded at the 2–3 mm distance from the fusion line in weld root zone. For this purpose the holes were drilled up to a required depth in as-assembled samples on the side of a bottom part (Figure 6). The results of estimation of crack resistance depending on the cooling rate are presented below:

$w_{6/5}$, °C/s	13	9.5–12.0	7.4–7.7	5.8
Presence of cracks	Cracks	Cracks/No cracks	No cracks	No cracks

The obtained results prove that cold crack formation in the joints of martensite steel with 9 wt.% Cr is eliminated at the cooling rate $w_{6/5} \leq 8$–10 °C/s.

It is known that effective measure of improving the resistance against cold crack formation is a low-temperature tempering [3], i.e. isothermal soaking of welded joints after welding. The purpose of this operation is to create the conditions for removal of H_{diff} from the joint, a partial increase in ductility and toughness of the hardened metal [3]. As applied to

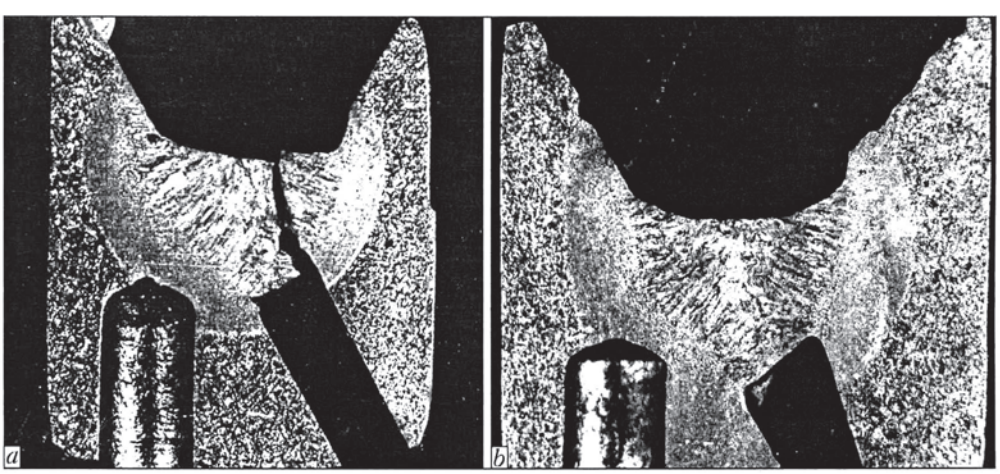

Figure 6. Macrostructure of cross section of the Tekken samples of steel 10Kh9MFB at $w_{6/5} \approx 12$ (*a*) and 7 (*b*) °C/s

the Implant method tests of welded joints of martensite steel with 9 wt.% Cr the durability of tempering after welding was estimated in the temperature range from 200 down to 160 °C, sufficient to provide the resistance against a delayed fracture. The temperature in welded joint was measured using a thermocouple welded to the specimen. The heating mode was controlled using a programmable temperature measuring-control device connected to the thermocouple and heating device. At the end of the tempering operation the welded joints were cooled down to room temperature and then the tests were carried out, the results of which are presented in Figure 7. The Figure shows that tempering at the temperature from 200 down to about 180 °C is more efficient than at lower temperature. Thus, to eliminate the crack formation at 200–180 °C the soaking from some tens of minutes up to 1.5 h will be sufficient. At the lower temperature the required duration of tempering takes several hours.

In the present experiments the tempering at 200, 180 and 160 °C per unit of thickness of section of welded joint (including weld and HAZ) was approximately 5, 15 and 30 min/mm. Hence, it follows that 3–10 h could be required for the operation of tempering the butt joint of 40 mm thickness at the temperature from 200 down to 180 °C. However this estimate can be somewhat overestimated. Probably, when selecting the tempering condition it is necessary to account not only for thickness of welded joint but also for the nature of hydrogen distribution across its thickness. Thus, for example, it follows from work [16] that during multi-pass welding with a concurrent preheating of welded joints of 2.25Cr–1Mo steel 55–100 mm thick the increased concentration of hydrogen was created at the depth of about 15–25 mm from the external weld surface; it was noticeably decreased closer to the weld root and its external surface. The concurrent preheating promotes also the decrease in concentration of H_{diff} (and low-temperature tempering of martensite). Probably, when optimizing the tempering conditions it is necessary to be oriented to the elimination of hydrogen accumulated at some depth in the section of welded joint near the surface. Here, the time of operation may be reduced. In general, the question about the duration of tempering of real welded joints requires additional study.

Thus, it was found on the basis of results of experiments using the Implant method that the resistance of welded joints of chromium martensite steels of 10Kh9MFB type against the cold crack formation is attained at $w_{6/5} \leq 8$–10 °C/s, and that of joints of steels with martensite-bainite transformation (of 10Kh9MFA type) is attained at $w_{6/5} \leq 12$–14 °C/s. By the example of martensite steel the efficiency of tempering after welding at the temperature from 200 down to 180 °C is shown.

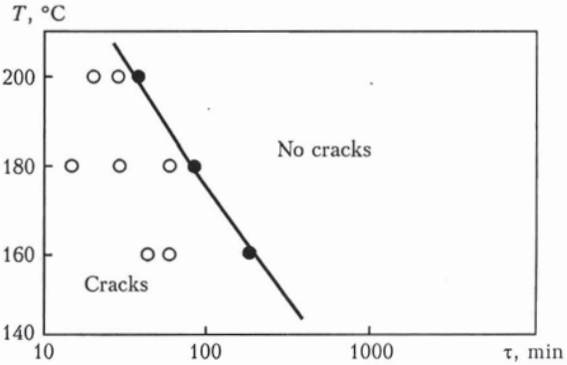

Figure 7. Effect of tempering duration on resistance of welded joints of steel 10Kh9MFB against cold crack formation (test using Implant method)

1. Zemzin, V.N., Shron, R.Z. (1978) *Heat treatment and properties of welded joints*. Leningrad: Mashinostroenie.
2. Kozlov, R.A. (1986) *Welding of heat-resistant steels*. Leningrad: Mashinostroenie.
3. Florian, W. (2006) Cold cracking in high metal. Possibilities to calculate the necessary preheating temperature. *IIW Doc. IX-2006-01*.
4. Burashenko, I.A., Zvezdin, Yu.I., Tsukanov, V.V. (1981) Substantiation of preheating temperature in welding of molybdenum-vanadium steels of martensitic class. *Avtomatich. Svarka*, **11**, 16–20.
5. Shorshorov, M.Kh., Chernyshova, T.A., Krasovsky, A.I. (1972) *Weldability tests of metals*. Moscow: Metallurgiya.
6. Hrivnak, I. (1984) *Weldability of steels*. Moscow: Mashinostroenie.
7. German, S.I. (1972) *Electric arc welding of heat-resistant steel of pearlitic class*. Moscow: Mashinostroenie.
8. Lanskaya, K.A. (1976) *High-chromium heat-resistant steels*. Moscow: Metallurgiya.
9. Skulsky, V.Yu. (2009) To problem of alloying of heat-resistant steel for power unit high-temperature components of new generation thermal plants. *Sovremennaya Elektrometallurgiya*, **1**, 52–56.
10. Skulsky, V.Yu. (2006) Effect of the degree of alloying of heat-resistant chromium steels on hardness of metal within the welded joint zone. *The Paton Welding J.*, **9**, 17–20.
11. Kasatkin, B.S., Brednev, V.I., Volkov, V.V. (1981) Procedure for determination of deformations in delayed fracture. *Avtomatich. Svarka*, **11**, 1–7, 11.
12. Grabin, V.F. (1982) *Metals science of fusion welding*. Kiev: Naukova Dumka.
13. Skulsky, V.Yu. (2009) Thermokinetic peculiarities of formation of cold cracks in welded joints of hardening heat-resistant steels. *The Paton Welding J.*, **3**, 8–11.
14. Moroz, L.S., Chechulin, B.B. (1977) *Hydrogen brittleness of metals*. Moscow: Metallurgiya.
15. Skulsky, V.Yu. (2009) Peculiarities of kinetics of delayed fracture of welded joints of hardening steels. *The Paton Welding J.* (to be publ.).
16. Takanashi, E., Twai, K., Horisutsuji, T. (1979) Prevention of the transverse cracks in heavy section butt weldments of 2 1/4Cr–1Mo steel through low temperature postweld heat treatment. Rep. 2: Correlation between hydrogen concentration and practical welding conditions. *Transact. of JWS*, **10(2)**, 20–27.

EFFECT OF ULTRA-DISPERSED CARBIDES CONTAINED IN FLUX-CORED WIRES ON PROPERTIES OF HEAT-RESISTANT DEPOSITED METAL

I.A. RYABTSEV[1], I.A. KONDRATIEV[1], N.F. GADZYRA[2], N.K. DAVIDCHUK[2], I.L. BOGAJCHUK[1] and G.N. GORDAN[1]
[1]E.O. Paton Electric Welding Institute, NASU, Kiev, Ukraine
[2]I.M. Frantsevich Institute for Materials Science Problems, NASU, Kiev, Ukraine

The effect of charge materials in flux-cored wires containing ultra-dispersed carbides on properties of the deposited metal corresponding to tool steels in composition was studied. It was established that application of such charge materials results in refinement of structure of the deposited metal and more uniform distribution of alloying elements in it, this leading to improvement of heat and wear resistance of the deposited metal.

Keywords: *cladding, flux-cored wires, microstructure, ultra-dispersed carbides and compositions, properties of deposited metal*

It is a well known fact that structure and properties of the deposited metal are interrelated [1–3, etc.]. However, the main consideration in investigation of principles of formation of structure of the deposited metal was given, as a rule, to its chemical composition and thermal cladding cycle, the problem of relationship between the initial structure of filler or electrode materials and structure of the deposited metal remaining little studied. Meanwhile, the so-called «structural inheritance» may take place in the cladding consumable–weld pool–deposited metal system [4, 5]. This is the case where the deposited metal «inherits» the structure of initial cladding consumables in grain size, composition, size and distribution of strengthening (carbides, carbonitrides, borides, etc.), as well as non-metallic inclusions, which contaminate the deposited metal, this having a negative effect on its performance.

The purpose of this study was to investigate the effect of ultra-dispersed carbide compositions added to the charge of flux-cored wires on properties of the deposited metal. Ultra-dispersed carbide compositions were produced by high-temperature CO_2 treatment of powders of high-carbon ferrochromium FKh800, ferrovanadium FVd50 and tungsten. Natural colloidal graphite was added to each of the powders.

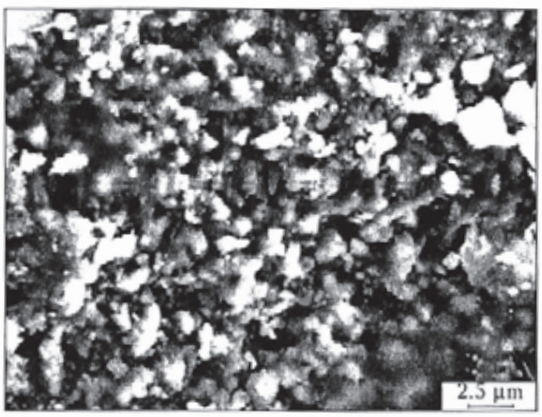

Figure 1. Appearance of ultra-dispersed carbide particles synthesised from powder of ferrochromium FKh800 and natural colloidal graphite after milling

Scanning electron microscopy of carbide compositions was carried out with microscope «Superprobe 733», and transmission electron microscopy – with microscope PEMU-125. Test specimens were prepared by using standard preparation methods.

Figure 1 shows appearance of ultra-dispersed carbide particles synthesised from the powder of ferrochromium FKh800 and natural colloidal graphite in carbon dioxide atmosphere after milling in a planetary-type mill. It can be seen from the Figure that most carbide particles are less than one micrometre in size. There are also particles of a smaller size. The presence of coarse particles was not detected, this being indicative of a high homogeneity of the produced material.

As follows from the X-ray phase analysis data, structure of the fused material is characterised by the eutectic state of carbide compositions Fe_7C_3 and Cr_7C_3. The streak contrast allows the size of the carbide eutectic to be estimated. The carbide compositions are 50–120 nm in size (Figure 2).

It was planned to use the ultra-dispersed carbide particles of the composition in the charge of flux-cored wires PP-Np-35V9Kh3GSF and PP-Np-30Kh4V2MFS, which are usually applied for cladding of tools for hot pressure treatment of metals [6] and provide deposited metal of the type of heat-resistant die steels. As follows from study [7], structural heterogeneity of this type of the deposited metal has a substantial effect on performance of tools and fixtures for hot pressure treatment of metals repaired by arc cladding.

The carbon content of the powders dramatically increased after treatment in carbon dioxide atmosphere (Table 1).

Flux-cored wire PP-Np-35V9Kh3GSF was made in two modifications: Op-1 and Op-2 – with a charge prepared by using untreated (standard) and treated

Table 1. Content of carbon in charge materials

Charge material	C, wt.%	
	Standard	After treatment
Ferrochromium FKh800	7.80	11.00
Ferrovanadium FVd50	0.46	4.70
Tungsten powder	≤ 0.01	4.10

tungsten powder, respectively. Flux-cored wire PP-Np-30Kh4V2MFS was also made in two modifications: Op-3 and Op-4 – with standard charge and charge containing treated ferrochromium and ferrovanadium powders, respectively. The calculated composition of charge of the flux-cored wires was adjusted to produce deposited metal of the identical chemical composition.

Cladding of specimens was performed with experimental flux-cored wires to determine chemical composition of the deposited metal and its hardness (Table 2). It was established that chemical composition and hardness of the metal deposited with all types of the flux-cored wires met requirements of the corresponding specifications. Assimilation of individual alloying elements was almost identical, independently of the charge components, whether they were standard or containing the ultra-dispersed carbides.

Test pieces were cut from the deposited plates to conduct metallographic examinations. Structure of the metal deposited with the standard flux-cored wire (Op-1) included lath martensite (with laths elongated in one direction) having microhardness *HV*0.5 5930 MPa, and a small amount of retained austenite with microhardness *HV*0.5 5090–5490 MPa (Figure 3, *a, b*). Carbide inclusions were also revealed.

Structure of the metal deposited with experimental flux-cored wire Op-2 had a bit different composition: along with lath martensite, it also contained plate-like martensite (Figure 3, *c, d*), the plates being of a lenticular shape. Its hardness was *HV*0.5 5930 MPa. The content of retained austenite was a bit higher than in the metal deposited with the standard wire, and its hardness was *HV*0.5 4410–5490 MPa. It should be noted that adding the components containing ultra-dispersed carbides to the charge of the experimental flux-cored wire led to refinement of structure of the deposited metal, this being especially pronounced at high magnification (Figure 3, *b, d*).

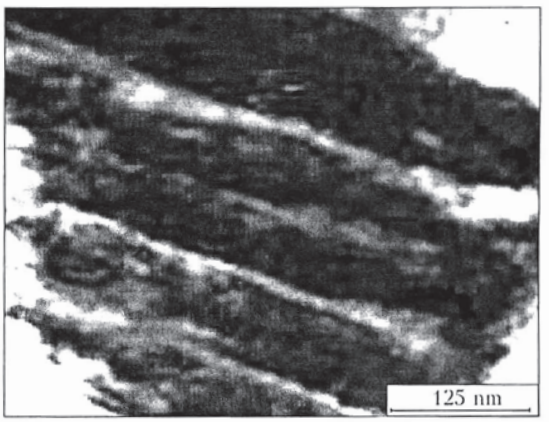

Figure 2. Microstructure of synthesised fused ultra-dispersed ferrochromium-base carbide powders

Microstructure of the metal deposited with flux-cored wire Op-3 is shown in Figure 3, *e, f*. The matrix consists primarily of lath martensite having microhardness *HV*0.5 5490–6440 MPa. Retained austenite (*HV*0.5 5020–5090 MPa) persists along the homogenisation boundaries.

Microstructure of the metal deposited with experimental wire Op-4 is shown in Figure 3, *g, h*. Compared with microstructure of standard deposited metal PP-Np-30Kh4V2MFS, the former is more dispersed, and it contains less regions of lath martensite, the plate-like martensite being dominant. Microhardness of the martensitic matrix is *HV*0.5 5490 MPa. The content of retained austenite is lower than in cladding with the standard wire, and its microhardness is *HV*0.5 4120–4660 MPa.

Therefore, the examinations showed marked differences in structure of the metal deposited with flux-cored wires containing the standard and experimental charge. In the latter case, structure of the martensitic matrix changed, and the deposited metal had a refined structure.

Uniformity of distribution of main alloying elements in the deposited metal was evaluated by using X-ray microanalyser «Camebax SX50». The examinations were conducted in the automatic mode at a depth of about 100 μm from the surface of the deposited metal. Distribution of alloying elements in the metal deposited with flux-cored wires containing the experimental charge materials was more uniform than in the case of using flux-cored wires with the standard charge. This was especially pronounced by an example of such an alloying element as tungsten (Figure 4).

Table 2. Chemical composition (wt.%) and hardness of deposited metal

Flux-cored wire grade	Designation	C	Mn	Si	Cr	W	Mo	V	Hardness *HRC*
PP-Np-35V9Kh3GSF	Op-1	0.39	0.60	1.00	2.97	8.05	–	0.70	51
PP-Np-35V9Kh3GSF	Op-2	0.34	0.60	1.00	3.00	9.30	–	0.76	54
PP-Np-30Kh4V2M2FS	Op-3	0.37	0.72	1.17	3.97	2.52	1.88	0.44	55
PP-Np-30Kh4V2M2FS	Op-4	0.35	0.70	1.17	3.80	2.33	1.97	0.45	53

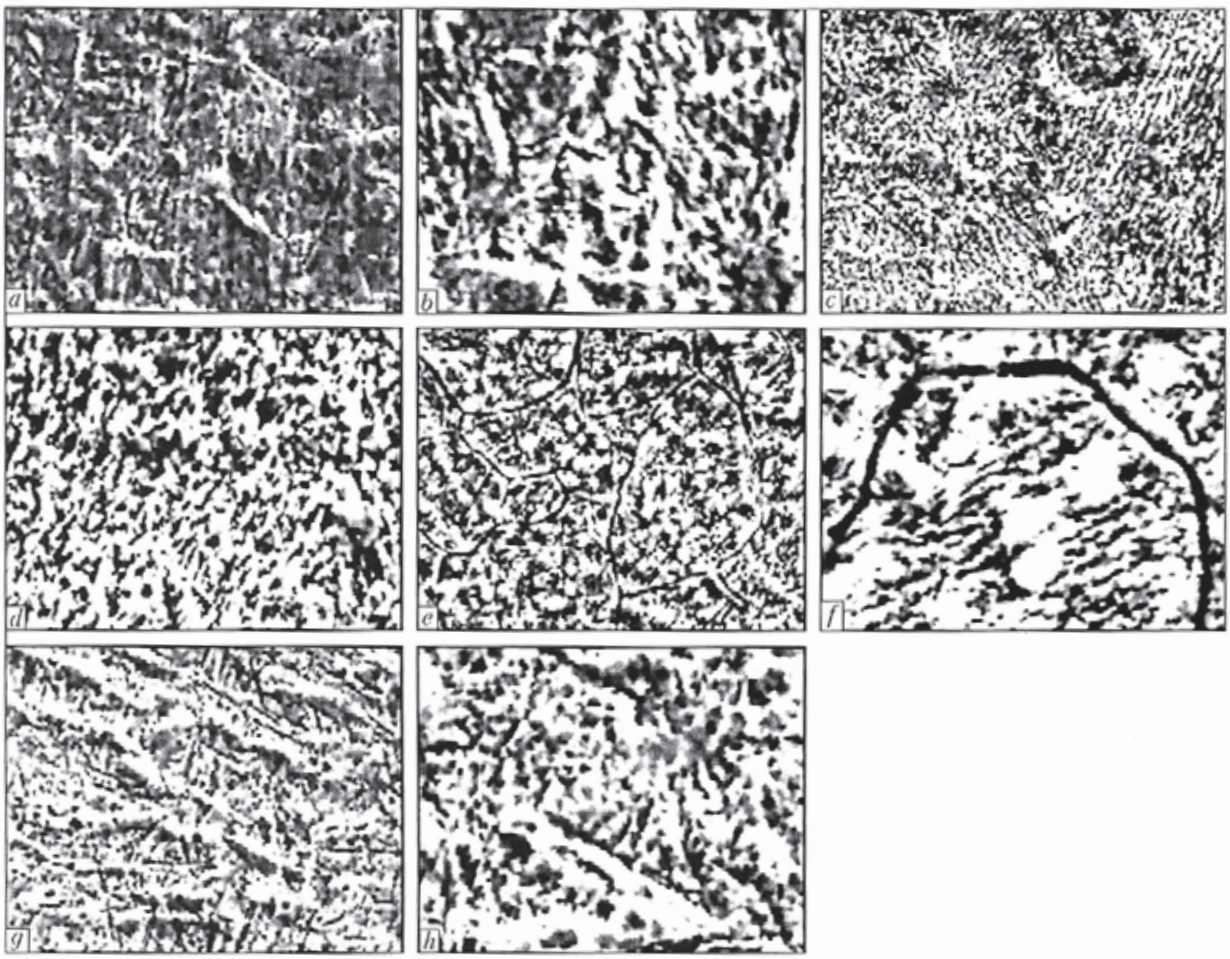

Figure 3. Microstructure of metal deposited with flux-cored wires: *a*, *b* and *e*, *f* — standard wires PP-Np-35V9Kh3GSF and PP-Np-30Kh4V2MFS, respectively; *c*, *d* and *g*, *h* — experimental wires PP-Np-35V9Kh3GSF and PP-Np-30Kh4V2M2FS, respectively (*a*, *c*, *e*, *g* — ×900; *b*, *d*, *f*, *h* — ×2400)

Heat resistance tests of the deposited metal were carried out with the machine and by the procedure [8] providing for heating of the deposited surface of a specimen measuring 40 × 40 × 30 mm to 800 °C by using a gas torch (heating spot with a diameter of 15 mm), followed by cooling to 60 °C with a water jet. The heating–cooling cycles were repeated up to formation of a fire crack network. The test results are given in Table 3. They are indicative of the fact that using ultra-dispersed carbide compositions in the charge of flux-cored wires increases heat resistance of the deposited metal, i.e. the quantity of the heating–cooling cycles to formation and development of the fire crack network is increased.

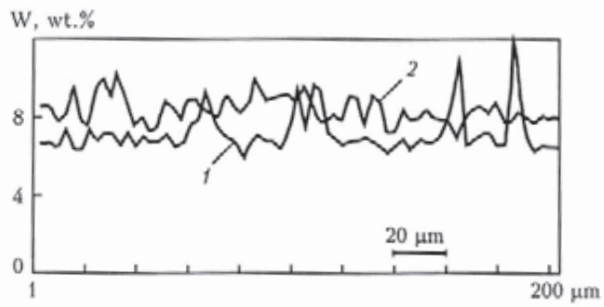

Figure 4. Distribution of tungsten in metal deposited with standard Op-1 (*1*) and experimental Op-2 (*2*) wire

The tests to wear at the metal on metal sliding friction at increased temperature were conducted by using a different testing unit of the same machine [8]. During the tests, a deposited specimen measuring 10× × 17 × 40 mm was pressed with a force of 175 N to a mating ring rotating at a speed of 30 rpm. The mating body 120 mm in diameter made from hardened steel 45 was heated during the tests with a gas torch. Temperature in the specimen to mating body contact zone was 600 °C, and time of the tests was 1 h. During the tests the specimen made reciprocal movements in the vertical plane with oscillation amplitude of 20 mm

Table 3. Heat resistance of deposited metal

Flux-cored wire grade	Designation	Quantity of heating–cooling cycles	
		Before formation of fire crack network	Before development of fire crack network
PP-Np-35V9Kh3GSF	Op-1	60	80
PP-Np-35V9Kh3GSF	Op-2	70	100
PP-Np-30Kh4V2M2FS	Op-3	40	60
PP-Np-30Kh4V2M2FS	Op-4	60	80

and frequency of 62 min^{-1}. The test results (average over three specimens) are given in Table 4.

The tests showed that wear of the metal deposited with flux-cored wires containing the experimental charge was lower than in the case of using wires with the standard charge. Wear of the mating bodies, which were tested in pair with the specimens deposited with flux-cored wire containing the experimental charge, was also lower.

Table 4. Wear of deposited specimens in metal on metal sliding friction at increased temperature

Flux-cored wire grade	Designation	Wear resistance $J \cdot 10^{-4}$, kg/km	
		Deposited specimen	Mating body
PP-Np-35V9Kh3GSF	Op-1	2.9705	37.7625
PP-Np-35V9Kh3GSF	Op-2	2.4589	28.1803
PP-Np-30Kh4V2M2FS	Op-3	2.7429	33.8164
PP-Np-30Kh4V2M2FS	Op-4	1.4529	17.6991

CONCLUSIONS

1. Application of charge materials containing ultra-dispersed carbides leads to refinement of structure of the deposited metal and more uniform distribution of alloying elements in it.

2. Metal deposited with flux-cored wires, the charge of which contains ultra-dispersed carbides, has higher heat and wear resistance in metal on metal sliding friction.

1. Frumin, I.I. (1961) *Automatic electric arc surfacing*. Kharkov: Metallurgizdat.
2. Livshits, L.S., Grinberg, N.A., Kurkumelli, E.G. (1969) *Principles of alloying of deposited metal*. Moscow: Mashinostroenie.
3. Khrushchev, M.M., Babichev, M.A., Berkovich, E.S. et al. (1971) *Wear resistance and structure of hard deposits*. Moscow: Mashinostroenie.
4. Ryabtsev, I.A. (2006) Structural inheritance in the initial materials–metal melt–solid metal system (Review). *The Paton Welding J.*, **11**, 8–12.
5. Ryabtsev, I.A., Pereplyotchikov, E.F., Mits, I.V. et al. (2007) Effect of initial structure and particle size composition of powder on structure of metal 10R6M5 deposited by the plasma-powder cladding method. *Ibid.*, **10**, 18–22.
6. Ryabtsev, I.A., Kondratiev, I.A. (1999) *Mechanised electric arc surfacing of metallurgical equipment parts*. Kiev: Ekotekhnologiya.
7. Kondratiev, I.A., Vasiliev, V.G., Dzykovich, I.Ya. (1996) Study of structural heterogeneity of the 35V9Kh3SF type deposited metal and its effect on performance of clad mill rolls. *Avtomatich. Svarka*, **6**, 17–20.
8. Ryabtsev, I.A., Chernyak, Ya.P., Osin, V.V. (2004) Modular testing machine for deposited metal. *Svarshchik*, **1**, 11–12.

FEATURES OF SOLIDIFICATION OF COMPLEX-ALLOYED FILLER METALS FOR BRAZING HIGH-TEMPERATURE NICKEL ALLOYS

V.V. KURENKOVA, L.K. DOROSHENKO and I.S. MALASHENKO
E.O. Paton Electric Welding Institute, NASU, Kiev, Ukraine

Applicability of differential thermal analysis to determine the character of phase transformations in boron- and silicon-containing filler metals intended for brazing of casting nickel alloys has been considered in relation with the results of microstructure and X-ray spectrometry analyses. The efficiency of adding 20 % powder (Ni–12 % Si) of eutectic composition to boron-containing filler metal (Ni–Co–Cr–Al–2.5 % B) is shown. Silicon disperses carboboride eutectics precipitating in the brazed seam metal and depresses the heterogenization of its structure, thus favouring improvement of physical-mechanical properties of the brazed joints.

Keywords: *high-temperature brazing, high-temperature nickel alloys, seam metal, boron- and silicon-containing filler metal, powder filler, differential thermal analysis, DTA curve, X-ray diffraction analysis, diffractogram, structure heterogenization*

Brazing of high-temperature nickel alloys is widely used for manufacturing complex structures [1, 2] and repair of gas turbine parts. The effectiveness of this technology is confirmed in practice in repair of parts after service, as well as items with casting defects [3–6]. Optimization of the modes of brazing, selection of filler metal types, results of laboratory testing and industrial application are presented in [4–7]. These are studies of brazed joints of nickel high-temperature alloys ChS70VI, ChS104, VJL12U, JS6U, JS26VI and NK, produced using complex filler metals of different types. The basic composition of the filler metals is a low-melting filler metal of Ni–Co–Cr–Al–2.5 % B system (trade mark Ni-377-2) of the manufacturer — PRAXAIR Surface Technologies (USA), and fillers are powders of Rene-142 nickel alloy. For simplification basic filler metal of Ni–Co–Cr–Al–2.5 % B system is further designated as #1.

Isothermal brazing of high-temperature nickel alloys with boron-containing filler metals runs into the problem of heterogenization of seam metal of the formed joints related to precipitation of centrally-axial and interdendritic boride eutectics during solidification [8–11], this leading not only to embrittlement of the brazed seam metal, but also to lowering of fatigue resistance and to gas corrosion of brazed joints. Under the conditions of isothermal brazing or long-term heat treatment of brazed objects boron having the diffusion rate of $6.22 \cdot 10^{-11}$ $m^2 \cdot s^{-1}$ (which is three orders of magnitude higher than carbon or silicon diffusion rate — $3.09 \cdot 10^{-14}$ $m^2 \cdot s^{-1}$) actively penetrates into the brazed alloys with boride phase formation along the grain boundaries, thus promoting their intercrystalline erosion. As follows from [8], the latter is aggravated at long-term diffusion interaction of boron, contained in the filler metal with the alloying components of the brazed alloy (for instance, titanium and chromium). Therefore, development of the methods of neutralizing the eroding action of boron on the contact boundary of the seam metal with the base at brazing of high-temperature nickel alloys is of considerable interest.

The aim of this work was investigation by the methods of metallographic, X-ray spectral, differential thermal (DTA) and X-ray diffraction analyses of the structure of filler metals of different chemical and phase composition and substantiation of the rationality of their selection for repair brazing to obtain a satisfactory combination of strength and low-temperature ductility of nickel alloy brazed joints (BJ).

During the experiments DTA was mainly used, which allows evaluation of the structural changes in the applied filler metals during melting–solidification by thermal effects. It was used to determine the characteristic solidus T_S and liquidus T_L temperatures of powder filler metals, as well as the influence of component ratio in complex filler metals on the process of their melting–solidification (Table 1).

DTA was performed in VDTA-8 M unit in helium atmosphere at a constant rate of heating–cooling of 80 K/min. Chamber was filled with helium (up to the pressure of 80–90 kPa) after pumping the chamber down to the rarefaction of not less than $1.33 \cdot 10^{-3}$ Pa. The operation of helium blowing was repeated two times.

Powder samples of approximately the same mass (1.09–1.20 g) in crucibles of zirconium dioxide were moistened by a solution of acrylic acid in acetone. This solution was used to prevent «leakage» of the filler metal powder from the crucible during the chamber pumping down and blowing with helium.

The nature of DTA curves is affected by such factors as heating rate, sample weight (there is a correlation between the thermal effect and sample weight), dimensions and degree of compactness of the powder, presence of an inert heat carrier, etc. [12]. As powder samples were practically of the same weight, presence of salient points in the thermograms was indicative

Table 1. Main temperature characteristics of complex-alloyed filler metals (by DTA results)

Number and type of filler metal mixture	Complex filler metal	T_S, °C	T_L, °C	Solidification interval ΔT, °C
1	Ni–Co–Cr–Al–2.5 % B	1040	1170	130
Ni-365-3	Rene-142	1310	1410	100
NS12	Ni–12 % Si	1140	1160	20
11	40 % #1 + 60 % Rene-142	1070	1310	240
12	20 % #1 + 20 % NS12 + 60 % Rene-142	1050	1250	200
13	25 % #1 + 15 % NS12 + 60 % Rene-142	1050	1250	200
14	15 % #1 + 25 % NS12 + 60 % Rene-142	1030	1260	230
19	60 % VPr-36 + 40 % Rene-142	1080	1310	230

of the change of enthalpy, which is related to transformation running in powder formulations of different chemical composition.

Studied were the processes of melting–solidification of powders of multicomponent filler metals, used in brazing of high-temperature nickel alloys [12–14]. The main aim of investigations was to derive DTA curves of heating–cooling of low-melting filler metal #1, Rene-142 filler powder and complex filler metals with addition of powder of eutectic composition Ni–12 % Si, in which silicon is used as a depressant (see Table 1).

X-ray diffraction measurements were conducted in the standard geometry of θ–2θ in DRON-4 diffractometer in Co_{K_α} radiation. Samples of filler metal ingots were studied after solidification. CaF_2 salt was used to increase the accuracy of determination of interplanar spacing, the salt being applied on a small section of sample surface after dissolution in the lacquer.

Structure of metal samples was studied in a scanning electron microscope CamScan-4, BJ chemical composition was determined using energy-dispersive spectrometer «Energy200».

BJ strength and ductility depend on phase composition of the used filler metal, as well as the brazed seam metal structure formed in brazing. DTA results allowed revealing the possible quantity of polymorphous transformations running at solidification in the filler metal systems and performing qualitative evaluation of the intensity of these processes (Figure 1).

At formation of nickel-base filler metals and increase of alloying element content the shape of DTA curves becomes more complicated. At the same time, the solidification temperature interval of the applied complex filler metals becomes wider. DTA curves have a multitude of peaks corresponding to structural transformations in the filler metal system at heating and melting.

Systems of cast filler metals of Ni–Cr–B–Si type are well studied and are used mainly for structural brazing. In repair of turbine hot section parts made from high-temperature nickel alloys, application of composite filler metals is preferable, which, in addition to the low-melting component proper, include powder-fillers from high alloys, providing not only a closer similarity of the composition of the metal of the brazed base and formed seams, but also high-temperature resistance, as well as scale resistance of metal in the repaired sections.

At addition of Rene-142 alloy powder as filler to the initial low-melting filler metal #1 (filler metal #11) an increase of T_S and T_L temperature values and a widening of the solidification range of complex filler metals was observed (see Table 1).

For filler metal #1 temperature T_S = 1040 °C and T_L = 1170 °C, which coincided exactly with the data of VBC Company (Great Britain) (Table 1, Figure 1). The thermogram of solidification of powder of filler metal #1 shows two clear-cut salient points. During solidification crystallites of matrix γ-solid solution and two types of eutectics — γ + Ni_3B and γ + Ni_3B + CrB precipitate from the melt. Chromium boride (dark precipitates) included into the composition of the ternary eutectics, has a grooved (skeletal) structure and as to its chemical composition corresponds to CrB (14.9–15.3 % Cr) (Figures 2, *d*, 3, *a* and Table 2). Primary chromium borides precipitate from the melt at the temperature of 1097 °C. Etching reveals another eutectic — γ + Ni_3B in the filler metal structure, which forms from the liquid phase by the reaction of $L \rightarrow \gamma$ + + Ni_3B (where L is the liquidus) approximately at 1042 °C [8] (Figure 2, *e, f*). As follows from DTA curve of Ni–Co–Cr–Al–2.5 % B filler metal solidification of the ternary eutectic most probably occurs at 997 °C by the following reaction: $L \rightarrow \gamma + Ni_3B$ + CrB.

The structure of the crystallized sample of filler metal #1 and intensity of peaks on DTA curve show that the seam metal contains eutectics of different morphology. Boride eutectics adversely affect BJ ductility and strength characteristics. Microhardness of CrB boride phases of the basic filler metal reaches *HV* 24930 MPa, thus exceeding the microhardness of the matrix solution (*HV* 3300 MPa). Forming borides and carboborides, boron leads to embrittlement of the solidified filler metal, and presence of low-melting boride eutectics increases the risk of their surface melting at BJ finish heat treatment. Intensively diffusing

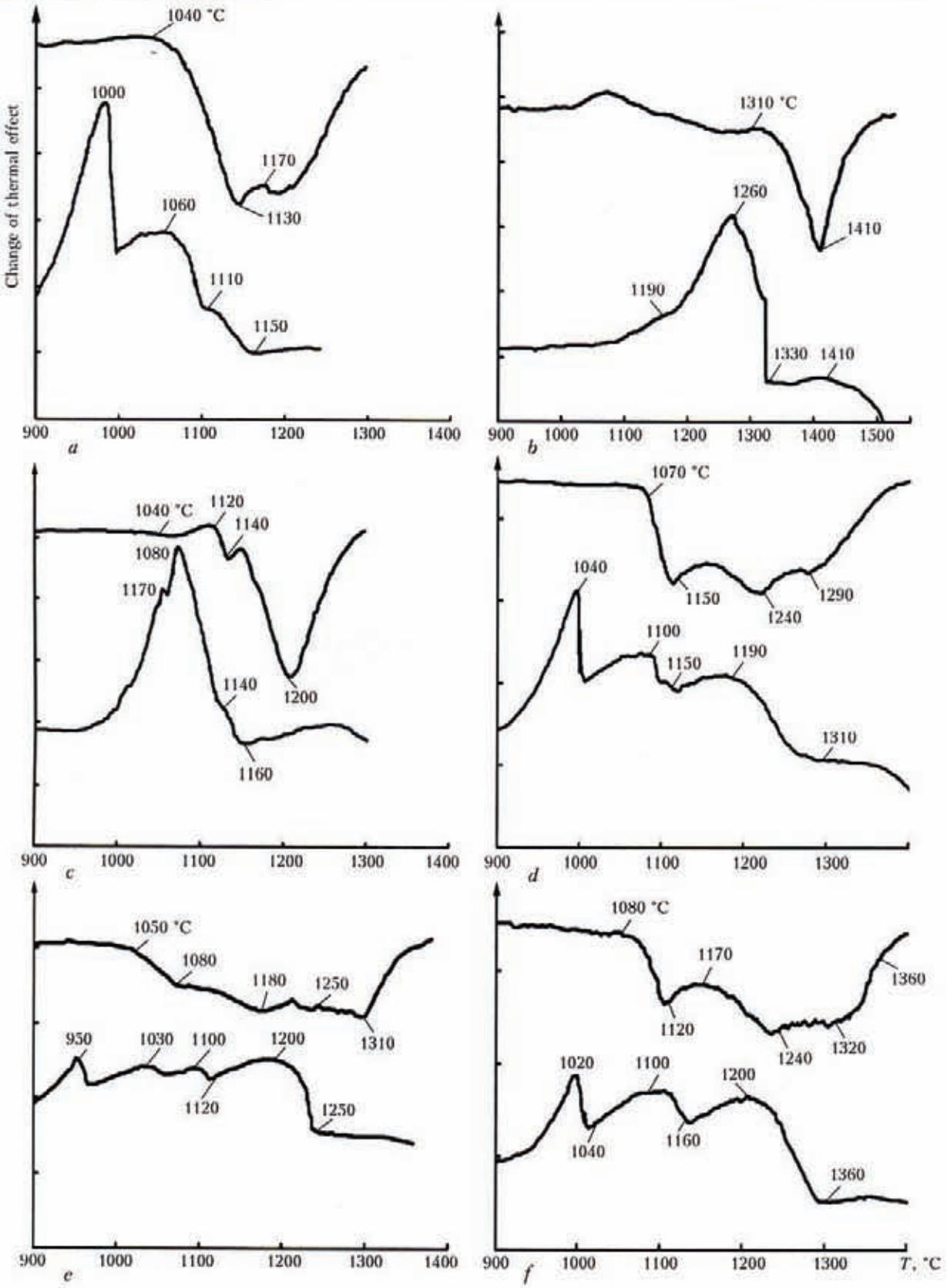

Figure 1. DTA curves obtained at solidification of molten powders of basic filler metal #1 (*a*), filler (Rene-142 alloy) (*b*), NS12 filler metal (*c*) and composite nickel filler metals #11 (*d*), 12 (*e*), 19 (*f*) according to Table 1

into the base metal, boron causes erosion of the brazed base.

In order to increase the viscosity and reduce the chemical activity of the melt relative to the brazed base, powder of Rene-142 superalloy was added to filler metal #1 as a filler (see Figure 1, *b*). This resulted in improvement of functional characteristics of BJ, for instance, of ChS70, VJL12U alloys [2, 3].

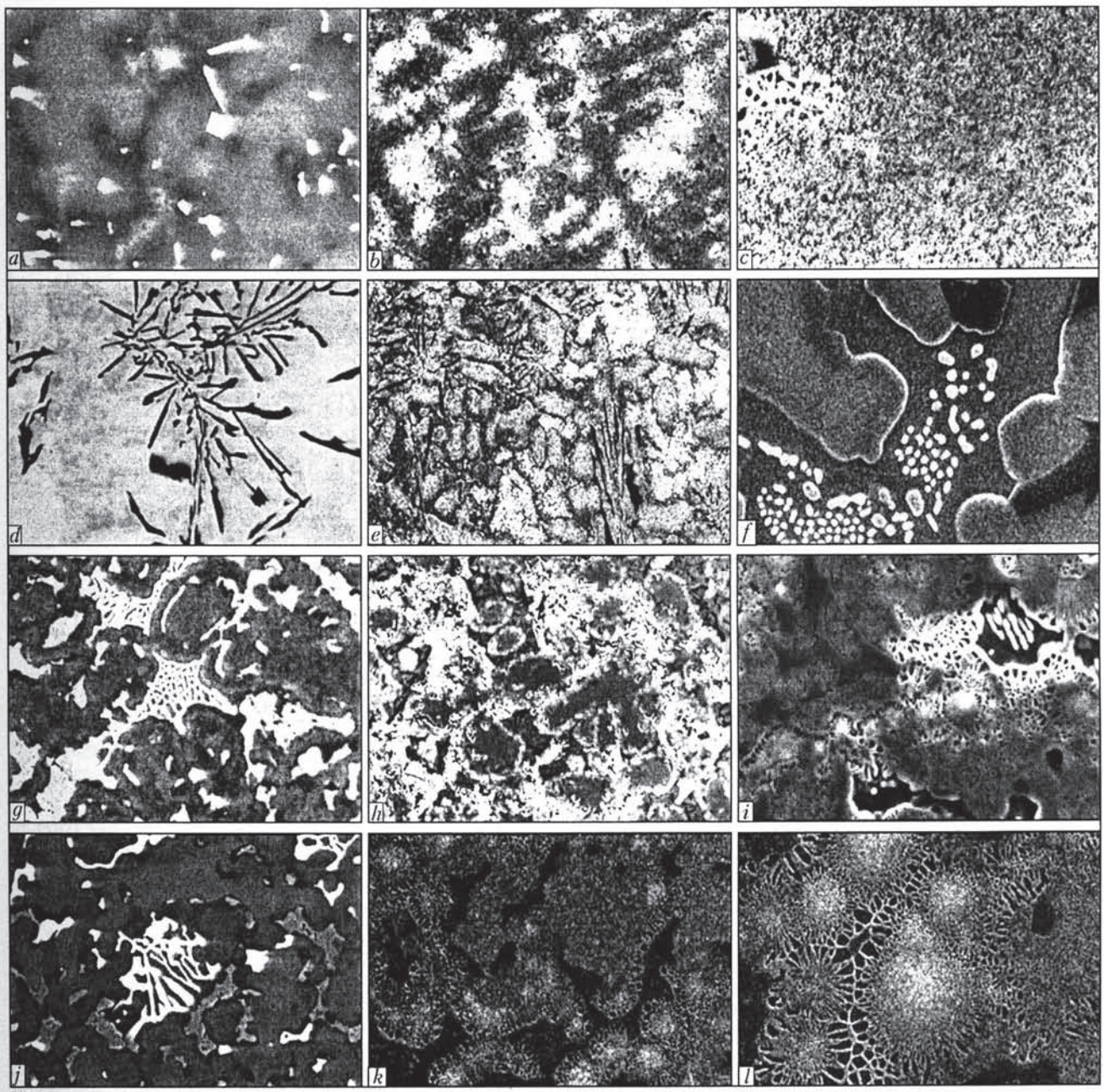

Figure 2. Metal microstructure of solidified Rene-142 alloy (*a–c*), filler metal #1 (*d–f*), composite filler metals #1 + 60% Rene-142 (#11) (*g–i*) and 60 % VPr-11 + 40 % Rene-142 (#19) (*j–l*): *a, d, g, j* — filming in back-scattered electrons (×500); *b, e, h, k* — in secondary electrons after metallographic etching (×200); *c, f, i, l* — same (×2000)

DTA was used to determine the liquidus and solidus temperatures for Rene-142 alloy: T_L = 1310 °C, T_S = 1410 °C (see Table 1). Rene-142 alloy in the solidified state has the structure of high-alloyed γ-solid solution based on nickel with discrete precipitates of the carbide phases on the interphase boundaries (Figures 2, *a* and 3, *b*). Matrix microhardness was *HV* 4450 MPa. Volume fraction of carbide particles was small (10–12 %), and the precipitates proper (by the data of X-ray spectral analysis) were structurally stable MeC carbides based on Ta (67–70 wt.%) and Hf (11–12 wt.%) (Table 2, Figure 3, *b*), their microhardness reaching *HV* 21000 MPa.

For Rene-142 alloy precipitation of γ′-phase particles from the liquid by an eutectic reaction in the interdendritic regions is characteristic at the end of solidification [14]. This phase contains 6–7 wt.% Al, 7 wt.% Ta and 2 wt.% Hf, stabilizing the γ′-phase. γ–γ′ eutectic melts approximately at 1310–1320 °C, which corresponds to the start of the peak on DTA curve of the alloy melting (see Figure 1, *b*).

The discernible peak in the DTA melting curve at 1010–1020 °C most probably corresponds to the start of dissolution of non-equilibrium γ′-phase, formed along the dendrite arms during solidification from the solid solution. This phase and γ–γ′ eutectic were detected by chemical etching of samples.

To produce a composite filler metal, Rene-142 alloy powder was added as filler to boron-containing filler metal #1. As a result, the shape of DTA curves changed, the solidification interval widened considerably (from 130 to 240 °C) as the filler metal was

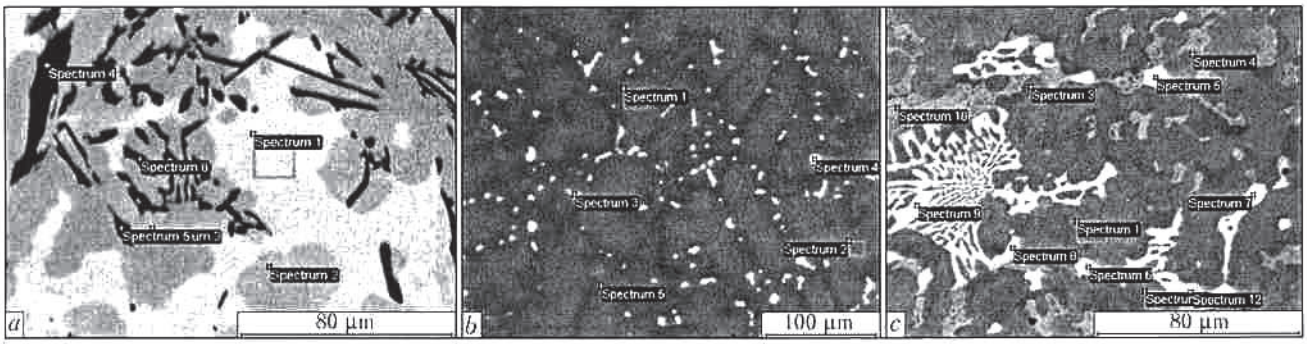

Figure 3. Microstructure of solidified metal of basic filler metal #1 (*a*), Rene-142 alloy (*b*) and composite filler metal #11 (*c*) with sections, in which X-ray spectral microanalysis of structural components was performed

alloyed (Table 2, Figure 1, *d*). Thermogram of composite filler metal #11 is of a complex three-stage mode, which is related to the diversity of the structural components precipitating during solidification.

At addition of Rene-142 alloy powder to filler metal #1, the weight fraction of boron in the melt decreases to 1 %, which results in the absence of a low-temperature peak on the DTA curve corresponding to formation of a ternary low-temperature eutectic γ + + Ni_3B + CrB. However, the volume fraction of the secondary components in the solid solution of the solidified filler metal is quite high (about 40 %). These are mainly two types of eutectics – light grooved eutectics and grey interdendritic eutectics (Figures 2, *g* and 3, *c*). The first eutectics, most probably, of a quasi-binary type, are γ-solid solution and chromium-based intermetallics with partial substitution of tungsten, molybdenum and rhenium (Table 3). They, probably, are carboforide compounds, which solidify on CrB primary intermetallics, precipitating from the liquid phase. Their carbo-boride components include the following elements (Table 2, Figure 3, *c*), wt.%: 33–34 Cr; 17–24 W; 9–16 Re; 7–10 Mo. This is close in its content to $Me_{23}C_6$ type carbides. $Me_{23}(C, B)_6$ compound isomorphous to $Cr_{23}C_6$ carbide can form during further heat treatment. Complex compound of $Me_{23}C_3B_3$ type has a large region of homogeneity, when substitution of carbon atoms by boron occurs with simultaneous increase of the compound crystalline lattice [15].

The second type of eutectic are interdendritic complex-alloyed eutectics with the following content of components (Figure 2, *c*), wt.%: 61.8–62.7 Ni; 14.0–14.3 Co; 7.3–9.6 Cr; 1.7–2.0 Al; 0.85 Mo; 2.7–4.5 Hf; 4.8 Ta; 1 W. According to DTA, the temperature, at which these phases precipitate, is equal to approximately to 1040 °C (see Figure 1, *d*). Volume fraction of these eutectic phases in the matrix solution is equal to 25–30 %, their microhardness being *HV* 7540 MPa at matrix solution microhardness *HV* 4035 MPa (see Figures 2, *g–i* and 3, *c*). These eutectics are of a complex structure, the base of which is $\gamma + Ni_3B$. On DTA curve (see Figure 1, *d*) the temperature of 1150 °C most probably corresponds to the process of the start of melting of $\gamma + Ni_3B$ eutectic.

During solidification a small amount of stable polyhedral MeC carbides based on Ta (63 wt.%) and Hf (14–17 wt.%) precipitate from the solution in the metal of filler metal #11. Volume fraction of these phases with microhardness of *HV* 18000 MPa, is relatively small (1–2 %) (see Figure 3, *c*).

Thus, when powders of the basic filler metal and Pene-142 filler are mixed, the range of melting–solidification of the brazing mixture (ΔT = 240 °C) is widened, compared to the initial components (see Table 1, Figure 1, *a*, *b*), which is not a positive factor for formation of homogeneous brazed seams. At a wide solidification interval and short time of this process running, heterogeneous systems form with a multitude of secondary phases precipitating both from the melt and from the solid solution. Many of these phases are stable and are preserved at subsequent heat treatment, which is negative for BJ ductility and strength characteristics.

On the other hand, addition of Rene-142 filler to filler metal #1 reduces the total content of boron to 1 wt.% at the expense of filler metal alloying by superalloy components and concentration of the low-melting boride eutectic in the seam metal (see Figure 1, *b*, *d*). This lowers the intensity of formation of chromium boride front along the fusion line and reduces the depth of boron penetration into the brazed metal. However, the quantity of boride phases in the solidified seam volume remains to be quite high, and heat treatment does not ensure a ductility margin of the BJ (all of them failed in the brittle mode).

To increase the fluidity of boron-containing filler metal at a simultaneous lowering of its reactivity relative to the brazed base, silicon in the form of powder of commercial filler metal NS12 (Ni–12 % Si) with T_L = 1143 °C (1150 °C) was further added as the second depressant to the composition of filler metal #1 + Rene-142 (see Figure 1, *c*). Silicon was added to boron-containing filler metal as a component lowering the melting temperature of the brazing mixture and affecting boron solubility in the seam matrix. Nickel added simultaneously with silicon, diluted the composite filler metal, preventing excess alloying.

Depressant content was varied in the ranges of 15–25 wt.%, thus promoting an improvement of such mechanical properties as BJ strength and fracture toughness. BJ Q-factor ($\sigma_t^{BJ}/\sigma_t^{BM}$, where σ_t^{BJ}, σ_t^{BM} is the ultimate strength of BJ and base metal, respec-

Table 2. Content (wt.%) of elements in structural components of solidified metal

DTA spectrum	B*	Al	Cr	Co	Ni	Mo	Hf	Ta	W	Re
Basic alloy #1										
1	–	2.43	8.42	8.68	80.47	–	–	–	–	–
2	2.03	4.08	11.46	8.24	74.18	–	–	–	–	–
3	2.30	4.34	11.87	7.92	73.57	–	–	–	–	–
4	14.90	–	83.93	0.89	1.27	–	–	–	–	–
5	16.07	–	81.60	0.93	1.40	–	–	–	–	–
6	15.32	–	82.24	0.80	1.64	–	–	–	–	–
Rene-142 alloy										
1	–	5.35	7.34	12.44	60.00	1.07	0.61	5.43	4.13	3.63
2	–	5.12	6.99	12.27	59.40	1.34	–	4.97	5.57	4.34
3	–	–	0.97	1.36	5.00	1.18	14.88	71.82	2.35	1.44
4	–	–	0.73	0.48	1.97	1.78	15.89	75.37	2.92	0.85
5	–	6.30	6.43	10.47	52.73	1.64	1.95	7.00	2.29	1.19
Complex alloy #11										
1	–	4.73	8.91	10.57	68.19	0.59	–	2.42	3.16	1.43
2	–	4.70	8.99	11.87	68.73	0.68	–	2.08	2.08	0.86
4	–	4.03	7.78	12.37	71.53	0.51	–	1.65	2.12	–
5	–	–	2.16	0.65	2.76	1.99	19.99	68.94	3.12	0.40
6	–	–	1.49	0.57	3.05	1.87	21.13	68.30	1.27	2.32
7	–	–	40.67	5.64	8.44	10.02	–	3.63	20.54	11.08
8	–	–	47.18	4.70	7.53	5.82	0.53	1.11	14.83	18.29
9	–	–	46.23	4.41	5.97	6.76	–	–	20.49	16.13
10	–	1.68	7.32	14.31	65.34	0.85	4.49	4.95	1.06	–
11	–	1.99	9.56	13.97	66.18	0.85	2.70	4.73	–	–
12	–	–	37.89	5.71	9.15	10.25	–	3.52	24.37	9.11

*At determination of boron content by the method of X-ray spectral analysis the complexity consists in superposition of molybdenum lines on boron lines.

tively) reached 0.96–1.00 at a stable relative elongation of 4–10 % [5–7].

Ni–12 % Si melt solidifies with simultaneous precipitation of two hard phases of a certain concentration – silicon hard solution in nickel γ(Ni) and eutectic γ(Ni) + Ni_5Si_2. Eutectic forms at the temperature of approximately 1150 °C and silicon content of 11.5–12.0 wt.%. In DTA melting curve it is seen that Ni_3Si (13.76 wt.% Si) undergoes two transformations at 1120 and 1040 °C, which results in formation of an eutectoid-like microstructure (see Figures 1, *c* and 5, *i*, *j*), which corresponds to Ni–Si constitutional diagram [16]. At the temperature of 20 °C the solidified filler metal is γ(Ni)-solid solution (microhardness *HV* 3870 MPa), and eutectic is γ(Ni)-solid solution and Ni_3Si(β) (11.3–12.8 wt.% Si, microhardness is *HV* 7740 MPa). The latter forms as a result of peritectic reaction between the alloy and Ni_5Si_2 at the temperature of 1165 °C and primary crystals of Ni_5Si_2 silicide (15.39 wt.%) (Table 3, Figure 5, *i*, *j*).

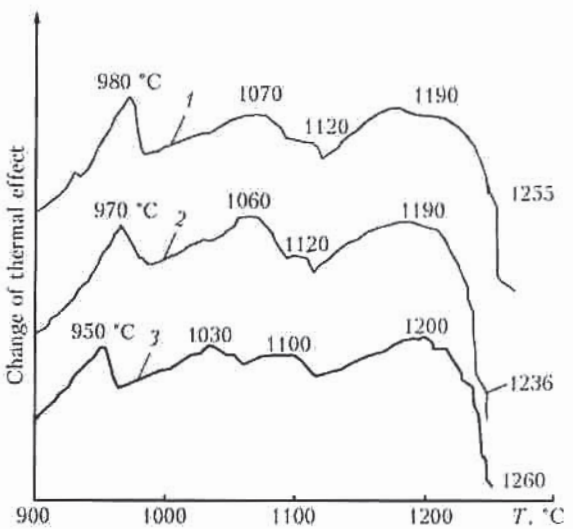

Figure 4. DTA curves obtained at solidification of molten ingots of complex alloys #1 + NS12 + 60 % Rene-142 with different content of silicon-containing component NS12: *1* – filler metal #13; *2* – 14; *3* – 12

Addition of eutectic filler metal NS12 to composite filler metal #11 changes the structure and phase composition of brazed seam metal, thus ensuring an improvement of BJ technological properties. Mode of thermograms of silicon- and boron-containing filler metal changes simultaneously: solidification processes are shifted towards lower temperatures with weakly expressed peaks on melting–solidification curves, and T_L value decreases by 60 °C compared to boron-containing filler metal #11.

Silicon added to the filler metal in the form of a eutectic component, promotes a reduction of the volume fraction and size of the secondary strengthening phases in the solidified filler metal, as well as a discrete mode of their distribution along the dendrite boundaries (see Figure 5, *c*). At the same brazing temperature the solidification range is narrowed by 40–50 °C in filler metals #11 and 12. The process of solidification in boron- and silicon-containing complex filler metal will run at a lower speed and in a more complete manner, respectively.

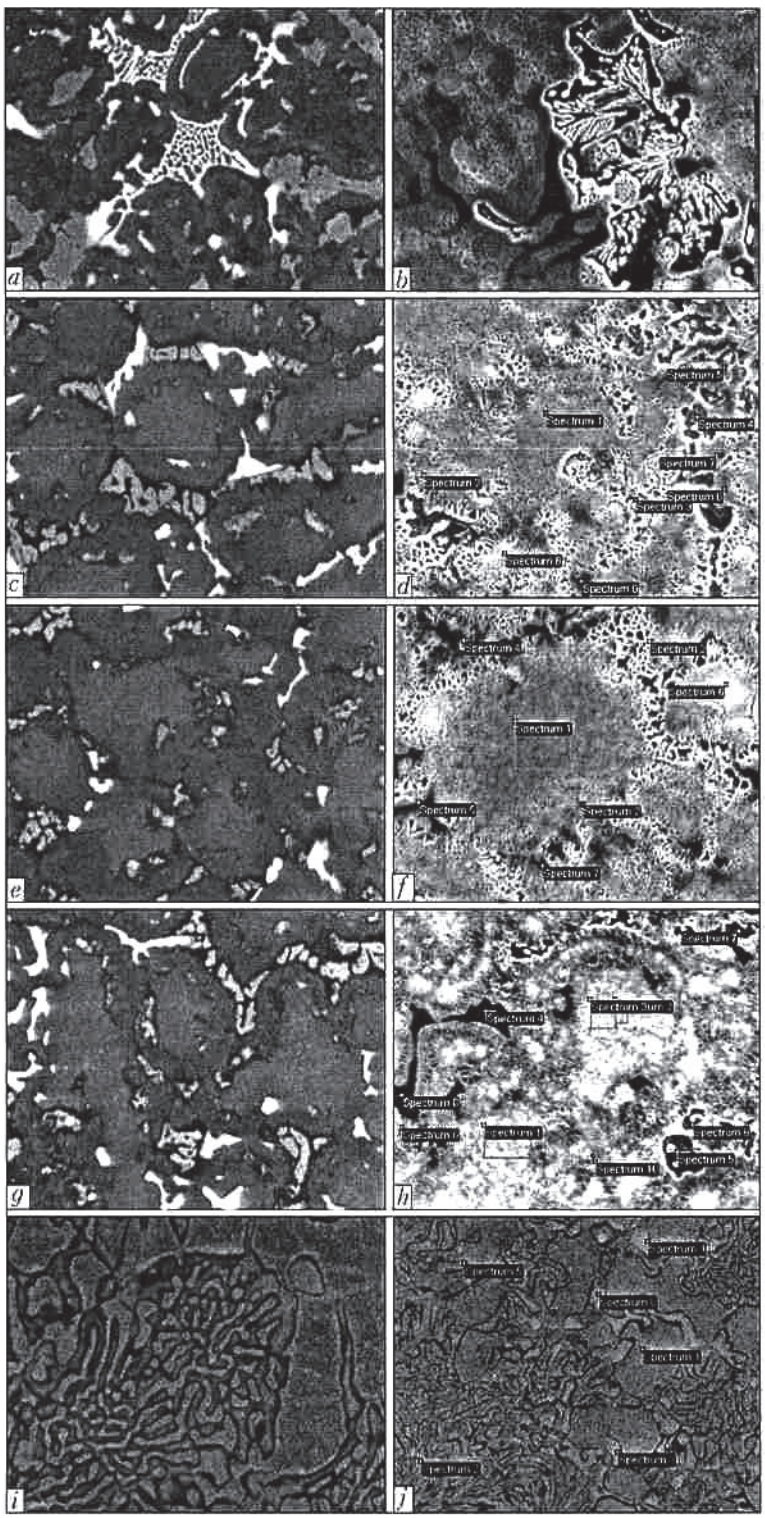

Figure 5. Microstructure of metal of solidified samples of complex filler metals of the type of #1 + 60 % Rene-142 without silicon (*a*, *b*) and with different content of NS12 additives: *c*, *d* — 15; *e*, *f* — 20; *g*, *h* — 25 vol.%; *i*, *j* — NS12 filler metal (*a*, *c*, *e*, *g*, *i* — ×500; *b*, *d*, *f*, *h*, *j* — ×1000)

As the filler metal melt is diluted by nickel at NS12 addition, the volume fraction of secondary phases in the brazed seam decreases (see Figure 5, *c*). Boron content in filler metal #12 varies from 1.0 to 0.5 wt.%, which results in a considerable reduction of the volume fraction of the precipitating chromium or nickel borides in the seam metal. No groove γ + CrB eutectics are observed in the solidified structure, and residual eutectics of γ + Ni_3B type are present in the form of isolated inclusions in the seam matrix. Minimum content of boride eutectics (up to 5–8 vol.%) compared to 35–40 vol.% in boron-containing filler metal #11 is the result of presence of silicon. Purely boride eutectics lead to BJ embrittlement at 20 °C, and at the annealing temperature (about 1080–1160 °C) they melt and sweat out of the seam, resulting in pores and cavities in the seam metal.

When a complex alloy with silicon is used, the composition of discrete eutectic phases of γ + Ni_3B type changes. A reduction of the weight fraction of cobalt (from 14 to 10 %) and chromium (from 9 to 4 %) is observed, with only a slight increase of the weight fraction of nickel (from 63 to 67 %) and hafnium (from 2.7–4.5 to 6–9 %). Discrete eutectics are formed on the base of intermetallic phase Ni_nHf_m (see Table 3 and Figure 5, *b*). Appearance of intermetallics is related to a low solubility of hafnium in γ-solid solution [17].

Systems of powder filler metals #1 + NS12 + 60 % Rene-142 with different content of NS12 were studied. Thermograms of filler metals #12–14 and the respective intervals of solidification of filler metals with 15–25 wt.% NS12 are shown in Figure 4 and Table 1.

Solidification of complex filler metals with silicon is of a complex nature — the thermograms have four exothermal salient

Table 3. Content (wt.%) of elements in structural components of solidified metal of complex filler metals with different content of NS12 additives

DTA spectrum	Al	Si	Cr	Co	Ni	Mo	Hf	Ta	W	Re
#1 + 15 % NS12 + 60 % Rene-142										
1	3.48	0.61	8.12	9.92	68.23	0.84	–	1.88	4.59	2.27
2	3.68	2.54	7.17	9.91	71.74	0.47	–	0.66	1.74	2.10
3	3.65	2.65	4.90	8.11	75.76	–	–	3.19	0.93	0.80
4	1.13	0.40	4.70	11.89	68.69	–	7.51	4.84	0.84	–
5	1.51	0.71	5.09	11.66	65.87	0.37	8.01	5.97	–	0.82
6	3.07	3.75	7.72	11.56	72.76	–	–	–	–	1.02
8	3.95	2.32	8.17	10.13	67.97	0.70	–	0.90	2.74	3.13
9	–	–	48.07	4.62	6.84	6.03	–	–	14.70	19.75
#1 + 20 % NS12 + 60 % Rene-142										
1	3.30	1.75	6.88	9.54	69.38	0.72	–	1.16	3.44	3.82
2	2.04	3.86	7.55	10.21	72.78	0.30	–	0.96	1.32	0.99
5	0.43	–	29.51	5.28	20.49	9.94	0.46	3.18	17.85	12.86
6	2.93	2.81	7.70	9.75	70.43	0.53	0.53	1.07	1.80	2.47
7	0.99	–	4.19	9.68	66.50	0.33	9.12	7.55	1.65	–
#1 + 25 % NS12 + 60 % Rene-142										
1	4.02	0.77	6.82	10.06	67.23	0.69	0.36	2.67	5.06	2.33
2	4.00	1.26	6.92	10.10	67.12	0.83	–	2.15	3.83	3.82
4	–	–	31.33	4.31	8.44	12.87	0.40	2.78	25.55	14.31
5	1.21	0.39	3.93	10.87	67.26	–	8.55	7.34	0.47	–
6	4.83	2.58	5.56	8.62	71.48	0.83	–	2.65	2.59	0.87
7	2.38	7.03	4.31	9.06	74.80	0.54	1.35	0.53	–	–
10	3.89	3.27	5.49	9.04	72.74	0.61	0.24	3.15	0.89	0.68
NS12										
1	–	8.24	–	–	91.76	–	–	–	–	–
2	–	12.08	–	–	87.92	–	–	–	–	–
3	–	15.39	–	–	84.61	–	–	–	–	–
5	–	13.78	–	–	86.22	–	–	–	–	–

points. T_S and T_L temperature of these alloys is practically the same (see Table 1), however, the volume fraction of the structural components is different. The main phases in the solidified seams are γ-solid solution, islet eutectics of γ + Ni_3B type, discrete carbide phases of $Me_{23}C_6$ type, dispersed MeC carbides and non-equilibrium γ′-phase. Content of complex-alloyed eutectic and chromium borides is higher in filler metal #13 than in filler metals #12 and 14, which is confirmed by brazed seam microstructure in Figure 5 and data of Table 3.

Increase of the amount of silicon added to the filler metal (with 25 % NS12) leads to appearance of isolated formations of up to 3 μm size on interdendritic boundaries, in which silicon content reaches 5.7–7.0 wt.%, and that of nickel — 71–72 wt.%. As to its composition, this compound is close to Ni_3Si silicide, the lower temperature of precipitation of which from the solid solution is equal to about 1040 °C [16].

Lowering of chromium content in the filler metal due to solid solution dilution by nickel resulted in variation of the carbide phase morphology: their tungsten content was increased (25 wt.%) compared to 14 wt.% in the basic system of filler metal #11 composition. Volume fraction of the carbide phases and their dimensions decreased with silicon addition.

System with 20 % NS12 turned out to be the optimum one, proceeding from the volume fraction of the secondary (boride and carboboride) phases in the brazed seam metal (Figure 6). This is exactly the weight fraction of NS12 additive, at which the solidified filler metal structure with minimum content of the secondary phases and liquation inhomogeneity was produced.

Table 4. BJ strength for a number of high-temperature nickel alloys at testing temperature T_{test} = 20 °C

Alloy type	Filler metal	σ_t, MPa (average value)		BJ Q-factor
		Base	BJ	
ChS70VI	#1 + 60 % Rene-142	813.5	732.5	0.90
	#1 + 20 % NS12 + 60 % Rene-142		778.0	0.96
VJL12U	#1 + 60 % Rene-142	833.0	721.0	0.86
	#1 + 20 % NS12 + 60 % Rene-142		873.0	1.00
JS26VI	#1 + 60 % Rene-142	727.0	692.0	0.95
	#1 + 20 % NS12 + 60 % Rene-142		718.5	0.99
JS26NK	#1 + 60 % Rene-142	868.0	766.0	0.88
	#1 + 20 % NS12 + 60 % Rene-142		835.0	1.00

X-ray diffraction patterns of the ingots (molten and solidified powders) of filler metals #1, 11 and 12 with silicon show lines, corresponding to γ-matrix solution based on nickel and CrB and Ni_3B borides. In filler metal #11 the intensity of solid solution lines is low, i.e. the volume fraction of the secondary phases is higher than in γ-solution. Relative intensity of diffraction lines of γ-matrix solution is indicative of the textured condition of the solidified filler metal, which is confirmed by the results of diffractometric analysis. Intensity of lines on the diffractograms identified as CrB, revealed that the highest volume fraction of this component is found in Ni–Co–Cr–Al–2.5 % B and #1 + 60 % Rene-142 filler metals. Chromium binding into boride compounds leads to a loss of high-temperature resistance of the alloy at lowering of this element content in the seam matrix.

For filler metals with silicon the intensity of these lines is low, as the content of these phases in the seam metal is minimum, which is confirmed by the results of different studies. Relative intensity of the lines of CrB and Ni_3B borides when filler metal #11 is used is higher than for filler metal #12. In the filler metal with silicon (#12) boron mainly precipitates in the form of dispersed Ni_3B particles of 0.3–0.7 μm size, both along dendrite arms, and in interdendritic regions. The above boride has the structure of cementite, i.e. of dispersion-strengthened type. Silicon somewhat stabilizes Ni_3B boride as a component «expanding the lattice» [15], and promotes boron penetration into the cementite lattice.

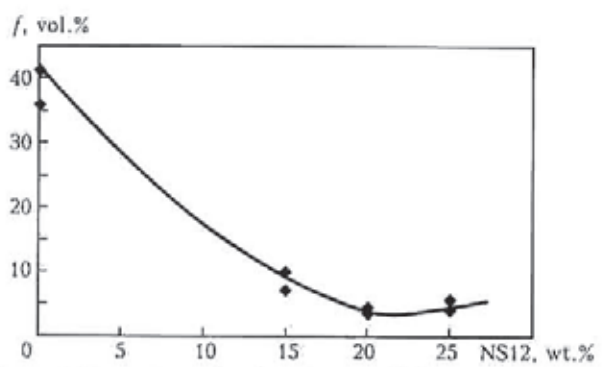

Figure 6. Dependence of volume fraction f of secondary phases in seam metal of #1 + 20 % NS12 + 60 % Rene-142 system on the content of added NS12

For a sample of filler metal #12 diffraction lines are found, which correspond to carbide phases of MeC type. Clear-cut peaks are indicative of their presence in the solidified filler metal. Structural and X-ray spectral analysis confirms the presence of carbide phases based on (Ta, Hf, W)C, having the form of dispersed particles of 3–7 μm size.

For silicon-containing filler metal #12 intensity peaks form on the X-ray diffraction pattern, identified as Ni_3M phase intermetallics, obviously, corresponding to γ′-Ni_3Al phase, which is the main strengthening phase, precipitating from the solid solution at its cooling. Its content is considerable already during solidification compared to boron-containing filler metal #11, in which no peaks are found on the roentgenogram. Addition of the second depressant in the form of NS12 to filler metal #11 (T_L lowering by 60 °C, respectively) at narrowing of ΔT_L–T_S interval promotes a more complete solidification of the filler metal melt without formation of developed eutectics. Low-temperature peak at the temperature of 950 °C on DTA curve of solidification of filler metal #12, most probably, corresponds to the start of precipitation of dispersed non-equilibrium γ′-phase from the solid solution (see Figure 1, *d*).

As follows from [4–6], two-step heat treatment after brazing reduces the liquational inhomogeneity inherent to all the cast alloys after solidification, and leads to formation of particles of γ′-Ni_3Al strengthening phase uniform as to composition, size and morphology, both on the arms and in the interdendritic spaces, and, therefore, promotes a higher long-term strength of the brazed seam metal [18].

With increase of weight fraction of Ni–12 % Si filler metal powder from 15 to 25 % the matrix microhardness along the dendrite arms varies in the ranges of *HV* 3940 to 4230 MPa, which is related to increase of γ′-Ni_3Al phase volume fraction. Dispersity of γ′-particles decreases (see Figure 5). Obtained data are indicative of the fact that in the case of application of filler metal with 20 wt.% NS12 redistribution of

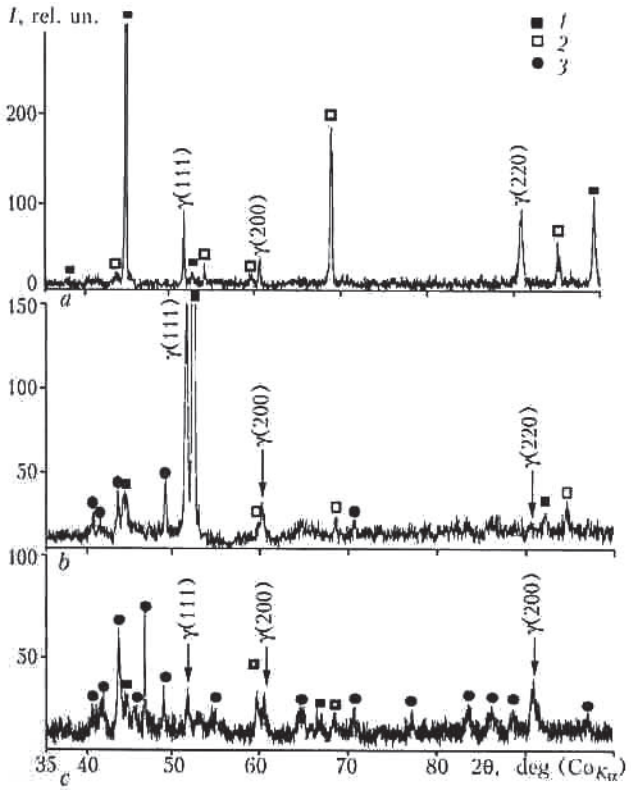

Figure 7. Diffractograms of basic filler metal #1 (*a*), composite filler metals of #1 + 60 % Rene-142 system without silicon (#11) (*b*) and with additive of 20 wt.% NS12 (#12) (*c*): *1* — CrB; *2* — Ni_3B; *3* — Ni_3Me

alloying elements in the dendrite volume occurs already during the solidification process.

Filler metal with 20 % NS12 (#12) approaches the equilibrium condition during solidification in the most complete manner (see Figure 5, *e*, *f*). This composition ensures the minimum content of the secondary strengthening phases in the filler metal, their discrete distribution along the dendrite boundaries, which results in smoothing of the peaks on DTA curve (see Figures 1, *e* and 5, *e*, *f*). Volume fraction of the boundary γ′-eutectic phase here is minimum, primary γ′-phase precipitates along the dendrite boundaries uniformly and in the maximum volume.

To confirm the rationality of selection of boron- and silicon-containing filler metal a system of composite filler metal #19 was studied (see Figure 1, *f*). DTA curves obtained for this filler metal show that the solidification range is widened up to 230 °C. At solidification of such a filler metal phase transformations take place, which are characterized by formation of diverse structural components in the seam metal (see Figure 2, *j*).

During investigations also the lattice parameters of matrix γ-solution were determined, and it was established that silicon, which is added to boron-containing filler metal, reduces the inner stress level of the solid solution, related to distortion of the crystalline lattice. Values of lattice parameter increase at addition of boron atoms to the nickel lattice, while silicon dissolves in nickel to the maximum, and, substituting boron, reduces the level of stresses, developing in the solid solution (see Figure 4). Values of lattice parameter of γ-solid solution of the seam metal formed with application of the studied filler metals are as follows, nm: Ni–Co–Cr–Al + 2.5 % B — 0.3555; Rene-142 — 0.3580; #1 + 60 % Rene-142 — 0.3566; #1 + 20 % NS12 + 60 % Rene-142 — 0.3549.

The interrelation between the structure of the brazed seam metal and BJ mechanical properties is shown in greater detail in [4, 5, 7] and Table 4. BJ of casting nickel alloys VJL12U, JS26VI, produced using filler metal 20 % #1 + 20 % NS12 + 60 % Rene-142, at 20 °C were characterized by strength equivalent to that of the base metal. Their ductility was 2.5–4 times higher than that of BJ, produced using regular boron-containing filler metals (40 % #1 + 60 % Rene-142). BJ short-time high-temperature strength at 900–1000 °C was 80 % of that of the base metal.

1. Khorunov, V.F. (2008) *Fundamentals of brazing thin-wall structures of high alloy steels*. Kiev: Naukova Dumka.
2. Peshcherin, E.I., Khorunov, V.F., Zhadkevich, M.L. (1997) Development of filler metals, technology and equipment for brazing of composite blades of aircraft gas turbines. In: *Brazing in development of current engineering products*. Moscow: Dom Zhanij.
3. Khorunov, V.F., Peshcherin, E.I. (1997) Search for technological processes for reconditioning of aircraft gas turbine engine parts. *Ibid*.
4. Malashenko, I.S., Kurenkova, V.V., Belyavin, A.F. et al. (2006) Strength and metal science of brazed joints of casting nickel alloy ChS70 VI. *Advances in Electrometallurgy*, **1**, 19–30.
5. Malashenko, I.S., Kurenkova, V.V., Belyavin, A.F. et al. (2006) Short-term strength and microstructure of brazed joints of alloy VJL12U produced using boron-containing brazing alloy with addition of silicon. *Ibid*., **4**, 23–38.
6. Malashenko, I.S., Kurenkova, V.V., Onoprienko, V.V. et al. (2007) Mechanical properties and structure of brazed joints of casting nickel alloy JS26VI. Pt 1. *Ibid*., **1**, 21–27.
7. Kurenkova, V.V., Onoprienko, E.V., Malashenko, I.S. et al. (2008) Structure and strength properties of brazed joints of casting nickel alloy JS26NK. Pt 2. *Ibid*., **1**, 24–33.
8. Chaturvedi, M.C., Ojo, O.A., Richards, N.L. (2004) Diffusion brazing of cast Inconel 738 superalloy. *Advances in Technol. Materials and Materials Proc*., **2(6)**, 206–213.
9. Idowu, O.A., Richardi, N.L., Chaturvedi, M.C. (2005) Effect of bonding temperature on isothermal solidification rate during transient liquid phase bonding of Inconel 738 LC superalloy. *Mater. Sci. and Eng*., Apr. **(397)**, fasc. 1, 2, 98–112.
10. Wikstrom, N.P., Ojo, O.A., Charurvedi, M.C. (2006) Influence of process parameters on microstructure of transient liquid phase bonded Inconel 738 LC superalloy with Amdry DF-3 interlayer. *Ibid*., **A417**, 299–309.
11. Ohsasa, K., Shinmura, T., Narita, T. (1999) Numerical modeling of the transient liquid phase bonding process of Ni using Ni–B–Cr ternary filler metal. *J. Phase Equilibria*, **20(3)**, 199–206.
12. Wendlandt, U. (1978) *Thermal methods of analysis*. Moscow: Mir.
13. Vertogradsky, V.A., Egorova, L.S. (1979) Interpretation of thermal curve in differential thermal analysis. *Inzh.-Fizich. Zhurnal*, 36(3), 480–485.
14. Doroshenko, L.K., Vasiliev, V.G., Grigorenko, G.M. (1995) Application of VDTA thermoanalyser for determination of transformation heat in metallic thermal spray coatings. *Avtomatich. Svarka*, **11**, 30–34.
15. Goldshmidt, H.J. (1971) *Interstitial alloys*. Vol. 1. Moscow: Mir.
16. (1996) *Constitutional diagrams of binary metallic systems*: Refer. Book. Vol. 1. Moscow: Mashinostroenie.
17. (1987) *Heat resistance of casting nickel alloys and their protection from oxidation*. Ed. by B.E. Paton. Kiev: Naukova Dumka.
18. Shalin, R.E., Svetlov, I.L., Kachanov, E.B. et al. (1997) *Single crystals of nickel heat-resistant alloys*. Moscow: Mashinostroenie.

CURRENT STATUS OF WELDING FABRICATION IN JAPAN

V.N. BERNADSKY and O.K. MAKOVETSKAYA
E.O. Paton Electric Welding Institute, NASU, Kiev, Ukraine

The review presents the data that characterize the state of the welding equipment market in Japan at the first stage of the global financial and economic crisis of 2008–2009.

Keywords: *welding fabrication, economic development, structural material market, welding equipment market, financial crisis*

Japan is the country of economic success, which managed to become one of the world leaders in a historically short time. Rate of economic growth of post-war Japan, having reached the highest point in 1950s (average annual increase of GDP was 14.9 %), began actively decreasing: in 1960s – by 11.3; in 1970s – 4.5; in 1980s – 3.8; in 1990s – 1.4; in 2008 – 0.7%. Such falling rates of growth are related to the change of the stages of the country's economic growth: reforms of the first post-war years (1946–1952), establishing industrial production (1955–1973), period of adaptation to the growing prices for raw material resources and fuel and internationalization of the economy (1974–1989), structural crisis of the 1990s and financial crisis of 2008–2009.

During the years of «economical miracle» Japan overcame the technical lag compared to the most developed countries and mastered the technologies of mass processing of the raw and fuel resources and mass output of standardized finished products. In 1950s ferrous metallurgy enterprises, coal mines and power stations were reconstructed and new merchant marine, destroyed during the war, was built. In 1960s manufacturing of household appliances and radiosets, automotive industry, as well as petrochemistry, production of synthetic fibres and resins and electronics were created on the basis of military enterprise conversion and new industrial construction from scratch. At the same time, almost all the coal mines which could not stand the competition of cheap import oil, were closed down, the oil becoming the fuel base of power economy.

In 1970s all the reserves of extensive growth by involvement of new labour resources and revising the industrial product range had been exhausted. The industry became more and more focused on science-intensive sectors, such as electronic engineering and manufacturing modern communication means. To intensify their development, a series of state programs was implemented for financial and organizational support of research performed by major companies in the field of high technologies.

In 1990s Japan went through a severe financial crisis, which had an essential influence on development of the real sector of the Japanese economy. Share of investments into the GDP dropped from 20 to 15–16 %. Lack of demand in the domestic market has been and still remains Japan's structural weakness, so that the 1990s crisis can be called structural crisis. Crisis phase lasted for more than 10 years and lead to a sequence of grave consequences in the production, financial and social spheres.

During the period of 2002–2007 Japan showed economical upturn, however no effective steps were taken towards a gradual re-orientation of the economy to domestic consumption. The complexity of Japan's situation at the current stage (2008–2009) consists in that it enters the recession, not having really recovered from the stagnation of 1990s. Japanese economy still has to cope with the burden of too large production capacities, high labour cost and huge amount of debt (Japan's internal debt was equal to almost 180 % of GDT at the beginning of 2008) [1].

However, as noted by the Japanese economists, despite the tremendous initial destruction, a crisis, like nothing else, reveals the need for vital reforms and helps mobilize their support by the population. Crisis periods (particularly, «oil» crisis at the end of 1970s) gave an impetus to understanding the importance of innovation development of the Japanese economy, in particular, welding technologies. Japanese welding specialists drew two very important conclusions. First, innovation technologies of material joining should be developed and introduced continuously, so as to be ready at any moment to become involved in an intelligent and promising overcoming of global crises and fulfillment of major national programs. Secondly, welding needs scientists, developers, technologists and qualified welders all the time and not only during the time of crises [2]. Such a concept was confirmed by development of new high-technology productions and high technologies, development and manufacturing of structural materials, welding equipment and consumables. If we focus more on the strategic perspective, to-day's crisis can also become a herald of positive reforms, which will increase the effectiveness and viability of the Japanese economic system [3].

Market of the main structural materials. Development of the modern Japanese market of welding equipment is closely related to the sectoral metal-proc-

Table 1. Volumes of steel and hot rolled stock production, thous t

Production type	2001	2006	2007	2008
Steel melting, total	102870	116226	120202	118737
Including:				
common	83960	90700	94078	92564
special	18910	25526	26124	26173
Hot rolled stock, total	94760	104121	108202	106087
Including				
common steel	78930	83139	86704	84322
special steel	15840	20982	21496	21765

essing markets — welding equipment users and structural material markets, primarily steel markets. In the Japanese steel industry such phenomena, as specialization, cooperation, and integration of production have changed and acquired new forms during globalization of the world economy. Steel consumption rises, being, however, the case of qualitative, rather than quantitative growth. A key factor of development of the country's metallurgy, are innovation solutions aimed at development of new steel grades for specific products. The forms of division of labour and cooperation between metal producers and users have changed and acquired new features. Products oriented to a specific application are formed together with steel users, and adaptation of all the production processes including joining technologies, materials and equipment, is performed. Cooperation of producers and users starts from the R&D field and ends by the final product entering the market. An example of it can be development in 1980s of the process of thermomechanically controlled processing by Nippon Steel for production of rolled stock from high-strength steel, as well as technologies of its welding, which, in its turn, led to appearance of new concepts in fabrication of pipelines, designs of welded off-shore platforms and lightweight ship structures [2]. Development of new types of steels subjected to thermomechanical processing is carried on, and new grades with improved properties, i.e. high environmental, brittle fracture, corrosion and fatigue resistance, and characterized by good weldability are regularly introduced into the market [4].

As to the volume of steel production (118.7 mln t in 2008), Japan takes the second place in the world after China. Export quota of this sector amounts to 24 % of Japan's share in the world market of ferrous metals of approximately 25 %. Volume of steel production in Japan in the last decade was equal to about 100 mln t, and in 2007 it reached the next peak of 120 mln t. Table 1 shows the data of steel and hot rolled stock production during 2001–2008 [5].

During 2001–2008 steel production in Japan rose by 15 %, the increase of common steel production being just 10, and that of special quality steels — 38 %, and the situation in hot rolled stock production is similar. In the structure of total steel production the share of special steels is equal to 22 % and exhibits a tendency to continuous growth [5].

Japan is one of the world leaders in stainless steel production. In 2007 the world production of stainless steel reached 27.6 mln t, 60 % of which was produced in the Asian countries (China — 7.2, Japan — 3.5 mln t). Sheet steel amounts to almost 80 % of stainless steel produced in Japan, the main users of which are construction, shipbuilding, industrial mechanical engineering, railway transportation, and container fabrication. Stainless steel export is equal to about 500 thous t.

Non-ferrous metallurgy of Japan, in which practically all the productions are material- and power-consuming, as well as environmentally unsafe, went through structural reorganization to the greatest extent. Primary production of non-ferrous metals was greatly reduced (for instance, for aluminium it decreased in 1980s from 770 to 32.4 thou t). A reduction of production facilities and taking production out to other countries takes place. By the data of the Japanese Aluminium Association in 2007 production of primary aluminium in the country amounted to just 6.6, and that of secondary aluminium — to 1111.7 thou t, which covered about 80 % of inner demand for metal produced from scrap. The country imports about 3 mln t of aluminium and aluminium alloys. The demand for metal has been steadily growing for the last five years, the main users being construction and automotive industry. It is predicted that the Japanese domestic demand should decrease somewhat, however, the total aluminium production in the country will grow.

Table 2 gives the pattern of consumption of aluminium rolled stock and extruded sections in Japan by individual industries and in construction [6].

The main fraction of extruded sections (78 %) is consumed in transport engineering and construction sectors, in particular, in fabrication of structures, where advanced welding technologies are widely used: friction stir welding, hybrid, electron beam and laser welding.

Welding consumables market. By the volume of welding consumables consumption (by deposited metal weight) Japan takes the third place in the world (268 thou after the USA (335 thou t) and EU countries (437 thou t) [7].

Japanese welding consumables market is closely related to structural metal market, in particular steel market. This dependence is clearly visible in Figure 1, which

Table 2. Sectoral structure of aluminium rolled stock and extruded section consumption

Industrial sector	Rolled stock, thou t		Extruded sections, thou t	
	2002	2007	2002	2007
Food	449.4	448.8	1.2	1.1
Dishware manufacturing	7.2	3.1	1.0	1.7
Foil	159.9	154.3	–	–
Metalware manufacturing	101.7	98.0	28.4	25.0
Power industry	90.3	109.5	29.6	28.6
Transport engineering	135.2	200.0	141.4	173.6
Industrial mechanical engineering	12.4	27.0	75.1	91.8
Construction/structures	62.9	48.9	642.2	573.6
Other	66.2	71.9	60.3	59.9
Total	1085.1	1161.5	979.3	955.3

Table 3. Volume and structure of domestic consumption of welding consumables

Welding consumables	1999		2007		2008 (estimate)		2009 (prediction)	
	thou t	%	thou t	%	thou t	%	thou t	%
Coated electrodes	56.2	18.3	44.6	12.4	42.7	11.7	39.9	11.7
Submerged-arc welding wire and flux	32.8	10.7	36.2	10.3	40.2	11.0	37.7	11.0
Thin solid wire	141.5	46.2	163.5	46.7	171.0	46.8	157.5	46.4
TIG welding wire	1.8	0.6	2.4	0.7	2.2	0.6	2.1	0.6
Flux-cored wire	74.2	24.2	105.0	29.9	108.7	29.9	103.3	30.3
Total	306.5	100.0	351.7	100.0	364.8	100.0	340.5	100.0

shows the data on welding consumable production and steel consumption in Japan during 1990–2007 [8].

Volumes and patterns of domestic consumption of the main groups of welding consumables in the period from 1999 to 2009 are given in Table 3 [9]. Data of Table 3 show that the tendencies exhibited by the Japanese welding consumables market in the recent decades, are quite stable. On the whole, welding consumables consumption showed positive dynamics with annual growth of about 3–4 %.

In the pattern of consumption a continuous reduction of the demand for arc welding electrodes should be noted. In the period from 1999 the volume of their application decreased by 30 %, and the fraction of coated electrodes in the structure of the applied welding consumables dropped to 11.7 %. A stable increase of the demand for flux-cored wires was still observed. The demand for solid wire continues to be high: its fraction amounts to almost half of all the used welding consumables. The fraction of consumption of wires for inert-gas welding is less than 1 %, however, the volumes of application of this welding process, rise, particularly, in mechanical and power engineering.

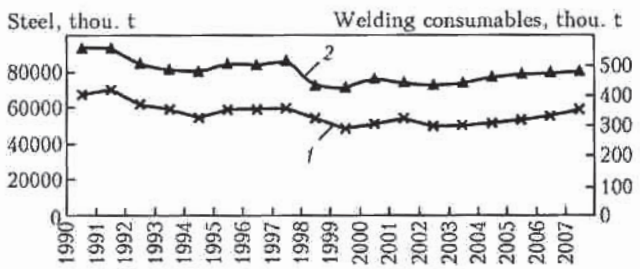

Figure 1. Dynamics of welding consumable production (*1*) and steel consumption (*2*) in Japan over the period of 1990–2007

In the production structure of welding consumables, the fraction of welding consumables designed for stainless steel welding is small, being 3–4 %, which corresponds to the stainless steel fraction in the structure of total steel production in the country. Table 4 gives the data on manufacture of welding consumables for welding stainless steels [9]. Over the recent years, positive dynamics of the volume of production of welding consumables for stainless steel welding has been observed with the annual output increase of 3–5 %, which is 2007 was equal to more than 13 thou t. In the production structure flux-cored wire constitutes the main fraction (50 %) and almost 25 % is taken up by solid wire for MIG welding, which is noticeably different from the total consumption pattern of common welding consumables (see Table 3). As a result of a considerable demand for stainless steel in the shipbuilding, petrochemical, nuclear and electric power industries, no considerable reduction of the demand for welding consumables in this sector in 2008–2009 is anticipated. A not more than 1–2 % lowering of production is predicted.

Volume of production of welding consumables for welding aluminium in Japan is small, despite the considerable volumes of consumption of this metal in the automotive industry, shipbuilding, railway transport engineering. This is determined by the structure of

Table 4. Volume of production of welding consumables for stainless steel welding, t

Welding consumables	2001	2002	2003	2004	2005	2006	2007	2008 (prediction)
Solid wire for submerged-arc welding	375	289	309	438	460	470	480	480
Filler materials for TIG welding	930	861	936	973	960	980	990	990
Solid wire for MIG welding	2049	2623	2832	2953	2860	2990	3230	3150
Coated electrodes for arc welding	1967	1868	2004	1976	1850	1740	1720	1700
Flux-cored wire	5081	5099	5519	5780	5910	6180	6600	6580
Total	10405	10740	11600	12120	12040	12360	13020	12900

aluminium welding processes applied in Japan, among which a considerable share is taken by such welding technologies as TIG, laser welding, friction stir welding, which require no welding consumables.

Figure 2 gives the statistical data of the Japan Light Metal Welding and Construction Association on production of welding consumables used for aluminium welding [10]. Consumption of this type of welding consumables in Japan (domestic production and import) was somewhat higher in 2008 and amounted to about 1.9 thou (1.5 thou t of welding wire and 0.4 thou t of electrodes).

Volumes of foreign trade in welding consumables in Japan are growing continuously. From 2001 to 2007, export of welding consumables increased two times, amounting to 49.5 thou t. In the export pattern flux-cored wires designed for gas-shielded welding account for more than 60 %. The main fraction of welding consumable supplies is taken up by countries of the South-Asian region, as well as the USA.

Welding consumable import is also growing. In 2007 it amounted to 48 thou t, which is 14 thou t more than in 2001. Solid wire import constitutes the main fraction (more than 70 %). The main trade partner is the Korean Republic, which supplies almost 2/3 of all the welding consumables imported by Japan, mainly, solid wire.

By estimates of the Japanese experts, under the influence of the world financial crisis consumption of all types of welding consumables will be reduced already in 2008, as a result of decrease of industrial production in all the industrial sectors, including construction, mechanical engineering, shipbuilding, and automotive industry. For 2009 a total decline of the demand for welding consumables by approximately 7 % is predicted, the export being reduced by 5.6 % to about 51 thou t, and import being reduced by 5.8 % to about 53.5 thou t.

Japanese companies, including the world leader in welding consumable manufacture — Kobe Steel Ltd. are actively developing and supplying to the market new types of welding consumables in all the market segments. Development of new welding consumables in Japan first of all is the response of welding consumable manufacturers to the problems, arising in different industrial sectors: improvement of product quality, productivity and cost-effectiveness of production, lowering of the ecological impact on the working medium and environment. With this purpose requirements are made of increase of the speed and productivity of welding processes, automation and robotization of welding production, widening flux-cored wire application for welding in all positions, ensuring ecological compatibility of welding processes [8].

In shipbuilding the demand for welding consumables for robotic welding of ship structure components in all positions is rising. At present developments of flux-cored wire designed for upward vertical welding in a wide gap at high current, are pursued more actively. The new wire ensures a high viscosity of the liquid metal, is characterised by an increased viscosity of the slag and its melting temperature. Another direction is development of flux-cored wire to improve the weldability during performance of welds in the vertical position and welding efficiency in all positions in ship and bridge building.

In construction R-bars are traditionally welded by YGW11 wire with a high content of alloying elements, which allows achieving a high impact toughness and strength of welds. However, the high content of slag-forming components impairs the weldability in the case of the wire application for robotic welding. In order to solve this problem, a new wire type — YGW18 was developed specially for robotic welding. The wire has excellent mechanical properties, namely ultimate tensile strength and impact toughness higher than that of the traditional wire.

Solid wire without copper cladding (YGW12) for MIG welding with a low spatter index and improved feeding characteristics was developed for robotic welding in the automotive industry and construction machinery engineering. This wire type has the highest feeding index and provides very high arcing stability. If we add a quite low spatter, thus preventing or minimizing cleaning after welding and equipment downtime, its application is cost-effective and highly efficient.

Development of up-to-date consumables for welding low-alloyed high-temperature steels for production of oil refining installations and construction of pipelines and thermal power plants is conducted successfully, to provide the possibility of welded struc-

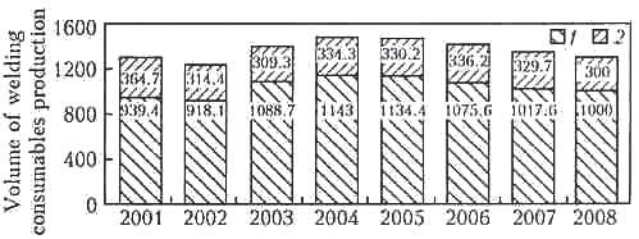

Figure 2. Volume of production of welding consumables (*t*) for aluminium welding: *1* — wire; *2* — electrode

Table 5. Welding equipment production

Welding equipment	Production indices, pcs (bln yen)				
	1999	2006	2007	2008	2009
Arc welding equipment, total	103900 (26430)	124500 (38001)	145100 (43837)	134800 (40500)	121300 (37721)
Including:					
rotary type converters	29300 (7891)	29600 (8802)	28500 (7489)	23600 (5893)	21700 (5881)
automatic and semi-automatic machines	27100 (8996)	59200 (17489)	72600 (21776)	70700 (23100)	63600 (22061)
power sources and other equipment	47500 (9543)	35700 (11905)	44000 (13268)	40500 (10800)	36000 (9720)
Resistance welding machines	7600 (16286)	10500 (11549)	10400 (11597)	9000 (10000)	8100 (9100)
Total	111500 (42716)	135000 (49550)	155500 (55470)	143800 (50500)	129400 (46821)

ture operation at an even higher temperature and pressure. An indubitable success is introduction of new wire of a high toughness for welding 2.25 % Cr–1 % Mo–V steel applied in manufacture of welded components of oil refining installations [11, 12].

Welding equipment market. Japan is one of the recognized leaders in the world production of up-to-date welding equipment. Japan's fraction of the world market of welding equipment accounts for approximately 15 %.

Table 5 gives the data on production volumes (in terms of figures and money) of the main types of welding equipment in the period from 1999 to 2007 and prediction for 2008–2009.

Over the period from 1999 till 2007 the volume of welding equipment production increased by almost 40 % in figures and by almost 10 % in value terms. Arc welding machines account for more than 90 % of the equipment manufactured in Japan. During 2003–2007 (after decline of production during the crisis period of 2001–2002) production of all types of welding equipment rose by 56 %. During this period the market registered the highest demand for automated arc welding machines, including submerged-arc welding machines. The volume of their production increased almost two times both in figures and in terms of value, and in 2007 it amounted to 72.6 thous pcs. Demand for resistance welding machines increased 30 % since 1999. Over the recent years it has been quite stable at about 8–10 thou pcs per year. Starting from 1999 the cost of one unit of welding equipment decreased considerably, which is particularly noticeable in the sector of resistance welding machines [13].

Short-term fluctuations of the volumes of welding equipment production are closely related to tendencies in development of the national economy. In 2008, 8 % decline in welding equipment production was noted. An almost 20 % reduction of production in the automotive industry predicted for 2009, will lead to lowering of the demand for welding equipment in the arc welding machine sector by another 10 % in figures and 7–8 % in terms of value. In the sector of automatic arc welding machines the volume of production in 2009 will be about 63.6 thou pcs (a 10 % drop compared to the previous year), while sales volume will decrease to 22061 mln yen (4.5 % decrease). In the sector of other kinds of arc welding machines, which includes DC and AC power sources, TIG welding equipment, special arc welding machines and air-plasma cutting machines production decline will continue also in 2009.

Decline in production of welding equipment in the sector of rotary type converters driven by an internal combustion engine (petrol or diesel), alongside the market stagnation in the civil and industrial construction sector was also affected by the initiated in 2007 revision of the Japanese national standards in con-

Table 6. Welding equipment export, pcs

Welding equipment	2004	2005	2006	2007
Arc welding equipment:				
Automatic and semi-automatic machines	9991	11838	9393	11570
other	10857	11772	11036	12839
Resistance welding machines:				
automatic and semi-automatic machines	4036	4293	5361	4142
other	3768	3868	2752	12828
Special welding machines	18209	14126	17719	18871
Total	46861	45897	46261	60250

Table 7. Welding equipment import, pcs

Welding equipment	2004	2005	2006	2007
Arc welding equipment:				
automatic and semi-automatic machines	20086	17469	16732	27984
other	51507	47397	45948	37953
Resistance welding machines:				
automatic and semi-automatic machines	540	1509	3107	594
other	860	1117	1063	361
Special welding machines:				
ultrasonic welding	1483	1716	2495	1858
other	39072	84821	42428	19455
Total	113548	154029	111773	88205

struction as regards the applied equipment. In 2008 compared to the previous year, the welding equipment sector showed the greatest decline in production: 17.4 % in figures and 25.5 % in terms of value. As predicted, the volume of production of this type of machines in 2009 will be reduced to 21.7 thou pcs (8 % drop compared to the previous year), while sales will be about 5.94 mln yen (10 % drop). It should be noted that manufacturing of welding transformers decreased abruptly, their manufacturing index being shown as a separate line in statistical reports just 10 to 15 years ago.

In the sector of resistance welding machines the volume of production in 2009 (prediction) will also be reduced, and will be equal to about 8100 pcs (9.1 mln yen). Annual decline in production will be equal to about 10 %.

Volumes of foreign trade in welding equipment are quite considerable. Over the recent years, import was equal to more than half, and export to almost 40 % of the volume of domestic production of welding equipment. During the financial-economic crisis of 2008–2009 export and import of different types of welding equipment will, obviously, be essentially reduced.

The prevailing fraction of arc welding application (more than 90 %) in the Japanese industrial production has largely determined the priorities in the field of development and production of welding equipment. The structure of welding equipment production has changed. Volumes of production of automatic and semi-automatic equipment increased considerably. The structure of production of individual groups of equipment has also changed. Up-to-date welding systems (welding machine–power source) mainly use digital control systems. Wide possibilities for high-speed effective control of the welding process are opened up by application of powerful computers and inverter circuits, this allowing a considerable increase of the efficiency and level of automation. The problem of transition from partial automation of the technological processes of welding to broad robotization and creation of completely unmanned technologies of welding and fabrication of welded structures is currently being solved.

Welding process automation is closely related to increased application of new welding technologies — laser, hybrid-laser, friction stir welding and robotization of the technological production process based on these welding processes [14, 15].

Volumes of production and sales of industrial lasers designed for processing various materials, including welding and cutting lasers, are negligible in Japan, compared to the European countries and the USA. The world volume of sales of industrial lasers and laser systems for welding and related technologies in 2008 amounted to about 2327 mln USD, and about 51.1 thou industrial lasers were manufactured. Process lasers designed for welding and cutting make up about 55 % of the total production of industrial lasers, while Japan accounts for about 23 % of the world consumption of industrial lasers and systems. Figure 3 gives the volume and structure of Japanese industrial laser manufacture. The volume of domestic production does not satisfy the demand for lasers and laser systems, which is growing continuously. Japan is one of the five countries, which are the main importers of lasers in the world. As to the volume of purchases, lasers take the second place in the total product import into the country [16, 17].

Volume of consumption of both CO_2 lasers (2005 — 1080 pcs) and YAG-lasers (2005 — 2900 pcs) is growing continuously. The demand for fibre lasers has increased considerably. From 2000 to 2005 the volume of purchases of this laser type (share of application in welding is 40 %) rose from 170 up to 830 pcs. A noticeable increase of application of disc lasers is observed, on the basis of which Japan is developing a new generation of machines for high-speed cutting and microwelding.

Laser and hybrid-laser welding technologies are widely used in many industrial sectors: automotive, shipbuilding, transport engineering. Development of mobile laser equipment for welding in shipbuilding is actively performed, and a process of diode laser welding in space was proposed, etc.

Japan in the world leader in the field of industrial robot manufacture and production automation based on welding process robotization. In 2007 volume of industrial robot sales was equal to 6.5 bln USD (575755 mln yen). In 2008 the total decline in the sales volume was equal to about 9 %.

Robots are intensively used in a number of sectors of the Japanese economy, particularly in automotive and electronic industry. Total added value created with involvement of robotics in industrial production, already in 1997 amounted to about 4.1 trln yen, which is equivalent to 0.8 % of GDP. Assessing the current status and prospects for development of robotics in the XXI century, the Japan Robot Association notes the need to switch to a new strategy of robotics development in the country: from robots to robotic technologies.

Welding robots account for about 24 % of the total volume of domestic supplies of industrial robots and about 15 % of the volume of export supplies. Tables 8 and 9 give the data on the volume of production, domestic market and export supplies of industrial robots and manipulators for welding [18, 19].

Overwhelming volume of robots produced in the country are robots for the traditional technologies of arc and resistance welding, more than 70 % of the domestic consumption of which falls to automotive industry [20].

In conclusion it should be noted that Japan is one of the countries of the world, which are world leaders in steel production and consumption, also per capita.

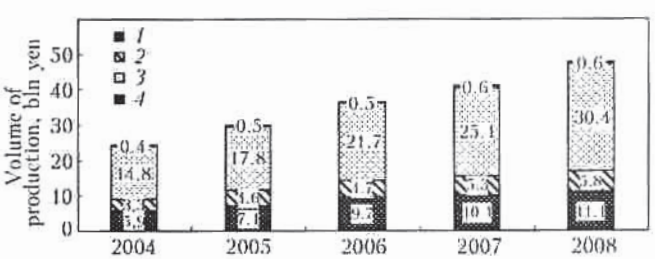

Figure 3. Volume of production of industrial welding lasers: *1* — CO_2; *2* — YAG; *3* — excimer laser; *4* — other

Table 8. Volume of production, domestic market and export supplies of industrial robots and manipulators for welding in terms of value for 2006–2008, mln yen

Application	2006			2007			2008		
	Domestic consumption	Export	Total	Domestic consumption	Export	Total	Domestic consumption	Export	Total
Total industrial robots	200324	355337	555661	212878	373134	586012	188999	345212	534211
welding robots	55017	44772	99789	51153	58535	109688	49494	57096	106590
for arc welding	29789	19785	49574	29327	24882	54209	29265	25322	54587
for resistance welding	24922	24942	49865	21723	33589	55312	20148	31737	51885
for laser welding	266	19	285	29	14	43	21	13	34
other	40	25	65	71	49	121	61	24	85

Table 9. Quantitative volume of production and domestic market and export supplies of welding robots and manipulators for 2006–2008

Welding robots	2006			2007			2008		
	Domestic consumption	Export	Total	Domestic consumption	Export	Total	Domestic consumption	Export	Total
Arc welding	5482	1888	7370	5181	3852	9033	5400	3700	9100
Resistance welding	5126	1353	6479	4481	5031	9512	4400	4700	9100

Here, it should be taken into account that for economically developed countries such as Japan, the USA and a number of others which have reached a high level of GDP per capita (more than 2000 USD), there is no more direct dependence of steel consumption growth on GDP growth. So, for instance, the rate of steel consumption growth in response to 1 % growth of the real GDP in 1994–2006 was equal to 0.94 in the countries of Central and Eastern Europe, 0.57 in Canada, and 0 % in Japan and the USA [21]. This is in line with the modern innovation tendencies of development of both ferrous metallurgy proper, and metal-processing industries in the developed countries. In particular, the share of production of special high-quality steels designed for manufacturing specific types of finished products is rising noticeably.

The national welding equipment market of Japan actually allows satisfying all the domestic demands of the leading sectors of industry and construction. Here, the volumes of foreign trade in welding consumables and welding equipment are considerable. Within the currently formed division of labour and specialization in the world market of welding equipment Japan is the main trade partner of East Asian countries, which are members of ASEAN, the USA and EC countries.

The world financial-economic crisis had an essential influence on the volumes of Japanese production and foreign trade. The predictive estimates given in the review may soon have to be significantly corrected. Japanese welding equipment manufacturers believe that the need to maintain reasonable market prices and returns on investment is the top priority under the crisis conditions. To increase the turnout in the welding equipment market the Japanese specialists proposed «New cost» and «Three in one» programs of activity, within which it is proposed to perform optimization of welding production organization, eliminating considerable overhead costs, optimization of the technological processes of welding, development of new high-quality products, achieve as close as possible coordination of the activity of manufacturers, dealers and users of welding equipment, increase the volumes of sales in the domestic market by studying the needs of welded structure manufacturers, particularly of small and medium-sized businesses.

1. *CIA*: The World Factbook. Japan. http://www.cia.gov
2. Shiga, T. (2007) New concept of steel structure production using innovative welding technologies. *J. JWS*, 76(**3**), 3–5.
3. Kennet, K., Jack, M. *Global financial shocks test Asia for strength*. http://www.inf.org
4. Siro, I. (2007) Advanced materials for modern large-sized structures. *J. JWS*, 76(**7**), 19–25.
5. Ohashi, T. (2007). Production and technology of iron and steel in Japan during 2006. *ISIJ Int.*, 47(**6**), 941–956.
6. *Japan Aluminium Association*. http://www.aluminium.or.jp
7. Middeldorf K, von Hofe, D. (2008). Trends in joining technologies. *The Paton Welding J.*, **11**, 33–49.
8. (2009) Welding consumables. *The J. Welding News for the World*, 13(**46**).
9. (2008) Welding consumables for stainless steel shipments. *Ibid.*, 12(**44**), Summer.
10. Aluminium Welding Consumables. *Ibid*.
11. Koshiishi, F. (2007) Promising welding consumables. J. JWS, 76(**7**), 61–64.
12. Koshiishi, F. (2008) Welding consumables. *Welding Technology* (Jap.), **1**, 66–69.
13. (2009) Welding machines. *The J. Weld News for the World*, 13(**46**), Winter.
14. Ueyama, T. ((2007) New approaches to development of welding power sources and equipment. *J. JWS*, 76(**1**), 55–60.
15. Era, T., Ueyama, T. (2007) New generation power sources for arc welding fitted with a digitization and visualization module. *Ibid.*, 77(**1**), 79–83.
16. (2008) Laser marketplace. *Laser Focus World*. www.laserfocusworld.com.
17. (2008) Welding in Japan. *Welding Technology* (Jap.), **6**, 129–137.
18. *Japan Robot Association*. www.jara.jp
19. (2008) Welding robots. *The J. Welding News for the World*, 12(**43**), Spring.
20. (2009) Arc welding robots. *Ibid.*, 3(**46**), Winter.
21. Vorobiov, P. How much steel is needed for love? *Nats. Metallurgia*. www.nmet.ru

PECULIARITIES OF LOW-AMPERAGE ARGON-ARC AND MICROPLASMA POWDER CLADDING ON NARROW SUBSTRATE

A.V. YAROVITSYN[1], K.A. YUSHCHENKO[1], A.A. NAKONECHNY[1] and I.A. PETRIK[2]
[1]E.O. Paton Electric Welding Institute, NASU, Kiev, Ukraine
[2]Open Joint Stock Company «Motor-Sich», Zaporozhie, Ukraine

Comparative analysis of technological characteristics of low-amperage argon-arc and microplasma powder cladding processes is conducted for a case of multilayer cladding on a narrow substrate 3.5 mm wide. Increase in viscosity of the weld pool metal provided by a dispersed additive in multilayer microplasma powder cladding allows increasing the effective heat input and thickness of the deposited layer, as well as reducing the risk of cracking of heat-resistant nickel alloys, which may be caused by re-heating in multilayer cladding.

Keywords: *low-amperage argon-arc cladding, microplasma powder cladding, multilayer cladding on narrow substrate, technological characteristics of arc, energy and thermal characteristics, hydrodynamic model of weld pool*

Traditional methods for repair welding of blades of ground-based and aircraft gas-turbine engines (GTE) from heat-resistant nickel alloys with a high content of the γ'-phase include manual low-amperage argon-arc cladding (AAC) using a filler wire [1–3] and laser cladding using an additive powder [4]. Microplasma powder cladding (MPC) has lately gained acceptance for repair of parts from heat-resistant nickel alloys [5–7], as the peculiarities of this process make it possible to perform a wide range of repair operations on blade edges (Figure 1). The Figure shows the welded joints produced by using a powder additive similar to the base metal (with a 30–50 % content of the γ'-phase), and additive having a lower strength at high temperatures.

Therefore, edges of the GTE blades can be repaired by different methods (Figure 2), the option including laser powder cladding, low-amperage AAC and MPC. Despite the fact that numerous publications are available on repair of the GTE blades [1–7], it is expedient to conduct comparative analysis of technological characteristics of the above cladding processes.

Specific feature of repair of edges of the GTE component blades by fusion welding is that the airfoil is installed in a vertical position and bead is deposited on a narrow substrate under the free formation conditions [1–7]. With such a cladding procedure, to decrease the sensitivity of welded joints on heat-resistant alloys to cracking as a result of re-heating, it is necessary to provide the maximum possible height (thickness) of the deposited layer to decrease the quan-

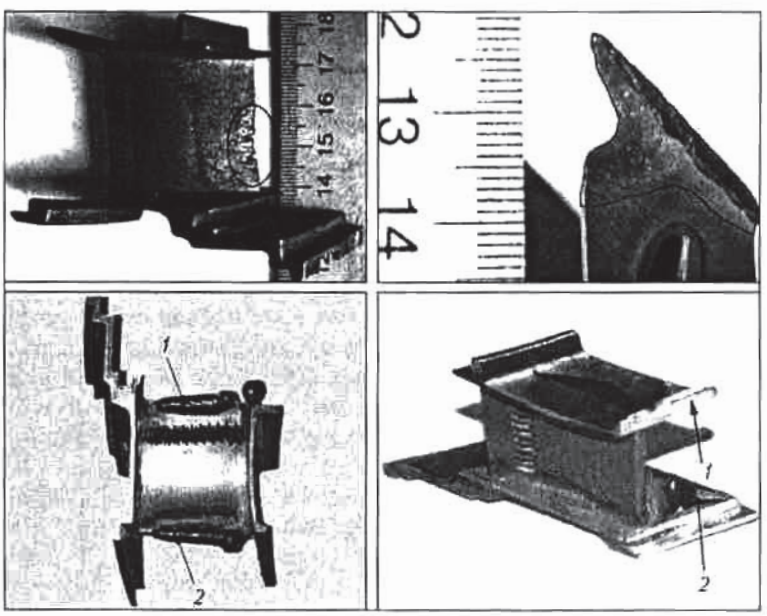

Figure 1. Appearance of operational damages (marked) and experimental claddings (*1*, *2*) made to repair the damaged regions of the AI-25TL engine nozzle blade made from alloy JS6U with 65 % γ'-phase content

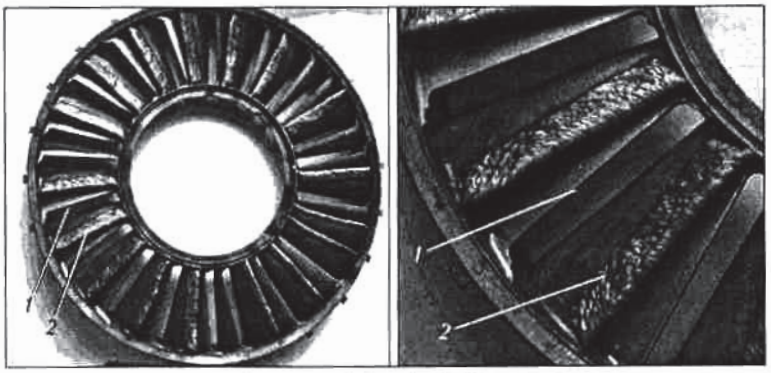

Figure 2. Appearance of the nozzle block with blades repaired by the MPC method: *1* – grooving of defective region; *2* – blade repaired by cladding

tity of layers of the deposited metal, which is also advisable for the technological reasons in order to reduce the scope of machining operations aimed at elimination of irregularities in formation of beads and removal of surface oxide films.

The process of repair of blade edges by laser powder cladding [4] is characterised by performing multilayer cladding at a speed of 0.1–0.8 m/min and thickness of the deposited layer equal to 0.5–1.0 mm. In the case of laser cladding of big amounts of metal on a narrow substrate (see Figure 2), it is necessary to deposit many layers, this increasing the risk of cracking as a result of re-heating. In this connection, low-amperage AAC or MPC is indicated for heavily damaged blade edges of heat-resistant nickel alloys.

The purpose of this study is to conduct comparative evaluation of technological characteristics of multilayer cladding on a narrow substrate by using the low-amperage argon-arc and microplasma processes for heat-resistant nickel alloys having limited weldability. Considered are energy characteristics of the arc (current, power, cladding speed), thermal characteristics (effective workpiece heating power, effective efficiency of heating of a workpiece), efficiency of deposition of a preset volume of metal, gas flow rate, and losses of filler metal in cladding.

The technological characteristics of the low-amperage argon-arc and microplasma processes were evaluated by an example of model multilayer cladding on a narrow substrate used to develop the technology for repair of the nozzle block of stage IV of the helicopter engine made from austenitic steel. The high degree of wear (see Figure 2) required deposition of a big amount of filler metal. Cladding was performed by using wire rods 2 mm in diameter and 50 mm long, as well as powder with a particle size of 53–153 μm of heat-resistant filler metal of the IN 625 type. Cladding on a narrow substrate was carried out under the conditions of free formation of the bead (Figures 3 and 4). To provide side allowance for machining, the deposited bead was formed at a contact angle of over 90° to the substrate (see Figures 3 and 4) [8]. Cladding was performed at a welding current of 30–40 A. Then each layer of the deposited metal was subjected to layer-by-layer dressing.

Machine UP-NS-304M was employed for AAC and MPC. The flow rate of argon (grade 1, according to GOST 10157–79) was 10 and 18 l/min for AAC and MPC, respectively. Mass of the deposited metal was evaluated by weighing on a balance with an accuracy of up to 1 g. Direct losses of filler materials during the cladding process were determined by weighing of the powder and wire on a balance with an accuracy of up to 0.1 g.

The technological characteristics of the two processes of low-amperage cladding for the conditions of building-up of the damaged region of a blade with a

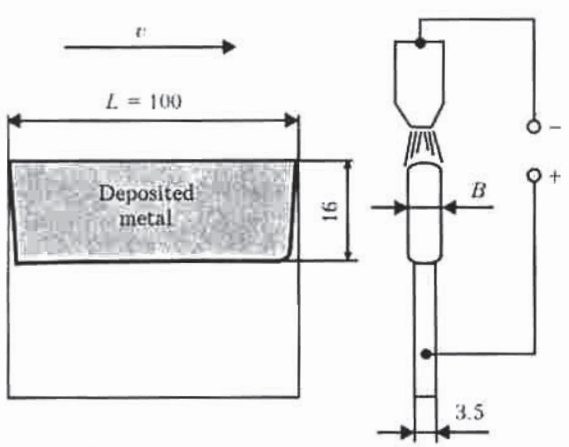

Figure 3. Schematic of grooving of the defective region and multilayer cladding of the nozzle block blade

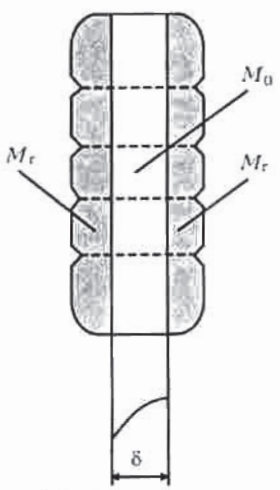

Figure 4. Schematic of the bead deposited on a narrow substrate by multilayer cladding: M_0 – zone of net size of repaired surface; M_t – zone of side reinforcements of the deposited bead

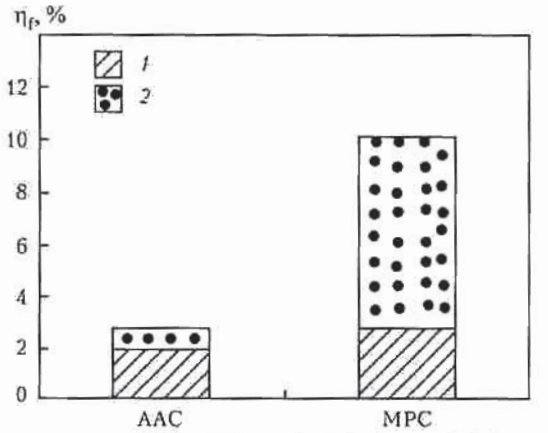

Figure 5. Direct losses of filler materials during cladding: *1* — waste; *2* — irreversible losses

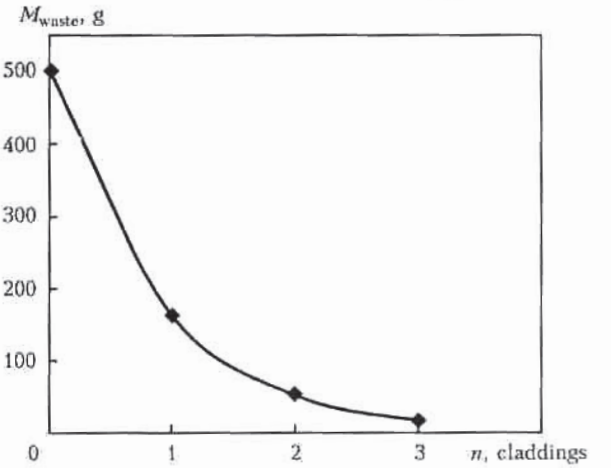

Figure 6. Dependence of variations in mass of the reference portion of powder, M_{waste}, in its repeated utilisation in MPC before (n = = 0) and after the first to third claddings

volume of 5.6 cm^3 * were as follows: current I for AAC (MPC) — 37 (32) A, respectively; speed v in deposition of one layer — 1.08 (0.667) m/h; quantity N of layers for deposition of the preset volume of metal — 9 (4); time t spent directly for deposition of the preset volume of metal to repair the blade — 0.833 (0.583) h; and deposition rate α_d — 2.6 (4.82) g/(A·h).

The deposition efficiency was evaluated from the quantity of layers of the deposited metal, time t directly spent for cladding of a blade, and value of deposition rate α_d [9]:

$$\alpha_d = M_d/(It), \quad (1)$$

where M_d is the actual mass of the deposited metal allowing for side reinforcements of the bead.

It was found that, compared with AAC, in MPC on a narrow substrate the value of the welding current was 15 % lower, speed was approximately 40 % lower, quantity of layers was almost twice as low, and blade cladding time was 30 % shorter. Results of check weighing of the nozzle block before and after cladding of the blades showed that the deposition rate in MPC was almost 1.85 times higher than in AAC.

Direct losses of a filler material in multilayer cladding on a narrow substrate were estimated from the following formula:

$$K_{l1} = 1 - M_d/M_f, \quad (2)$$

where M_f is the mass of the filler material spent for cladding of a blade, and M_d is the actual mass of the deposited metal in cladding of the blade.

Direct losses of wire in AAC (Figure 5) consisted approximately of 1 % losses for fumes and 2 % for the rod stub. Direct losses of a powder in MPC were estimated allowing for the powder consumption, mass of the deposited metal and mass of the powder that passed through the arc column and was collected then from outside the cladding zone. Checking consumption of the reference batch of the powder with a mass of 0.5 kg (Figure 6) allowed determining the average value of the powder utilisation factor (PUF) equal to 0.625, and value of irreversible losses of the powder equal to 5 %. Including wastes of the powder, which cannot be used for cladding after its three times utilisation (3.4 %), the losses of the powder additive in MPC on a narrow substrate were about 10.5 % (see Figure 5), which is similar to the losses of powder in plasma power cladding [8].

Experimental studies of the technological characteristics showed, in general, that despite a lower rate of deposition of a layer, MPC is characterised by the higher deposition efficiency than AAC. To substantiate the obtained experimental data, investigations were conducted to study energy and thermal characteristics of the free and constricted arc in a range of currents of up to 50 A.

The thermal characteristics were evaluated by using the continuous-flow calorimetry method [8]. In our case, the current and arc voltage were measured with a digital voltmeter of class 0.5. The constant flow of water via the continuous-flow calorimeter and cooling jacket of plasmatron PPS-4 was maintained with an accuracy of±1.5 %. It was provided by discharging water from a vessel with a constant volume using the precise water regulation valves. The voltage from thermocouples was measured in millivolts using analogue-digital converter ADAM 4118 with an accuracy of ±0.1 %. The calorimetry system was calibrated with standard mercury thermometer TL-4 (GOST 215–73) having a scale division value equal to 0.1 °C. The effective power of heating of a workpiece, q_w, and effective efficiency of heating of the workpiece, η_w, were determined during the experiments [10]:

$$\eta_w = q_w/(UI). \quad (3)$$

Total power of heating losses Σq_l in the plasmatron (torch) and arc was

$$\sum q_l = (1 - \eta_w)UI. \quad (4)$$

The maximal error of experimental data on the effective heating power, allowing for temperature fluctuations in the calorimetry system, was no more than 3 %. The adequacy of measurements was con-

*Here and below in the article, the required volume after final machining of the rectangular cross section equal to 3.5 × 16 mm.

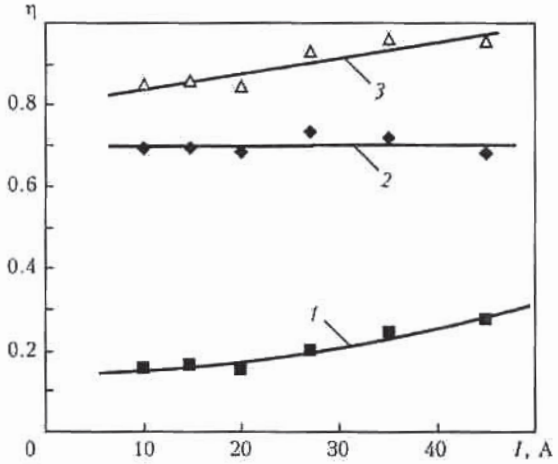

Figure 7. Energy balance of the constricted arc in MPC: *1* – share of heat losses for plasmatron cooling, η_p; *2* – η_w; *3* – $\eta_p + \eta_w$ (specific flow rate of argon: q_{plasma} = 1 l/min, q_{trans} = 7.5 l/min, workpiece to plasmatron distance – 5 mm)

firmed by convergence of the energy balance in MPC (Figure 7).

Figures 8 and 9 show dependencies of arc power *UI*, effective heating power q_w and total power of heating losses Σq_l upon the arc current at constant values of the arc length and argon flow rate for the conditions of burning of the constricted and free arcs, which corresponded to the above parameters of cladding of the nozzle block blade. The energy and thermal characteristics for the operating currents in multilayer cladding on a narrow substrate 3.5 mm wide, calculated from the results of regressions of the experimental data shown in Figures 8 and 9, are given in the Table. It was found that in multilayer cladding on a narrow substrate the higher deposition efficiency of MPC, compared with AAC, is provided by the higher values of arc power (2.1 times) and effective heating power (1.62 times).

Consider peculiarities of formation of a bead on a narrow substrate depending upon the type of a filler material. Geometric characteristics of cross section of the first layer bead deposited on the narrow substrate for MPC and AAC, respectively, are as follows: B = = 7.6 (6.0) mm, $h_{b.m1}$ = 1.5 (1.0) mm, and h_{d1} = 4.4

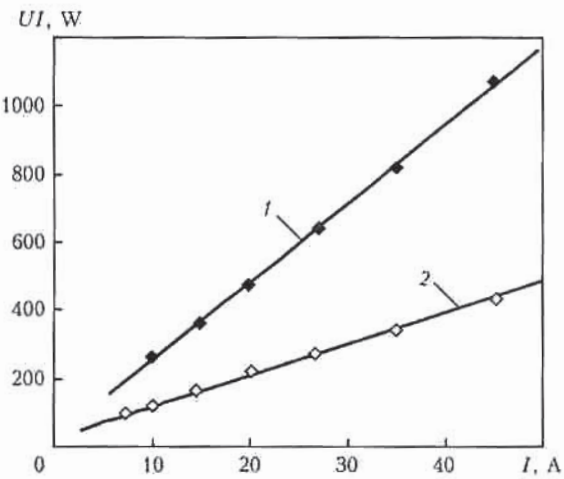

Figure 8. Energy characteristics: *1* – constricted arc, q_{plasma} = = 1 l/min, q_{trans} = 7.5 l/min, workpiece to plasmatron distance of 5 mm; *2* – free arc, q_g = 10 l/min, workpiece to plasmatron distance – 2 mm

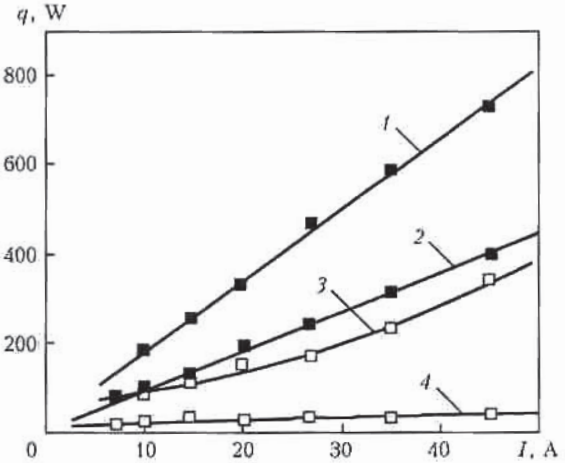

Figure 9. Thermal characteristics of the arc: *1*, *2* – heating power q_w with the constricted and free arcs, respectively; *3*, *4* – power of heating Σq_l with the constricted and free arcs, respectively, at different specific flow rates of argon: *1* – q_{plasma} = 1 l/min, q_{trans} = = 7 l/min; *2* – q_g = 10 l/min (arc length from plasmatron to workpiece – 5 mm (*1*), and from electrode to workpiece – 2 mm (*2*))

(2.0) mm (Figure 10). It was experimentally shown that height of the deposited layer may amount to more than 4 mm in layer-by-layer MPC on the narrow substrate under the conditions of free formation of the bead. This is twice as high than in AAC, where the height is limited because of the probability of flowing out of liquid metal of the weld pool over the side walls of the narrow substrate at a much lower q_w/v ratio (see the Table).

To substantiate the experimental data in terms of hydrodynamics, the moving weld pool on a narrow substrate can be regarded as a region of the thin layer of viscous fluid flowing over the plate end [11]. The character of the fluid flow (laminar, turbulent) is determined by the kinematic similarity criterion, i.e. Reynolds number [12]:

$$\mathrm{Re} = 4Q/\nu, \qquad (5)$$

where Q is the consumption of the fluid per unit width of the flow; ν is the kinematic viscosity of the fluid determined from the time of flowing of a set volume of the fluid via a calibrated hole under the effect of gravity [13].

Normal formation of the bead corresponds to a laminar character of flow of the thin layer of the viscous fluid and Reynolds number $5 < \mathrm{Re} < 60$, and unstable formation corresponds to a turbulent character and Reynolds number $50 < \mathrm{Re} < 200$ [11].

For the case of welding (cladding) on a narrow substrate, consumption of the the viscous fluid per unit width of the flow can be written down as follows [11]:

$$Q = vF_{pen}/\delta, \qquad (6)$$

where v is the welding (cladding) speed; F_{pen} is the cross section area of penetration bead; and δ is the width of the narrow substrate.

Given that the cross section of the bead deposited on a narrow substrate is close in shape to ellipse, its surface area can be written down as follows:

$$F_{pen} = 0.25\pi Bh, \qquad (7)$$

Energy and thermal characteristics for the free and constricted arcs in multilayer cladding on a narrow substrate 3.5 mm wide

Type of arc	I, A	UI, W	v, mm/s	UI/v, J/mm	q_w, W	η_w	q_w/v, J/mm
Free arc	37	364.34	0.316	1152.96	328.83	0.902	1040.60
	32*	320.23*	–	–	288.21*	0.902	–
Constricted arc	32	760.63	0.185	4111.51	532.74	0.700	2879.68

*The data are given for qualitative comparison.

where $h = h_{b.m} + h_d$.

Assume that the maximum possible height of the bead deposited on a narrow substrate, where the weld pool metal is still kept from flowing out over the narrow substrate walls due to viscosity, corresponds to a fixed value of Reynolds number for the considered range of the cladding speeds. Then the maximal possible cross section of the deposited bead, F_{pen}, which can still be kept on the narrow substrate, other conditions being equal, can also be increased by changing viscosity of the weld pool metal.

According to the data of study [8], the powder with particle diameters of 53–153 μm for the range of the parameters under consideration, while flying through the arc column, gets into the weld pool in the solid state, thus lowering its average temperature [8]. Due to the weld pool heat the relatively cold powder particles in it, while melting, form the overcooled microvolumes, i.e. freezing nuclei, which act as solidification centres [14]. In this case the weld pool is a set of the changing volumes of solid and solid-liquid states of metal, this increasing resistance to motion of one part of the weld pool metal relative to the other.

Therefore, from the standpoint of hydrodynamics of the weld pool and within the framework of considered physical model, it can be justifiably assumed that the addition of a dispersed material causes changes in kinematic viscosity ν of liquid metal, which can be expressed in terms of dependencies (4) through (6) as follows:

$$\nu = 0.25\nu\pi Bh/(\mathrm{Re}\,\delta). \qquad (8)$$

Using the experimental data on geometric characteristics of the deposited beads (Figure 10), estimate a change in kinematic viscosity ν of liquid metal of the weld pool for MPC (ν_1), compared with AAC, for the first deposited layer (ν_2):

$$\nu_1/\nu_2 = \nu_1 B_1 h_1/(\nu_2 B_2 h_2),$$
$$\nu_1/\nu_2 = 0.667{\cdot}7.6{\cdot}6.0/(1.08{\cdot}6.0{\cdot}3.0) \approx 1.6. \qquad (9)$$

Thus, as established, a 60 % increase in viscosity of metal of the weld pool caused by adding a dispersed filler metal to it allows the effective heat input into a workpiece to be increased approximately 2.75 times in multilayer cladding on a narrow substrate 3.5 mm wide, this leading to a more than 2 times increase in height (thickness) of the deposited layer and more than 2 times decrease in the quantity of layers of the deposited metal at a preset volume of the deposited metal.

Application of MPC to repair heavily damaged edges of the blades from heat-resistant nickel alloys with a more than 30–50 % content of the γ′-phase will make it possible to substantially reduce the risk of cracking as a result of re-heating in multilayer cladding.

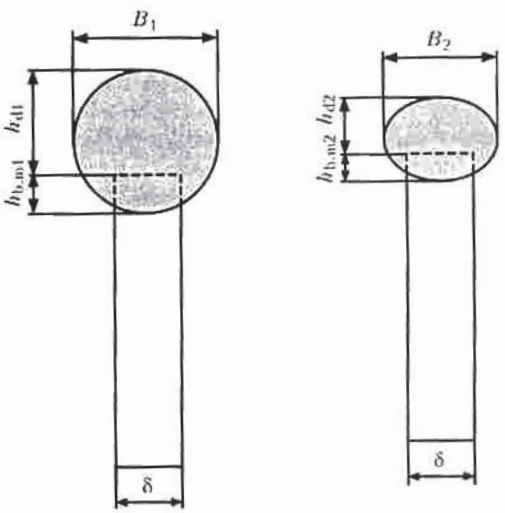

Figure 10. Schematic of measuring height h and width B of one-layer bead deposited on a narrow substrate: h_{d1}, $h_{b.m1}$, B_1 – height of the deposited bead, base metal penetration depth and width of the bead, respectively, in MPC; h_{d2}, $h_{b.m2}$, B_2 – same in AAC

1. Peremilovsky, I.A., Gejchenko, V.S., Frumin, I.I. (1976) Cladding repair of turbine blades of aircraft engines. *Avtomatich. Svarka*, **5**, 54–56.
2. Arzhakin, A.N., Stolyarov, I.I., Turov, A.V. (2003) Development of technology for repair of 8th stage blades of high-pressure turbine of aircraft engine by automatic cladding method. *Svarshchik*, **4**, 8–9.
3. Martyshin, G.V., Trunova, V.B. (1993) Argon-arc cladding with pulse feed of filler wire in repair of parts. *Svarochn. Proizvodstvo*, **10**, 16–17.
4. Krause, C. (2003) Improved technology of repair: laser powder cladding. *Gazoturb. Tekhnologii*, **5**, 24–26.
5. Savchenko, V.S., Yushchenko, K.A., Savolej, N.I. et al. (1993) Specifics of welding of high-nickel dispersion-hardened heat-resistant alloys and repair of parts made from them. *Avtomatich. Svarka*, **10**, 31–33.
6. Yushchenko, K.A., Savchenko, V.S., Chervyakova, L.V. et al. (2005) Investigation of weldability of nickel superalloys and development of repair technology for gas turbine blades. *The Paton Welding J.*, **6**, 2–5.
7. Yushchenko, K.A., Yarovitsyn, A.V. (2007) Experience of application of microplasma powder cladding. In: *Proc. of 4th All-Ukr. Sci.-Techn. Conf. of Junior Scientists and Specialists on Welding and Related Technologies* (23–25 May, 2007, Kiev). Kiev: PWI.
8. Gladky, P.V., Pereplyotchikov, E.F., Ryabtsev, I.A. (2007) *Plasma cladding*. Kiev: Ekotekhnologiya.
9. Frolov, V.V., Vinokurov, V.A., Volchenko, V.N. et al. (1970) *Theoretical principles of welding*. Ed. by V.V. Frolov. Moscow: Vysshaya Shkola.
10. Rykalin, N.N. (1951) *Calculations of thermal processes in welding*. Moscow: Mashgiz.
11. Shneerson, V.Ya. (1979) Formation of welds of flanged joints. *Avtomatich. Svarka*, **2**, 5, 6, 9.
12. Kapitsa, P.L. (1948) Wave flow of thin layers of viscous fluid. *Zhurnal Elektrotekhn. Fiziki*, **18**, Issue 1, 3–28.
13. Frenkel, Ya.I. (1975) *Kinetic theory of fluids*. Leningrad: Nauka.
14. Ivochkin, I.I. (1965) Suppression of columnar grain growth by method of welding pool «freezing». *Svarochn. Proizvodstvo*, **12**, 1–3.

PRODUCING PERMANENT JOINTS IN STRUCTURED POLYETHYLENE PIPES

N.G. KORAB, S.V. KABYSH and A.V. KOSTENKO
E.O. Paton Electric Welding Institute, NASU, Kiev, Ukraine

The possibility is considered of producing a permanent joint in structured polyethylene pipes by using the indirect heating method. As shown by mechanical tests, strength of the joint can reach 90 % or higher of that of the base material. Noted is the possibility of automated selection of heating conditions and their efficient utilization for development of a commercial technology for joining structured polyethylene pipes.

Keywords: *indirect heating, structured polyethylene, permanent joint, polymer pipeline*

In many countries, including Ukraine, structured (cross-linked) polyethylene pipes are successfully used for pipelines of different application. In comparison with many thermoplastics, this material has higher factors of impact toughness at low temperatures, resistance to slow and quick crack propagation, chemical resistance and strength. For this purpose a three-dimensional cross-linked structure is generated in material by different methods, and a distinguishing feature of this structure is a strong molecular bond between polymer chains, which significantly increases stability of polymer and provides higher density [1]. At present, a standard [2] is in force in the territory of Ukraine, according to which four types of structured polyethylene pipes can be produced: PE-Xa, PE-Xb, PE-Xc and PE-Xd. They are designed for building and repairing of pipeline systems for cold and hot water supply and heating, and transport water with temperature of 5–95 °C. Welding of these pipes by using known methods does not allow receiving the required strength properties of the joints [1, 3] (strength factor k does not exceed 0.1–0.3 of that of the pipe material). Today structured polyethylene pipelines are mounted with the help of metallic fasteners of different configurations [4], this having a range of disadvantages, such as a high price, corrosion of metal parts and probable loss of tightness in long-term operation. Analysis of existing publications shows that studies on welding of structured polyethylene are carried out abroad [3, 5–7], although their results do not have a wide industrial application so far, which is related to different reasons, for example, complexity of fasteners production, increased emission of harmful substances due to a high welding temperature, etc.

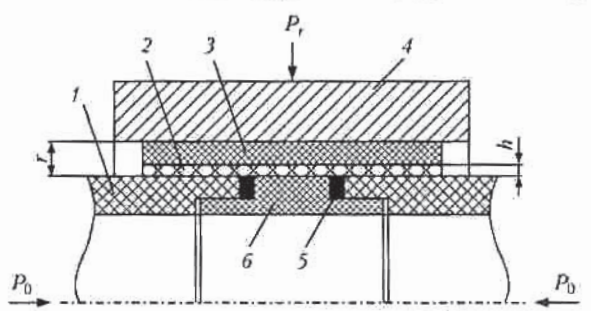

Figure 1. Scheme of permanent joint on structured polyethylene pipe produced by the indirect heating method: *1* – pipes to be joined; *2* – interlayer (from high density polyethylene); *3* – outer coupling (of structured polyethylene); *4* – nozzle of the heating tool (t_h = 200–300 °C); *5* – washer (from high-density polyethylene); *6* – guide insert

Based on the above-said, the possibility of producing permanent joints on PE-Xa structured polyethylene pipes by the method of indirect heating, which is performed by «fusion» of the mating surfaces through interlayer of PE80 grade high-density polyethylene with 0.5 mm thickness, was investigated by the E.O. Paton Electric Welding Institute. In this case, heat input to the «fusion» zone is carried out through one of the mating surfaces (indirect heating) (Figure 1) [8–10]. The proposed technology consists of several basic operations. The first operation is fit-up of the joint. Then parts *3*, *2* and pipe surface *1* are heated from the outer surface of coupling *3* with outer diameter of 6.3 mm and wall thickness of 5.8 mm, made from the PE-Xa material, to depth $h = r + (1–1.5)$ mm up to a temperature of around 170–200 °C (heating duration τ = 4–11 min). Axial pressure P_0 = 0.02–0.05 MPa should be applied to the pipes joined, and radial pressure P_r = 0.1–0.2 MPa – to the coupling outer surface *3* during heating and cooling (pressure P_0 is generated by the loading system of the aligner, where the joint is fixed during heating and cooling, and P_r is provided by squeezing coupling *3* with a metallic band or special nozzles of the heater). On completion of heating, cooling is performed for 10–15 min, after which the nozzles of the heater (or band) are removed. To provide the maximum possible level of relaxation of thermal stresses caused by formation of the melt of high-density polyethylene in the joining zone, it is recommended to run the pipeline 6–20 h after the end of heating. Insert *6* serves for prevention of misalignment and displacement of ends of the joined pipes, and ring *5* – for additional sealing by their partial melting and interaction with the pipe ends and insert *6*. The main investigations were carried out for

pipes of structured polyethylene of the PE-Xa type with an outer diameter of 50 mm and wall thickness of 4.6 mm.

Mechanical properties of the joints were evaluated according to tensile test results (Figure 2). The strength factor was determined on the basis of the forces which samples withstood before failure:

$$k = \sigma/\sigma_y, \quad (1)$$

where σ is the maximum tensile stress in the pipe wall, which the joint withstood before failure, MPa; σ_y is the yield strength of the material of the pipes joined (σ_y = 19.6 MPa for PE-Xa type polyethylene).

Strength of the joints is provided by adhesive interaction between the material of the interlayer in zones of its contact with the parts jouined. As shown by investigations of physics of the process, Van der Waals forces underlie this interaction [1, 11], and the presence of heating up of the interlayer material and mating surfaces up to polyethylene melting temperature T_{melt}, i.e. not less than 125–130 °C, is the first necessary requirement of its occurrence. The second necessary requirement is the presence of compression pressure P_r in the heating zone. In this case it occurs as a result of thermal expansion of the heated material of the parts joined and interlayer. For this purpose, the joint is tightly squeezed by the heater cavity or band.

Dependence of strength of the joint on duration of heating at different temperatures of a heating tool (Figure 3) was studied. Increase of the strength factor is observed with an increase of duration of heating in an entire interval of heater temperature variations. At $k > 0.2$, in all the cases, dependence $k = f(\tau)$ monotonously increases, reaching the $k = 1$ value. By linear approximation of the experimental data [12] in the $k = 0.2, \ldots, 1.0$ range, we obtain dependencies $k = f(\tau) = a\tau + b$ for each value of heater temperature (curves *1–3* in Figure 3). Curve *6* is an example of passing of the approximation curve. After this, by determining dependencies $a = f(T_h)$ and $b = f(T_h)$ (which also satisfy the linear law in the selected interval) and substituting them in the equation $k = f(\tau) = a\tau + b$, we obtaine

$$k = f(\tau, T_h) = [(0.153T_h - 20)\tau + 0.0697T_h - 25]\cdot 10^{-2}. \quad (2)$$

Evaluate the limits of variations of T_h, in which equation (2) will make sense in description of the process of formation of adhesion strength in the joint. Set the following conditions meeting the technological process: $k, \tau \geq 0$ may and take on the values of $0 \leq k \leq 1$, $\tau_0 \leq \tau \leq \tau_m$. In this case, τ_0 and τ_m are determined for each particular value of T_h from the dependencies derived through substitution of the $k = 0$ and $k = 1$ values to equation (2):

$$\tau_0 = \frac{25 - 0.0697T_h}{0.153T_h - 20} \text{ (min)}, \quad (3)$$

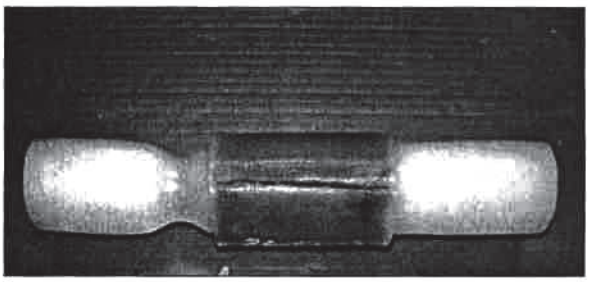

Figure 2. Sample that withstood a tensile test without fracture of the joint (a «neck» – sign of residual deformations can be seen on a pipe close to the coupling)

$$\tau_m = \frac{125 - 0.0697T_h}{0.153T_h - 20} \text{ (min)}. \quad (4)$$

To determine the range of T_h variations, $\tau_0 = 0$ value is substituted to equation (3), and denominator of equation (4) is set equal to zero.

After calculations $T_h = 358.7 \approx 360$ °C from equation (3), and $T_h = 130.7 \approx 130$ °C for the denominator of equation (4). Consequently, equation (2) makes physical sense at $130.7 < T_h < 358.7$ °C, as at $T_h > 358.7$ °C $\tau < 0$ and at $T_h = 130.7$ °C $\tau \to \infty$. As shown by the measurements, the temperature of the heating tool is higher than that in the area of its contact with a part by 40 °C on the average. In order to correct the limit of T_h variations, we set the lower limit by assuming that the contact temperature should be not less than T_{melt} = 130 °C, i.e. $T_{h\,min} = T_{melt} + 40 = 130 + 40 = 170$ °C. In the similar way we determine also the upper limit, considering that the temperature of thermal destruction of polyethylene is T_d = 280 °C [1], $T_{h\,max} = T_d + 40 = 280 + 40 = 320$ °C, since in the case of excess of the destruction temperature the probability of decomposition (that is, weakening) of joining part material in a place of contact with the heater is run. Equation (2) should meet the following conditions: $k, \tau \geq 0$, $T_h > 0$; $k = 0$–1, T_h = 170–320 °C; $\tau = \tau_0 - \tau_m$, where τ_0 and τ_m are determined according to the equations (3) and (4) for each specific T_h value. By finally determining the conditions, for which equation (2) can be used, the special cases in a form of $k = f(\tau)$ for temperatures of the heating element, $T_{h\,max}$ and $T_{h\,min}$ (320 and 170 °C,

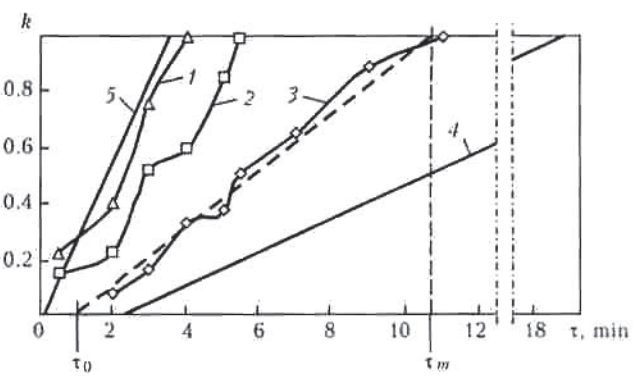

Figure 3. Dependence of strength factor of the joint on heating time τ at different temperatures of the heating tool: *1* – T_h = 300; *2* – 270; *3* – 200; *4* – 320; *5* – 170 °C (curves *4* and *5* were plotted on the basis of calculation data, and curve *6* – on the basis of approximation results)

Figure 4. Sample of the joint on PE-Xa grade structured polyethylene pipe with outer diameter of 50 mm and wall thickness of 4.6 mm after hydraulic tests

respectively) are found, and plotted in the form of curves *4*, *5* (Figure 3):

$$\text{for } T_h = 320\ ^\circ\text{C} \quad k = f(\tau) = [28.96\tau - 2.696]\cdot 10^{-2}, \quad (5)$$

$$\text{for } T_h = 170\ ^\circ\text{C} \quad k = f(\tau) = [6.01\tau - 13.151]\cdot 10^{-2}. \quad (6)$$

Dependencies (5) and (6) show that the higher the temperature of the heating tool, the higher is the rate of increase in strength, and vice versa, which is supported by experimental data.

The statement is valid that at the initial stage of heating the strength of adhesive interaction of the joint is zero up to the time moment τ', when the interlayer is molten and in the zone of its contact with mating surfaces there appear the areas with a temperature equal to or higher than the melting temperature of polyethylene T_{melt}, where formation of the adhesion interaction in the contact zone becomes possible. Assuming that dependence $k = f(\tau)$ is linear at $k < 0.2$, it can be considered that $\tau' = \tau_0$, i.e. this is the time necessary for achieving the temperature equal to T_{melt} in the surface of contact of interlayer and pipe at specified values T_h and r (see Figure 1). The optimum duration of heating for each specified T_h value, at which the adhesion interaction is observed in the entire area of the joining zones (in our case this is a point at $k = f(\tau)$ curve, conforming to the $k = 1$ value and equal to τ_m, which can also be calculated from equation (4)) can be determined in a similar way. Thus, upon achieving heating duration τ_m in the entire area of contact of interlayer with the mating surfaces, temperature $T \geq T_{melt}$ is also reached, and strength of the adhesion interaction is maximal. Further heating has no influence on increase of the joint strength, which is proved by a character of failure of samples in tensile tests (see Figure 2). With the help of the derived dependencies it is possible to automate the process of selection of heating modes, which, in turn, leads to the optimum combination of high strength properties with a minimum level of power inputs.

The conducted hydraulic tests showed that pipe samples did not fracture at a working liquid temperature of 95 °C, pressure of 1 MPa and duration of 165 h. To determine the maximum strength of a sample and

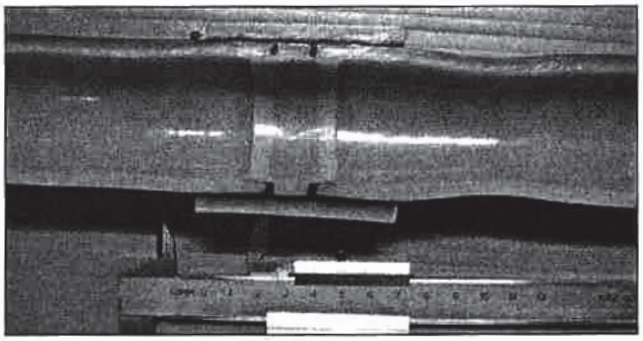

Figure 5. Cross section of joint after hydraulic tests

character of its probable failure, the pressure was increased after the tests. The sample fractured in a wall of the pipe joined, by withstanding the maximum pressure of 2.1 MPa, while the area of joints had no visible signs of deformation or frcature (Figures 4 and 5).

Thus, this study covers only an insignificant part of what is related to production of permanent joints on new polymer materials. Analysis of publications of many researches in Ukraine, as well as abroad, showed that the significant interest is expressed not only in development of the applied technologies, but also in welding of the new types of polymers, including the difficult-to-weld ones.

In the future it will be necessary to investigate the influence on joint properties by such parameters as interlayer material and thickness, wall thickness of the joining part, and pipe wall thickness. From the point of view of the proposed technology, it is also important to study other types of structured polyethylene: PE-Xc, PE-Xd and, first of all, PE-Xb, since it is characterized by higher strength properties and finds an increasingly wide acceptance. This method, as shown above, provides the maximum possible performance of pipelines, not requiring utilization of complicated and expensive equipment. Based on the results of these investigations, the corresponding patents for a set of joining parts and method for producing permanent joints on structured polyethylene pipes by means of indirect heating [9, 10] were issued in Ukraine and Russia.

CONCLUSIONS

1. Possibility of producing the permanent joints on structured polyethylene pipes by thermal method (method of indirect heating) is shown.

2. Strength properties of the produced joints are not inferior to those the pipes joined (for structured polyethylene pipes of the PE-Xa type).

3. Based on the experimental data the dependence of strength properties of the joints on basic technological parameters was derived, allowing automation of the process of selection of heating modes, and also making some assumptions on the mechanism of formation of the adhesive interaction in the zone of contact of mating surfaces.

1. Losev, I.P. (1981) *Chemistry of synthetic polymers*. Moscow: Khimiya.

2. *DSTU B V.2.5-17–2001*: Plumbing and heating installations. Extranets and works. Structured polyethylene pipes for cold, hot water supply and heating systems. Kyiv: Derzhbud Ukrainy.
3. Tobias, W., Bernshtein, G. (2000) Welding of PE-X pipes — cross-linked polymer. *Polimergaz*, **2**, 28–32.
4. *DBN V.2.5-22–2002*: Code of established practice. Rules. Plumbing and heating installations. Extranets and works. Extranets of hot water supply and hot-water heating using structured polyethylene pipes with thermal insulation from foamy polyethylene and protective corrugated polyethylene envelope. Kyiv: Derzhbud Ukrainy.
5. Eckert, R., Shlachter, R., Gessel, J. (1999) Studies of welded joints of pipes and fittings with embedded heating element in combinations of PE 80, PE 100 and cross-linked polyethylene — PE-Xa. *Polimergaz*, **4**, 16, 33–36.
6. Ilavsky, I.J. (2001) Spajanie sietovanych polyetylenovych rur (typ PEX-b). In: *Proc. of 8th Int. Gas Conf. on Plastic Materials in Gas Distribution* (Prague, 27–28 Febr., 2001).
7. Tobias, W., Bernstein, G. *Method for butt welding cross-linked polyethylene pipes (PE-X pipes)*. Pat. 6 524 424 BI US. Publ. 25.02.2003.
8. Shestopal, A.N., Vasiliev, Yu.S., Mineev, E.A. et al. (1986) *Reference book on welding and gluing of plastics*. Kiev: Tekhnika.
9. *Set of fittings for welding of pipes from structured (cross-linked) polyethylene and method of welding by heated tool of pipes from structured (cross-linked) polyethylene*. Pat. 77212 Ukraine. Publ. 15.11.2006.
10. *Set of fittings for welding of pipes from structured (cross-linked) polyethylene and method of welding by heated tool of pipes from structured (cross-linked) polyethylene*. Pat. 2293656 RF. Publ. 20.02.2007.
11. Zajtsev, K.I., Matsyuk, L.N. (1987). *Welding of plastics*. Moscow: Mashinostroenie.
12. But, E.D. (1992) *Numerical methods*. Kiev: Naukova Dumka.

INVERTER ACCELERATED VOLTAGE SOURCE FOR ELECTRON BEAM WELDING MACHINES

N.K. CHAJKA
PA «SELMI», Sumy, Ukraine

Key diagrams of design of the power part of accelerated voltage sources with frequency conversion for electron beam guns used in real practice are considered. The principle of operation of the non-resonance type of a power source, wherein the voltage regulator and converter are made as one unit, is described. Its advantages and disadvantages are noted, and specifications are given.

Keywords: *electron beam welding, source, accelerated voltage, inverter*

Inverter power sources steadily displace those traditionally used in equipment for most welding methods. Power sources for electron beam welding (EBW) do not make an exception. Good regulation characteristics, small size and weight, and increased efficiency are the reasons of popularity of the inverter power sources.

Certain requirements are imposed on the accelerated voltage sources designed for use in EBW machines [1]: output voltage instability (≤ 1 %), pulsing of output voltage (≤ 2 %), energy storage in output circuits (≤ 1–2 J/kW), presence of system for suppression of high-voltage discharges in a gun, and time for recovery of high voltage after breakdown should not increase several milliseconds.

Inverter accelerated voltage sources can be divided into two groups — resonance and non-resonance.

As a rule, non-resonance inverter power sources are built according to the scheme, at which the voltage regulator feeds the inverter operating at a constant conversion frequency with the output voltage close in shape to a meander.

The resonance group of inverter power sources is more diverse in designs. Consider a scheme (Figure 1, *a*) which is most often used now. It comprises, in addition to step-up transformer T, three additional reactive elements — inductance L_S, capacitance C_S and inductance L_P. Inductance L_P and capacitance C_S form a parallel oscillation circuit, which, as is well known, has the input resistance of a capacitance character at a frequency above the resonance one. This virtual capacitance forms, together with inductance L_S, the series resonance circuit having a minimum resistance, in contrast to the parallel one, which at the resonance frequency has a maximum resistance. Therefore, the ratio of resistances of reactive elements

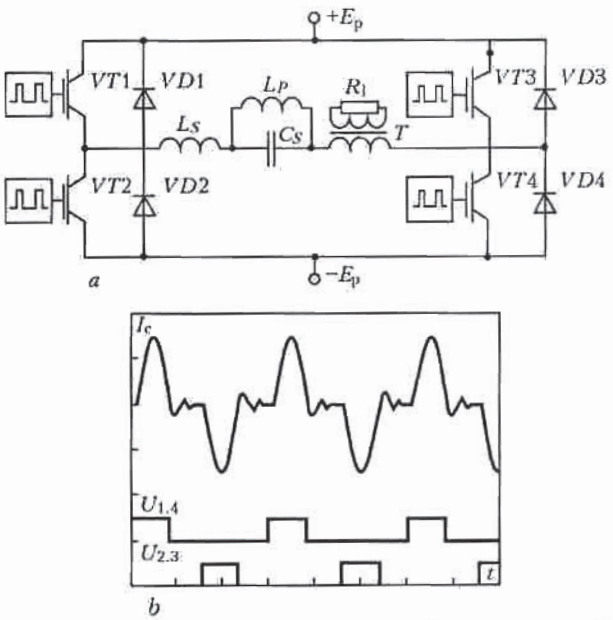

Figure 1. Scheme of inverter power source of resonance type (*a*) and oscillograms of inverter currents (*b*)

and load can be changed by varying the conversion frequency between two resonance frequencies and, thus, regulate voltage at the source output. Since resonance circuit $L-C$ is an enhancer, the current flowing through a primary winding of the step-up transformer acquires a sinusoidal shape, when its frequency is approximately equal to the resonance one. Oscillograms of the current of such an inverter are given in Figure 1, *b*.

The resonance group of inverter power sources used as accelerated voltage has the following structure. Two quasiresistor inverters work for the summing intermediary transformer, which in turn is loaded to the primary winding of the step-up transformer. The control circuit works at a fixed frequency and generates a series of rectangular pulses for the first and second inverters. Regulation of output voltage is provided by changing the phase shift between them. Analytically, this can be represented in the following way:

$$I_1 + I_2 = I_0 \sin \omega t + I_0 \sin (\omega t + \varphi) =$$
$$= 2I_0 \left[\sin \left(\omega t + \frac{\varphi}{2} \right) \cos \left(- \frac{\varphi}{2} \right) \right].$$

As cos φ is the even function, then cos $(-\varphi 2) =$ $= (\varphi/2)$. By designating the $2I_0$ cos $(\varphi/2)$ product as amplitude I_Σ of the sum, we obtain an expression for the sum of the currents:

$$I_1 + I_2 = I_\Sigma \sin \left(\omega t + \frac{\varphi}{2} \right),$$

where I_Σ if the function of phases shift between the driving pulses.

The following design is used to obtain the high output voltage in such sources: sectioning of a secondary winding of the step-up transformer, which reduces parasitic capacitance of the secondary winding and allows using rectifier diodes with a lower reverse voltage; using the double voltage transformation scheme [2] in the case of a lack of room for allocation of step-up windings in a window of the output transformer core; applying the step-up transformer and diode-capacitor multiplier combination, which makes it possible to dramatically reduce requirements to high-voltage isolation of the secondary winding of the step-up transformer.

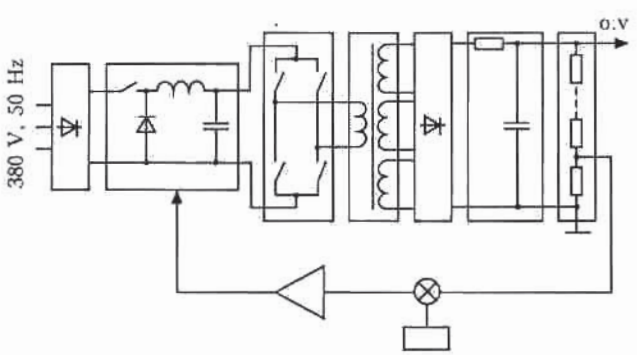

Figure 2. Scheme of inverter power source of non-resonance type: o.v — output voltage

A source described in study [3], the scheme of which is given in Figure 2 [4], can be considered as an example of realization of the non-resonance type of the accelerated voltage power sources. Both power sources are assembled according to the similar structural scheme and designed to have the same power (15 kW) and voltage (150 kV). The difference lies in a higher conversion frequency used in the second source (20 kHz), as well as in the fact that if in the first source the high voltage is provided due to summing up the rectified voltages of three section of the step-up transformer secondary winding, then in the second source it is provided due to the step-up transformer with an output voltage equal to 20 kV, and its diode-capacitor multiplier. Simplicity of design and control of the power part, and sufficiently high dynamic characteristics are advantages of such schemes. Their disadvantage is that switching of power keys takes place at high currents, which results in increased losses in the keys, as well as the necessity of series switching of two power energy converters (regulator and inverter), this reducing the overall efficiency of the power source.

Scheme of the resonance type of the accelerated voltage source with additional reactive elements designed for generation of current pulses was used by French Company TECHIX in commercial power sources SR60-N-6.000-EBWS (power 6 kW, voltage 60 kV), SR-60-N-15.00/TC1 (power 15 kW, voltage 60 kV) and others. Since the main advantage of all resonance inverters is switching of power keys at a zero current (see Figure 1, *b*), which leads, first of all, to reduction of losses in the keys at the moments of switching and dU/dt and di/dt values, and, as a consequence, decrease in the level of generation of higher order harmonics. Besides, leakage inductance of the secondary winding recalculated into the primary one can be taken into account in calculation of additional inductances. Thus, the inverters based on such a scheme are characterized by a high efficiency (more than 90 %). A disadvantage of this scheme includes reduction of its dynamic characteristics [5] because of usage of the resonance circuits for formation of current pulses.

Scheme of the accelerated voltage source with phase control and two quasiresistor inverters operating for one summing transformer was implemented in a source (power 10 kW, voltage 50 kV) developed by CJSC «Elektro-Intel» (Nizhnij Novgorod, RF). The high voltage in this source is provided through utilization of double transformation. Advantages of this scheme of power sources, like all the resonance ones, include switching of the power keys at zero currents, and disadvantages include the need for two inverters, summing transformer and a range of secondary step-up transformers, this leading to increase in cost and volume of a source.

In addition to the above traditional schemes of inverter power sources, consider also the scheme of an inverter source (power 6 kW and voltage 60 kV)

developed by OJSC SELMI (Sumy, Ukraine). The scheme is shown in Figure 3. The source consists of three-phase bridge rectifier with a filter in a form of capacitance *1*, bridge type key inverter with controlled width of output pulses *2*, step-up transformer *3*, diode-capacitor full-wave bridge voltage multiplier *4*, high-voltage feedback divider *5*, element *6* for comparison of the voltage taken from the lower arm of feedback with voltage of reference source *7*, feedback DC amplifier *8*, and former *9* of the inverter variable-width driving pulses.

The dosed capacity charge through inductance used in pulse-width constant-voltage regulators of the L–C type underlies the principle of operation of the given power source [6]. The difference is that leakage inductance of the step-up transformer secondary winding is used as inductance, and capacitances of the voltage multiplier serve as capacitance. Protective diodes of the inverter, connected in parallel to each key, perform the role of a diode allowing the energy stored in inductance in charging of the capacitor charge to be returned to the source. Although the pulses change their polarity at a conversion frequency, this fact has no influence on the operating regime, as the full-wave multiplier of the bridge type has a balanced input.

Owing to this design of the power source, it was possible to combine the voltage regulator and inverter in one unit, use leakage inductance of the secondary winding of the step-up transformer in operation, and decrease requirements both to size of the core window of the step-up transformer and to high-voltage isolation of the secondary winding.

Determination of parameters of the main power elements, such as the step-up transformer, inverter power keys and diode-capacitor multiplier, became the main points of the development of this source. It is known that output resistance of diode-capacitor voltage multipliers is proportional to the number of cascades in cubic quantity. In this connection, the multipliers containing not more than 4–6 cascades are used in power circuits. Based on above-said and the required output voltage of $60{\cdot}10^3$ V, four-cascade full-wave bridge multiplication circuit having the balanced input was selected. The main advantage of the given scheme is a doubled ripple frequency of the output voltage relative to the frequency of power supply of the transformer, as well as a flatter load characteristic.

The selected four-cascade multiplication circuit at a set output voltage and minimum inverter supply voltage (three phase voltage of 380 V, 50 Hz rectified by Larionov's circuit at offset of the circuit to minus 10 %) determined the transformation ratio equal to 33.

Four Philips cores U 100/57/25 of the 3C80 grade (μ_e = 1900) [7] (two UU stand for the closed combinations taken together) were used as a magnetic core of the step-up transformer. Calculation of the number of turns in the transformer primary winding at a square shape of the supply voltage, made by method described in study [7], allowing for offset of the supply circuit to plus 10 %, showed that the number of turns in the primary winding should be not less than 32. The number of turns in the secondary winding is determined by the transformation ratio and is equal to 1056. General view of the step-up transformer is shown in Figure 4. The number of turns in primary winding W_1 (secondary winding W_2) is 32 (1056), respectively; resistance is 0.02 (12) Ohm; leakage inductance is 0.02 (24) mH; and capacitance between the winding and screen is 173 (86) pF.

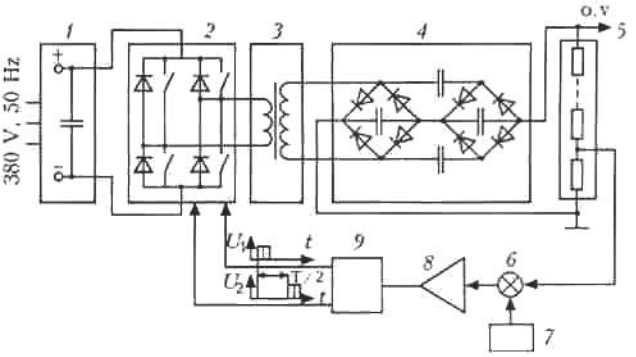

Figure 3. Structural scheme of power source with functions of frequency transformations and stabilization of output voltage combined in one unit

The multiplier capacitors were selected on the basis of two conditions: the operating voltage should be not less than $18{\cdot}10^3$ V (taking into account the gun training mode, where the output voltage of the source may exceed the operating one by 10–15 %); the value of capacitance of the discharge capacitor bank should provide the necessary level of high-frequency pulsing. It is natural that the maximum value of pulsing corresponds to the maximum value of the source current. By setting the value of high-frequency pulsing equal to 1 %, and knowing the load resistance at the source maximum current the expression of voltage at capacitance in its discharge ($U_{C(t)} = U_0 \exp(-t/RC)$, we find the capacitance when it run down to 1 % during the time equal to one fourth of the transformation period.

The time of discharge equal to one fourth of the inverter switching period is selected to estimate the

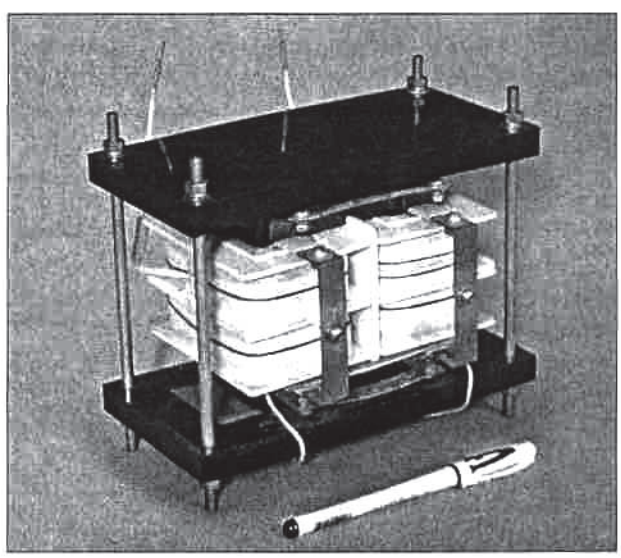

Figure 4. General view of step-up transformer

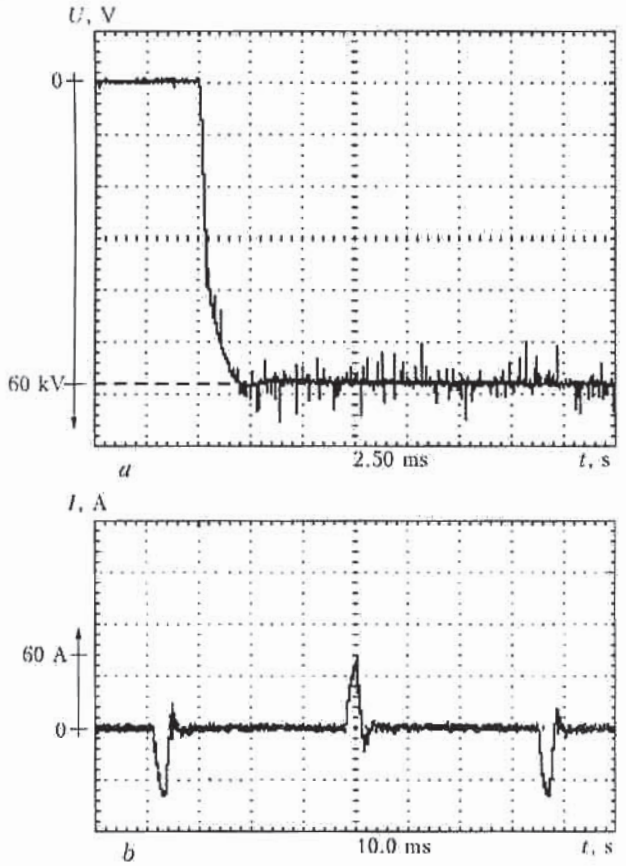

Figure 5. Oscillograms of open-circuit operation of power source: *a* — transition to high-voltage mode; *b* — shape of current pulses of primary winding of step-up transformer

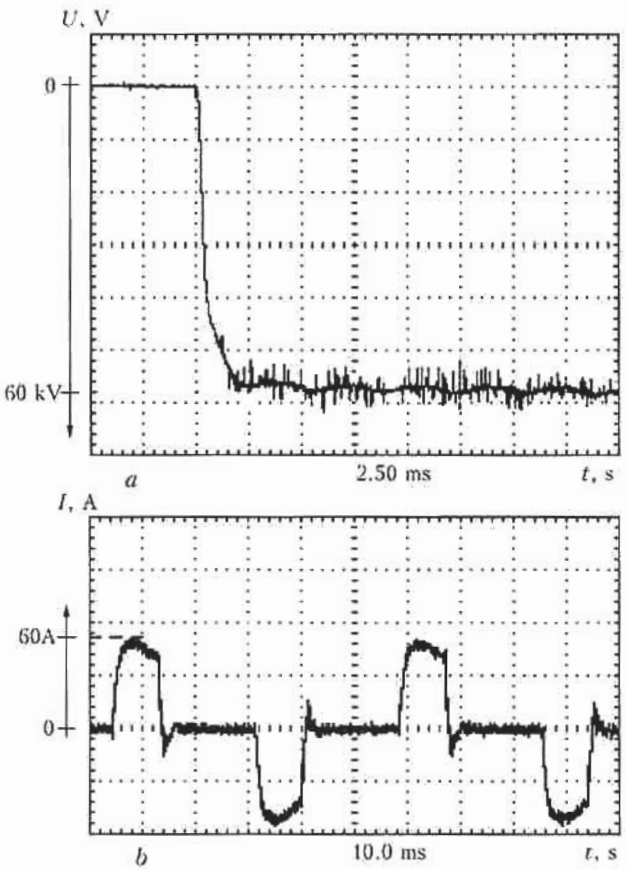

Figure 6. Oscillograms of operation of power source at nominal load (*a*, *b* — see Figure 5)

capacitance value for the following reasons. Recharging the discharge capacitor bank of the multiplier takes place two times per transformation period. Duration of a current pulse at the maximum supply voltage and maximum load current is assumed to be equal approximately to one forth of the transformation period. The time from the end of a current pulse to the second current pulse, which is also equal to about one forth of the period, is used for widening of the current pulse with decrease in the supply voltage and reduction of the safety gap time. This time is a maximum discharge time of the discharge capacitor bank. Capacitance of the discharge capacitor bank after the calculations should be not less than $2.54 \cdot 10^{-9}$ F. Therefore, the cascade capacitance should be equal to $2.54 \cdot 10^{-9} \cdot 4 \approx 10 \cdot 10^{-9}$ F. In fact, it was implemented with allowance for the capacitance of a high-voltage connecting cable with two capacitors K73-14-3300 pF (voltage 25 kV) [8] connected in parallel. For unification, capacitors of the charge bank were assumed to be similar to capacitors of the discharge bank.

It should be noted that increase of output capacitance of the source above the required level leads to increase of the stored energy, the value of which is a negative characteristic of the source. In our case, the expression for calculation of the stored energy has the following form:

$$E = \frac{CU^2}{2} = \frac{2.54 \cdot 10^{-9} \cdot (60 \cdot 10^3)^2}{2} = 4.5 \text{ [J]},$$

which corresponds to the specific stored energy equal to 0.75 J/kW.

Power keys used in the inverter of the source should provide switching of voltages of up to 600 V (bridge circuit rectified voltage of the three-phase 380 V mains at offset of the circuit to plus 10 % is equal to 565 V), overload currents during switching and in moments of reaching the operating mode after a high-voltage breakdown in the gun, which from three to four times exceed the rated ones, and also have an operating switching frequency of $20 \cdot 10^3$ Hz. Proceeding from these requirements and an operating transformation frequency selected to be equal to $18 \cdot 10^3$ Hz, the Mitsubishi Electric power module PM 150 DSA 120 consisting of two IGBT transistors connected in series, each being shunted by a high-speed diode, was used as a power key for the source. The module is designed for a maximum voltage of 1200 V, operating current of 150 A, and switching frequency of $20 \cdot 10^3$ Hz. The module has a built-in protection for overload current (320 A), short-circuit current (450 A) and transition temperature (110 °C).

The following requirements are imposed on the multiplier diodes:

Operating frequency without reduction of parameters, Hz	$\geq 20 \cdot 10^3$
Mean direct current, A	≥0.15
Reverse voltage, V	$\geq 18 \cdot 10^3$
Reboot capability, A	≥2.5

In order to fulfill all the above requirements, the control circuits for 108 V [9], connected in series with three columns in each, were used as diodes, each column for rectifying the voltage being shunted by resistor S3-14-10 mOhm. Rectifying column of the 108 V control circuit is designed for a maximum reverse voltage of $6 \cdot 10^3$ V, mean direct current of 0.18 A and pulse overload direct current of up to 5 A.

Oscillograms of switching to the high-voltage mode for sources operating at an open circuit and nominal load, as well as shapes of current pulses in the primary winding of the sep-up transformer without load and at nominal current load are shown in Figures 5 and 6.

Oscillogram of current pulses in the primary winding of the step-up transformer in source switching the source to a nominal load is shown in Figure 7. Measurements of the current in the primary winding were carried out with the help of a current transformer connected in series with the primary winding. Based on the measurement results, it can be seen that the maximum value of the current in the primary winding of the transformer was 213 A at switching on to the load, and after reaching the operating mode it was only 60 A, i.e. the maximum current in switching on may exceed the current in the stationary mode four times; and time of reaching the high-voltage mode depends but insignificantly on the load is equal to $(3–5) \cdot 10^{-3}$ s.

Specifications of the source

Nominal accelerated voltage, kV	60
Nominal power, kW	6
Accelerated voltage instability, %	±0.5
Accelerated voltage pulsing, %	1
Transformation frequency, kHz	18

This scheme of the inverter accelerated voltage source has the following advantages:

- lower requirements to high-voltage isolation of the step-up transformer due to a comparatively low voltage in the secondary winding;
- possibility of using a magnetic core with a smaller window and smaller size at the same output power and voltage;
- higher efficiency than in known non-resonance sources due to a combination of the regulator and inverter in one unit, as well as no-current switching of the power keys;

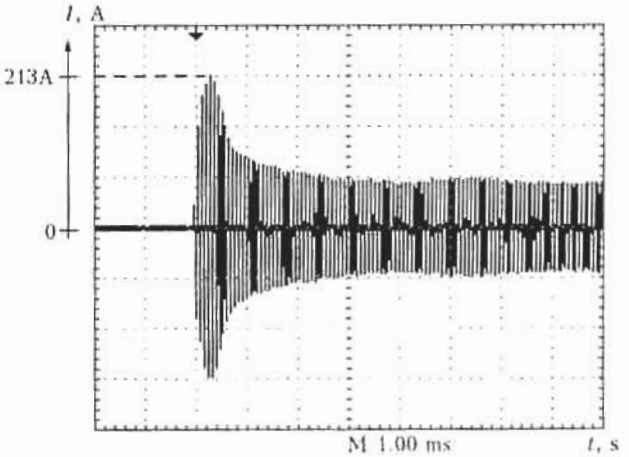

Figure 7. Oscillograms of envelope curve of voltage at measuring resistor of current transformer connected to primary winding of the step-up transformer at switching on of the source to nominal voltage

- better dynamic characteristics than in resonance sources due to the absence of resonance circuits with a resonance frequency close to the switching frequency;
- no need to adjust power circuits to the resonance.

Disadvantage of the above scheme of the inverter power source is switching off of the inverters keys at a current, this increasing losses in the keys at the moment of switching off and leading to decrease in the efficiency, compared with the resonance sources, where switching on and off of the power keys occurs as a zero current.

1. *DSTU 3014–95*: EBW installation.
2. Nazarenko, O.K., Lokshin, V.E. (2005) Dynamic characteristics of high-voltage sources for electron beam welding. *The Paton Welding J.*, **1**, 31–33.
3. Kostikov, V.G., Nikitin, I.E. (1986) *High voltage power supplies REA*. Moscow: Radio i Svyaz.
4. Ferrapio, J.D., Kyselica, S.R., Lawrence, A. (1989) Switch-mode accelerating – voltage regulator for electron beam systems. *Welding J.*, **2**, 44–47.
5. (1989) High-power EBW machines incorporate microprocessor control. *Ibid.*, **5**, 51–53.
6. Golovatsky, V.A. (1974) *Transistor pulse accelerators and constant voltage stabilizers*. Moscow: Sov. Radio.
7. (1993) *Philips components, magnetic products*: Data Handbook MA 01.
8. Diakonov, M.N., Karabanov, V.I., Prisnyakov, V.I. et al. (1983) *Handbook for electric capacitors*. Ed. by I.I. Chetvertkov, V.F. Smirnov. Moscow: Radio i Svyaz.
9. Gitsevich, A.B., Zajtsev, A.A., Mokryakov, V.V. et al. (1989) *Semiconductor devices. Rectifier diodes, stabilitrons, thyristors*. Ed. by A.V. Golomedov. Moscow: Radio i Svyaz.

EQUIPMENT AND CONSUMABLES FOR HARD-FACING OF LINING PLATE ELEMENTS

A.P. ZHUDRA[1], A.P. VORONCHUK[1] and S.I. VELIKY[2]
[1]E.O. Paton Electric Welding Institute, NASU, Kiev, Ukraine
[2]Experimental Design Bureau of the E.O.Paton Electric Welding Institute, NASU, Kiev, Ukraine

The data are presented on the developed, manufactured and applied machine AD 380.03M, which is intended for hard-facing of low-carbon steel plates with thickness of 5 to 30 mm and dimensions of 1500 × 3000 mm. Thickness of the deposited layer can be varied from 3 to 17 mm. Characteristics of the machine, main point of the process, hard-facing consumables, and fields of applications of hardened plates are described.

Keywords: *plate, machine, control system, hard-facing, flux-cored strip, technology, application*

Working surfaces of machine parts operating under intensive abrasive wear conditions should meet high requirements for wear resistance. The known method of extending life of the parts by increasing their thickness leads to increase in weight of structures, decrease in their load-carrying capacity, performance, etc. In addition, frequent replacements of such parts cause slowdown of productivity of process equipment. In this connection, the processes of hardening of wearing surfaces of parts by hard-facing are receiving an increasingly wide acceptance.

For flat parts (bins, chutes, bucket walls, truck bodies, sieves, pans of charging devices of blast furnaces, etc.) operating under intensive abrasive wear conditions, it is economically and technically more expedient to protect wearing surfaces by lining them with wear-resistant plates.

The technology for hard-facing of plates, developed by the E.O. Paton Electric Welding Institute, is based on utilisation of self-shielding flux-cored strips with a cross section of 16.5 × 4.0 and 10.0 × ×3.0 mm as an electrode material, as these strips allow hard-facing without deep penetration of base metal and exclude the labour-consuming process of removal of slag crust [1].

The process of hard-facing of plates using flux-cored strips is based on a continuous reciprocal movement of electrode and jog movement of a part treated.

The deposited layer of a wear-resistant metal contains cracks, which do not propagate to the base metal and have a negligible effect on performance. The developed technology provides high productivity — up to 25 kg of deposited metal per hour.

The hardened plate after full cooling has an insignificant distortion, i.e. the maximal sag is no more than 30–40 mm over a length of 2500 mm.

This technology was first applied at the Novolipetsk Metallurgical Works. It was done by using machine UD-249 designed by the Experimental Design Bureau of the E.O. Paton Electric Welding Institute [2], which allowed producing deposited plates measuring 2100 × 1100 mm.

In the last years Ukraine and other CIS countries have been intensively replacing traditional charging devices of blast furnaces by no-bell charging devices. The main element of such equipment, which is most vulnerable to wear, is a pan. Intensive wear of pans is caused by a very big amount of charging materials passing through them. As a rule, service life of such devices is no more than a year.

We proposed using wear-resistant plates to manufacture lining elements of pans. Finished wear-resistant elements for pans of charging devices and other wearing elements of such equipment can be made by cutting and bending of the plates.

To realise these proposals, the existing equipment was employed for hard-facing of plates with a standard size of 15 + 10 mm. Hard-facing was performed using flux-cored strip PLAN-T-179 with a cross section of 16.5 × 4.0 mm. Then these plates were bent to a diameter of 900 mm under conditions of a metallurgical plant, based on our recommendations. As a result, the finished wear-resistant parts of a pan of the blast furnace charging device were thus produced.

The interest expressed in this technology by a number of metallurgical plants became a key incentive for the development of a new generation of equipment for deposition of wear-resistant bimetal plates.

Machine AD 380.03M (Figure 1) was designed with allowance for both experience of operation of the existing equipment and numerous requests of a customer. For example, sizes of the billet to be hard-faced were increased, and functions of submerged-arc and gas-shielded welding and surfacing, as well as welding and surfacing with electrode oscillations, were added. The most important point was the development of a new, up-to-date control system for the machine.

As a result, the specialised machine for hard-facing of steel plates from 5 to 30 mm thick, 3 m long and 1.5 m wide by the electric open-arc method was developed and manufactured. The machine consists of a carriage with two welding heads moving along the

guiding line. The machine is equipped with two work tables to fix the steel plates, which provides a continuous deposition process. The carriage can move at a working and travel speed.

Specifications of the machine AD 380.03M are as follows:

Rated welding current at duty cycle = 100 %, A	1200
Electrode strip sizes, mm	16.5–4.0 10.0–3.0
Range of adjustment of flux-cored strip feed speed, m/h	4–120
Range of adjustment of wire feed speed, m/h	20–600
Speed of longitudinal movement of device, m/h	0.01–106
Speed of transverse movement of device, m/h	4–106
Speed of vertical movement of device, m/h	10–100
Accuracy of positioning of movable operating element, mm	±1
Overall dimensions of machine, mm	11100 × 3498 × 3468
Weight of machine, kg, not more than	15000

The machine is controlled by means of control system SU-320, which provides a high accuracy of movement of operating elements and automatic adjustment of parameters of the hard-facing process. This control system is designed to control the process of hard-facing of plates. It is based on the OMRON (Japan) components and consists of the following main parts:

- programmable controller of the CQM1H type with software to control the hard-facing process;
- inverter frequency electric drives of the Varispeed F7 and Varispeed V7 types for motors of machine AD-380;
- operator's panel (terminal) of the NT-11S type to enter process parameters;
- starting up and protection equipment, measuring instruments and controls.

Table 1. Thicknesses of hard-faced plates, mm

Plate thickness	Thickness of base metal	Thickness of deposited layer
5 + 3	5	3
6 + 4	6	4
8 + 5	8	5
8 + 8	8	8
8 + 10	8	10
10 + 5	10	5
10 + 8	10	8
10 + 10	10	10
12 + 5	12	5
12 + 10	12	10
12 + 12	12	12
12 + 17	12	17
15 + 5	15	5
15 + 10	15	10
20 + 12	20	12

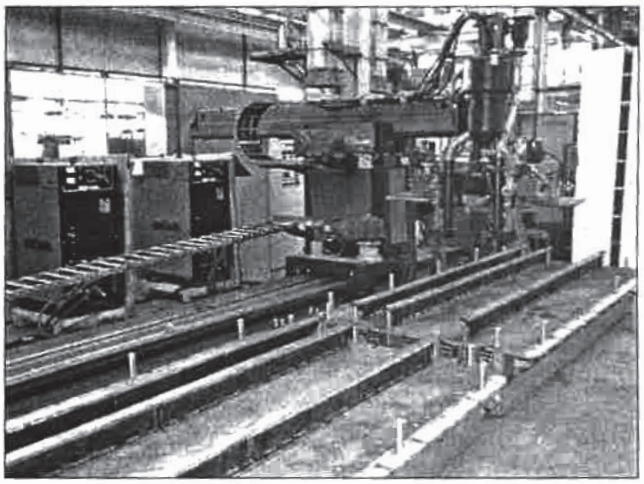

Figure 1. General view of machine AD 380.03M

Electric equipment of the control system is housed in a control cabinet located near the machine. Controls are situated on the panel located on the cabinet door.

The control system provides functioning of the equipment in three modes: setting up–strip–wire (the mode is selected with a switch located on the panel). Mode «setting up» is meant to check operation of all the mechanisms of the machine and perform the set movements prior to hard-facing. Modes «strip» and «wire» are intended for automatic control of the welding and hard-facing process following the set program. Depending upon the process consumable (strip or wire), the control system tests the set process modes. Indication of the process parameters on digital devices and operator's panel, as well as the possibility to adjust the parameters during welding or hard-facing are provided in all the operation modes.

Technological or emergency messages of the type of «no current, stop process», «failure of feed drive», «parameter outside the limits», etc. are displayed on the operator's panel to monitor operation of the equipment.

The machine is fitted with two power sources of the VDU-1250 type with constant external characteristic.

Self-shielding flux-cored strips of different compositions, providing high hardness of the deposited

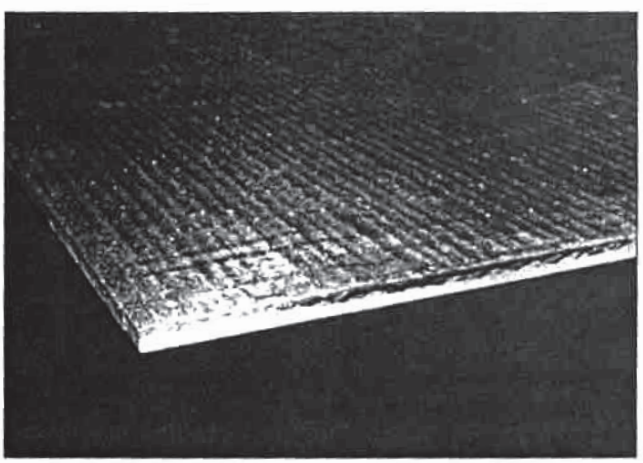

Figure 2. Appearance of clad plate

Table 2. Chemical composition and hardness of metal deposited by using flux-cored strips

Flux-cored strip grade	Chemical composition of deposited metal, wt.%							Hardness *HRC*
	C	Cr	Mn	Nb	Mo	V	W	
PLAN-T-180	4.5	30.0	–	–	1.0	–	–	58–62
PLAN-T-181	4.5	30.0	3.0	–	–	–	–	58–60
PLAN-T-179	5.0	22.0	–	7.0	6.0	1.0	2.0	58–62

metal and high wear-resistance at normal and increased temperatures, can be used as the electrode material.

Flux-cored strip with a cross section of 10.0 × × 3.0 mm is used for hard-facing of plates 5–7 mm thick, and strip with a cross section of 16.5 × 4.0 mm is used for hard-facing of plates 8–20 mm thick. Hard-facing can be performed in one, two or three passes.

The resulting bimetal plates can be readily transformed by laying-out, cutting and bending into a wide range of parts for hardening different assemblies and units, thus extending several times their service life.

The machine was manufactured by the Pilot Plant for Welding Equipment of the E.O. Paton Electric Welding Institute and delivered to the customer (Mechanical-Repair Plant of the Magnitogorsk Metallurgical Works, Russia). The machine was commissioned in February 2009.

The developed hard-facing technology and equipment allow producing plates of a wide range of standard sizes (Table 1). It should be noted that the sizes in the Table are given without allowance for the base metal penetration depth. The penetration depth in hard-facing of plates 5–8 mm thick is 1.5–2.0 mm, and above 8 mm — 2–3 mm.

Flux-cored strips providing chemical composition of the deposited metal and its hardness as given in Table 2 are used for hard-facing of plates.

Other materials can also be used at the request of customers.

Appearance of the hard-faced plate is shown in Figure 2.

The developed technology, equipment and consumables make it possible to produce a wide range of wear-resistant lining elements, which can be used to advantage to manufacture and repair equipment in different industrial sectors. Also such parts are competitive in the world market, which is confirmed by delivery of these products to the USA, Germany, Greece, Russia, Poland and other countries.

1. Danilchenko, B.V., Shimanovsky, V.P., Voronchuk, A.P. et al. (1989) Hard-facing of rapidly wearing parts by self-shielding flux-cored strips. *Avtomatich. Svarka*, **5**, 38–41.
2. Terpilo, V.N., Shimanovsky, V.P. (1988) Technology of hard-facing of thin sheets by flux-cored strips. In: *Proc. of Conf. of Junior Scientists and Specialists* (Kiev, 1988).

11th INTERNATIONAL SCIENTIFIC-PRACTICAL CONFERENCE IN St.-PETERSBURG

The International Scientific-Practical Conference «Resource-Saving Technologies for Repair, Reconditioning and Hardening of Machine Parts, Mechanisms, Equipment, Tools and Fixtures from Nano- to Macrolevel» took place in St.-Petersburg on 14–17 April 2009. The Conference was organised by Research and Production Company «PlazmaCentre» and St.-Petersburg State Polytechnic University. This traditional annual conference has been held since 1997, and is the largest event in Russia and other CIS countries focused on these topics. It is dedicated to industrial technologies, which at the time of the economic crisis are capable of providing the maximum possible reduction of costs and raising the efficiency of manufacturing.

About 450 people representing different enterprises and organisations of Russia, Belarus, Ukraine, Kazakhstan, Azerbaijan, Moldova, Armenia, Uzbekistan, Lithuania, Poland and Korea took part in the work of the Conference. The main information sponsor of the Conference was the Limited Liability Company «Mashinostroenie» Publishing House». Also, the information support was rendered by over 50 periodical scientific-and-technical journals.

The focus of the Conference was on the following four topics:

- technologies for reconditioning of the initial surface geometry using welding, surfacing, spraying and other processes (41 papers);
- surface engineering, structural and operational methods for improving reliability and extending service life, tribotechnology and surface treatment of parts (29 papers);
- hardening technologies, modification and restoration of physical-mechanical properties of surfaces, and deposition of thin-film coatings (62 papers);
- technologies for diagnostics, flaw detection, washing and cleaning (25 papers).

P.A. Topolyansky, Director General of Research and Production Company «PlazmaCentre», noted in his opening speech that the Conference held in St.-Petersburg is the most important and major event of this kind in Russia and other CIS countries. It is attended not only by specialists, scientists and lecturers of institutes of higher education, i.e. developers of the repair, reconditioning and hardening technologies, but also representatives of the industry — direct customers of the above technologies, who came from different regions of Russia and CIS countries. The Conference allows direct communication between developers and customers of the innovation projects. It is the dialogue and sharing of experience that such conferences are famed for. The main purpose of such conferences is to popularise technologies and obtain the new ones, which are capable of providing reliable and competitive products, as well as advocate the need for generation of the new knowledge to improve quality and reliability, and extend life of technical parts, which are manufactured now or are already in operation. Such conferences are characterised by orientation to practical application and possibility of finding performers to introduce into practice the repair, reconditioning and hardening processes, by demonstration and deposition, together with the participants, of wear-resistant coatings on parts they brought with them. This Conference is of a high educational sig-

nificance, as it is attended by post-graduates and students who chose the line of their future labour activity — creative work in engineering.

About 50 plenary papers were presented at the Conference. Each organisation that presented a paper was awarded the honorary diploma.

One should note an increased scope of research and new efficient developments made at different institutions of higher education and intended for practical application. The integrated approach to addressing the topical problems can be illustrated by an example of the technology developed by the St.-Petersburg Agrarian University in collaboration with the Bryansk Agricultural Academy for arc cladding of parts of tillage machines allowing for interaction of soil with the clad surface. The cladding performed not in a solid layer, but in separate strips following the certain diagram makes it possible to improve the quality of cultivation of soil, decrease wear of parts, and save cladding consumables. The technology can be applied not only by manufacturers of agricultural machinery, but also by small business companies providing technical service.

Developers of the repair and hardening technologies pay much attention to mechanisation and automation of both processes and information systems for automated choice of materials for deposition of coatings (e.g. development of the Military-Technical University, Balashikha).

We cannot but note the active participation in the Conference by representatives of remote regions: Yakutsk, Magadan, Khabarovsk, Chita, Novosibirsk, etc., who presented interesting developments on currently important topics.

The largest quantity of papers (62) presented at the Conference were dedicated to new resource-saving technologies for hardening of surfaces and deposition of thin-film coatings. The technologies are characterised by a wide diversity and high efficiency. Interesting developments were presented by specialist from Belarus, Irkutsk, Moscow and St.-Petersburg. The Conference noted topicality of development of non-vacuum technologies for production of hardening nano-coatings.

Traditionally, a visit to industrial sections for reconditioning and deposition of functional coatings using the thermal spraying, cladding and hardening technologies was arranged for the Conference participants. They were shown a new process of finishing plasma hardening with deposition of diamond-like coatings, which can provide a many times increase in life of parts by a few minutes treatment, as well as the technology for spray cladding (PTA-process). Tools and technological fixtures brought by the participants were hardened during the Conference.

The new generation of equipment developed by specialists of Research and Production Company «PlazmaCentre», Messer Eutectic Castolin Ltd., Limited Liability Companies «OTsPN» and «Energiya 3000», was demonstrated at the exhibition facilities to the Conference participants.

Workshops were held in parallel within the framework of the Conference for industry representatives: «All Methods for Increasing Strength of Tools, Cold Deformation Dies, Press Moulds and Other Technological Fixtures», «Surfacing and Spraying — Selection of Technology, Equipment and Materials», «Repair, Reconditioning, Hardening and Quality Inspection of Casting Fixtures, Press-Forging Tools and Dies» and «Design of Friction Components and Parts with Increased Life and Wear Resistance».

During discussions, the Conference participants noted political aspects and problems with application of the advanced repair, reconditioning and hardening technologies. Actively expressed were the opinions on the expediency of arranging regional centres for renovation of technical facilities, enhancement of efforts on application of new, science-intensive technologies for repair and, particularly, hardening of critical parts and tools. The Conference participants noted an extensive use of plasma, laser, ultrasonic and other highly efficient electrophysical processes aimed at the extension of life of parts, tools and process fixtures. Nanotechnologies are going out from research laboratories and finding an increasingly wide application for hardening of various parts. Scientists and practical workers from different CIS countries take an active part in collaborative efforts. International conferences of this format promote development of practically all sectors of economy of both Russia and other countries.

The annual St.-Petersburg Conference dedicated to the repair, reconditioning and hardening technologies is an important link for integration of science and industry. The Conference proceedings in two books and in about 1000 pages were published for Conference opening. «Encyclopaedia of Repair, Reconditioning and Hardening Technologies» stored on the compact disk, including proceedings of all previous conferences (about 6000 pages) and software for retrieval by key words to address scientific and practical problems, was disseminated among the Conference participants.

N.L. Ivanova

4th INTERNATIONAL CONFERENCE ON LASER TECHNOLOGIES

Over the period of May 26–29, 2009 the 4th International Conference on LTWMP-2009 «Laser Technologies in Welding and Processing of Materials», organized by the E.O. Paton Electric Welding Institute of NASU, Research Institute of Laser Technique and Technology of the National Technical University of Ukraine «KPI» and International Association «Svarka» took place in Crimea on the base of «Katsiveli» House of Scientists. The co-chairmen of its Programme Committee were Academician B.E. Paton and Prof. V.S. Kovalenko.

Starting from 2003 the conferences on the mentioned subject are held regularly gathering the specialists on this progressive technology from all over the world. The official language of conference is English. This year in spite of all doubts of organizers as to the reasonability of Conference conductance under the conditions of severe global crisis the experts of laser technology from seven countries of the world (at the previous conferences the number of countries-counterparts usually exceeded 20) have successfully overcome all problems of their participating in the conference.

After welcome the plenary part of the Conference was opened by the report of Prof. V.S. Kovalenko «Modern tendencies of development of high technologies in mechanical engineering». It was told about the new paradigm of mechanical engineering development (Competitive Sustainable Manufacturing) and challenge of implementation of innovations based on the progressive technologies and include automation of processes of assembling and disassembling in industry, development of high-efficient lasers (diode, fibre optic and other).

The fundamental report «Laser hybrid welding of pipe steel – modeling and technology» was delivered by Prof. G.A. Turichin with the colleagues from St.-Petersburg Technical University. The report of Prof. I.V. Krivtsun with colleagues from the E.O. Paton Electric Welding Institute «Interaction of dense gas-discharged plasma with metal surface evaporating during the plasma and laser-plasma welding» was also devoted to the theoretic analysis of hybrid processes. Dr. A. Gumenyuk from the Federal Institute of Material Research (Berlin, Germany) reported the results of research works of laser hybrid welding of thick-walled structures using fibre laser. The Chinese colleagues presented two reports from Laser Centre of Zhejiang Technology University (Guangzhou). In one of them «The investigations of residual stresses and

mechanical properties of turbine blades of stainless steels modified by laser radiation» Prof. Jianhua Yao presented the results of joint investigations with the colleagues from the Research Institute of Laser Technology of the National Technical University of Ukraine «KPI». Prof. A.N. Grezev from the Institute of Laser and Informational Technologies of RAS (Shatura) presented the report «Laser equipment and methods of laser cutting, welding and surface treatment» which were recently developed in this Institute for different enterprises.

In number of reports the possibility of control of local thermal deformations using laser radiation to change the shape and rigidity of parts of sheet materials were examined by M. Grden and Prof. F. Wolersten (Institute of Beam Technology, Bremen, Germany), and A. Kaglyak, the young researcher with his colleagues of Research Institute of Laser Technology presented the report on the subject «Forming of workpieces of metal sheet materials using laser». The possibilities of application of laser radiation for perforation and drilling of oil and gas drilling wells were discussed by specialists of Ukrainian State Geological Research Institute (Kiev). The Lithuanian colleague Prof. S. Sipyavichus (Institute of Physics of AS of Lithuania, Vilnius) suggested the application of laser radiation for production of nanoparticles of metals.

In some reports from «KPI» the possibilities of manufacture of stands for cardiosurgical operations were described (R. Zhuk, N. Anyakin and others). One of them was presented by the student I. Vakhdatinia (Iran), who prepared magister work on this subject. Among other topics of wide interest were the report of Prof. L.F. Golovko from «KPI» (manufacturing of diamond cutting tool using technology of laser growth of workpieces) and others.

During the plenary and stand sessions over 50 reports were considered. At the end of the Conference the round table was organized for discussion of actual problems of laser technologies development. The serious discussion was devoted to the peculiarities of physical phenomena observed at the interaction of laser radiation and plasma in the realization of hybrid «laser + plasma» treatment.

In the course of discussion on the application of different modeling methods it was outlined that development of physical and mathematical models of processes is reasonable in the cases when modeling results are perfectly correlated with practical (experimental) results.

Before opening of the Conference the collected theses and Conference program were published. By the end of November, 2009 the Proceedings of the Conference will be published in English (the works of the previous conferences LTWMP-03, LTWMP-05, LTWMP-07 can be ordered in the editorial board of journal «Avtomaticheskaya Svarka»).

Friendly, hospitable and creative atmosphere of the Conference promoted the development of useful discussions and establishment of business contacts. The absolute success of the Conference made its participants from different countries adopt unanimous suggestion on holding the next 5th International Conference on Laser Technologies in Welding and Processing of Materials (LTWMP-11) in May 2011, Katsiveli, Crimea, Ukraine.

Prof. V.S. Kovalenko
Dr. A.T. Zelnichenko